NASA
Technical
Paper
2607

June 1986

Development Testing of Large Volume Water Sprays for Warm Fog Dispersal

V. W. Keller,
B. J. Anderson,
R. A. Burns,
G. G. Lala,
M. B. Meyer,
and K. V. Beard

NASA

NASA Technical Paper 2607

1986

Development Testing of Large Volume Water Sprays for Warm Fog Dispersal

V. W. Keller,
B. J. Anderson,
and R. A. Burns
George C. Marshall Space Flight Center
Marshall Space Flight Center, Alabama

G. G. Lala
and M. B. Meyer
State University of New York at Albany
Albany, New York

K. V. Beard
University of Illinois at Urbana-Champaign
Urbana, Illinois

National Aeronautics
and Space Administration

Scientific and Technical Information Branch

ACKNOWLEDGMENTS

This work was supported by the NASA/MSFC Center Director's Discretionary Fund (CDDF), Project No. 84-15. Pumping module operations were conducted by Mr. James Manser, Fire Marshal Program Administrator, U.S. Navy, and his very capable team of firemen. Navy participation was coordinated through Mr. Ismail Akbay, Director of the MSFC Technology Utilization Office. Mr. Tom Troutner of the Akron Brass Company contributed in many ways to the success of the tests. Mr. David Bowdle, Universities Space Research Association (USRA), contributed to many stimulating discussions on various aspects of this study. The enthusiastic support of these individuals and the engineering, technical and clerical staff of MSFC is gratefully acknowledged.

TABLE OF CONTENTS

LIST OF SYMBOLS

A	Horizontal area over which water spray is distributed
a, a′, b, b′	Constants in the exponential spray drop distribution function. (Primes indicate corresponding parameter for surfactant treated spray).
B_h, B_o	Brightness of the background horizon and object, respectively.
C_p	Specific heat
D	Diameter of fog or spray drops; diffusivity of water vapor in air
d_o	Diameter of equivalent volume sphere
d_h	Drop major (horizontal) axis
d_v	Drop minor (vertical) axis
E	Collection efficiency
E′	Collection efficiency of surfactant treated drops; integral mean collection efficiency
E	Collision efficiency
F	Non-dimensional "ventilation coefficient"
f	Non-dimensional "ventilation factor" for mass transfer
F_D, F_D'	Fraction loss of droplets in spray. (Prime indicates corresponding parameter for surfactant treated spray)
f_1, f_1' f_2, f_2'	Substitution parameters in fog removal formulation. (Prime indicates corresponding parameter for surfactant treated spray)
K	Extinction factor; thermal conductivity
L	Length of spray curtain
LWC	Liquid water content
L	Latent heat of condensation
M	Mass of the drops
m	Mass of a drop
N	Number concentration of fog or spray drops
N_{Re}	Reynolds number

N_{Sc}	Schmidt number
N_{We}	Weber number
n	Concentration of fog droplets
n_o	Initial concentration of fog droplets
P	Pressure
Q	Water spray rate
R	Spray drop radius
R_o	Radius of equivalent volume sphere
r	Fog droplet or particle radius
$\bar{r}$	Mean droplet radius
S	Surface area of fog or spray drops
S_v	Saturation ratio of moist air
T	Temperature
T_a	Temperature of air
T_i	Initial temperature of falling water drop
t	Time
U	Velocity of drop
ΔU	Change in velocity
u	Component of wind velocity normal to the spray curtain
V	Total volume of water sprayed
ΔV	Volume of water dispersed into drops of radius R
V_R	Standard meteorological visual range
Y_c	Initial horizontal separation of drop centers on a grazing trajectory
z	Height above ground
α	Particle size parameter; constant in drop terminal fall speed relation
β	Constant in drop terminal fall speed relation

Γ	Drop axis ratio (vertical/horizontal)
Γ_o	Equilibrium drop axis ratio
γ	Constant in drop terminal fall speed relation
ϵ	Threshold of contrast; coalescence efficiency
λ	Wavelength of light
ν	Kinematic viscosity of air
π	Pi = 3.141592...
ρ_a	Density of air
ρ_L	Density of liquid water
$\rho_s(T)$	Saturated vapor density at temperature T
Σ	Summation
σ, σ'	Total extinction coefficient; surface tension for untreated and surfactant treated spray
τ	Thermal relaxation time constant

TECHNICAL PAPER

DEVELOPMENT TESTING OF LARGE VOLUME WATER SPRAYS FOR WARM FOG DISPERSAL

1.0 INTRODUCTION

Since Space Transportation System (STS) launches and landings are conducted along fog prone coastal areas, there is a potential for costly disruption to the Space Shuttle schedule due to incidence of fog (Fig. 1-1). Launch delays imposed by visibility restrictions at the return to launch site (RTLS) location can result in failure to meet narrow launch window constraints. Likewise, low visibility at the landing site can postpone a landing or cause diversion to an alternate site resulting in a five to seven day schedule delay for the following mission. As the frequency of Shuttle flights increases and as launches are initiated from the West Coast where fogs are more prevalent, the potential for fog induced disruptions will rise.

Disruptions resulting from low visibility due to fog are not unique to the Space Program. Even with the recent technological advances made in electronic aids, fog is still the most serious natural hazard to navigation whether by land, sea, or air. For example, direct costs attributable to fog disruptions at Los Angeles International Airport (LAX) alone, exceed $3,000,000 annually (in 1975 U.S. Dollars); indirect costs at LAX exceed $13,000,000 annually [1]. Loss of human life in occasional fog related aircraft accidents cannot be measured in monetary terms.

In an attempt to minimize these disruptions many fog dispersal schemes have been proposed and tested in the past, but with only limited success. Supercooled fogs can now be dispersed operationally, but these represent a very small fraction of the cases of interest. No satisfactory operational method is presently available for dispersing warm fogs, i.e., the most common type fogs. More than a decade ago it was concluded that no successful warm fog dispersal technique other than a brute force method is possible because of the thermodynamic and physical stability of these systems [2,3,4]. Despite this restriction there remained optimism that an operationally useful technique would eventually be developed [4].

Recently, a new brute-force method of warm fog dispersal has been proposed [5]. The method uses large volume recycled water sprays to create curtains of falling drops through which the fog is processed by the ambient wind and spray induced air flow. Fog droplets are removed by coalescence/rainout. The efficiency of the technique depends upon the water drop size spectra in the spray, the height to which the spray can be projected, the efficiency with which fog-laden air is processed through the curtain of spray, and the rate at which new fog may be formed due to temperature differences between the air and spray water. This paper describes a small field test program which was implemented to investigate these effects. The project was undertaken to develop the data base necessary to assess the feasibility of the proposed method. Analytical calculations based upon the field test results indicate that this proposed method of warm fog dispersal is feasible. Even more convincingly, the technique was successfully demonstrated in the one natural fog event which occurred during the test program.

2.0 BACKGROUND

By accepted definition the term "fog" is given to any cloud that envelops the observer and restricts his horizontal visibility to 1 km or less. Fog is usually a localized event. Both the moisture and

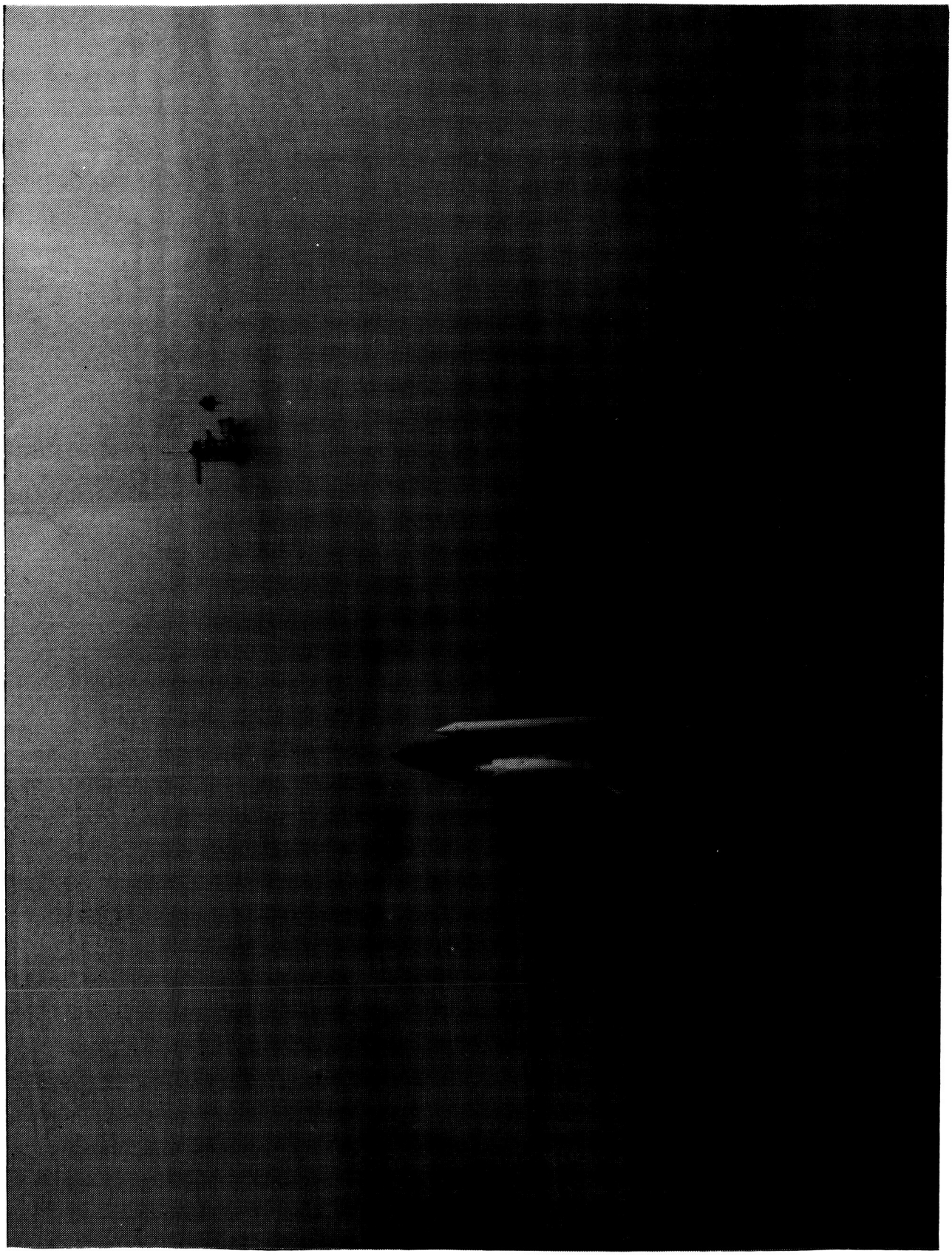

Figure 1-1. Incidence of fog can result in costly disruption to the Space Shuttle schedule. This photograph shows occurrence of a shallow fog at Kennedy Space Center during orbiter rollout.

cooling required for its formation are affected by local geography and meteorological conditions. Since fog consists of a suspension of numerous very small water droplets or ice crystals, it can, from the standpoint of dispersal, be categorized according to its composition and temperature as ice fog, supercooled fog, or warm fog. An ice fog is comprised of ice particles and rarely exists at temperatures warmer than -25°C. Therefore, its existence is limited to winter months at the very highest latitudes. It results almost entirely from water vapor introduced into the environment by human activity. Thus, it can be effectively prevented by controlling the man-made particle and moisture sources that lead to its formation.

Supercooled fogs are composed of water droplets in colloidally-stable equilibrium with their environment at below-freezing temperatures, i.e., colder than 0°C. They are by far the simplest to disperse. Although they are colloidally stable they exist in a thermodynamically metastable state; the transition to the lower energy ice phase is easily induced. If ice crystals are introduced into a supercooled fog they grow rapidly by vapor deposition at the expense of the surrounding water droplets since the equilibrium vapor pressure over ice is less than that over water at the same temperature. Thus, the water droplets are evaporated and the resulting ice crystals become large enough to be removed by gravitational settling. The final result is dispersal of the fog. Ice crystal formation is usually induced by airborne seeding with dry ice, i.e., solid carbon dioxide, or by ground-based propane systems which depend upon the instantaneous vaporization and expansion of the liquid propane to produce ice crystals at temperatures as warm as -1°C. Operational systems which exploit this principal have been in use at airports since the early 1960s.

Warm fogs, which are comprised of water droplets at above-freezing temperatures, develop when air cools or has its moisture content increased sufficiently to cause saturation in the presence of an adequate concentration of condensation nuclei. They occur throughout the United States but most frequently in coastal areas. They are by far the most common type of fog, accounting for 95 percent of the occurrences in this country. However, no satisfactory operational method for dispersing these fogs has ever been developed due to the fact that they are both colloidally and thermodynamically stable.

Warm fogs are often classified according to their formation mechanism. Those initiated primarily through cooling of the ambient air are called air mass fogs. This classification is subdivided according to the dominant cooling mechanism into advection, radiation, and upslope fogs. Radiation fogs are characteristic of inland valleys. Upslope fogs are dependent upon gradual orographic lifting. Typically, advection fogs occur along coastal areas or near other large bodies of water. This is a consequence of warm, moist air cooling as it passes over cold ocean currents. The California current, for example, is responsible for the high fog frequency during summer months along the California coast. Fogs formed by saturating the air through addition of water vapor, such as occurs when warm rain falls through cold air at a frontal surface, are called frontal fogs. Quite often more than one formation mechanism is operative, with one process being dominant. The physical properties of the fog are usually related to its dominant formation mechanism as well as to the number of available condensation nuclei. High nuclei concentrations characteristic of continental or polluted air typically result in large numbers of small fog droplets. It should be noted, however, that fog properties can vary considerably with fog type and age. In general, radiation fogs have a high concentration of small droplets and are associated with light winds. Advection fogs, on the other hand, have larger droplets but at a lower concentration and usually higher wind speeds. Table 2-1 gives typical values for the physical properties of these fogs.

The objective in dispersing fog is to improve the visibility or visual range. The theory of visual range and the relationship to the various fog parameters is discussed in Appendix A1.0. Equation (2.1) defines the standard meteorological visual range, V_R, as the distance at which a black target can just be detected against a horizon sky in daytime with a contrast threshold of 2 percent, i.e.,

$$V_R = \frac{3.912}{\pi \sum_{i=1}^{M} (K_i N_i r_i^2)} , \qquad (2.1)$$

where K is the extinction factor, i.e., scattering efficiency of a fog droplet; N is the number concentration of fog droplets; r is the fog droplet radius; and the summation, Σ, is taken over all fog droplets. For visible light and spherical fog droplets, the scattering efficiency has a constant value of approximately two. Note that the visibility can be improved by decreasing the number concentration of droplets, by decreasing their size, or by both. Modification techniques which decrease the number concentration must do so by physical removal, whereas, a reduction in droplet radii is accomplished via evaporation.

TABLE 2-1. WARM FOG CHARACTERISTICS

Fog Parameter	Fog Type	
	Radiation	Advection
Average droplet diameter (μm)	10	20
Typical droplet size range (μm)	4–35	7–80
Equivalent water content (g m^{-3})	0.11	0.17
Droplet concentration (No. cm^{-3})	200	40
Horizontal visibility (m)	100	300
Typical wind speed (m s^{-1})		
Near the ground	0.5–1.5	1.0–3.0
At 25 to 50 m	1.0–3.0	2.0–6.0

The clearing requirements, i.e., the size and shape of the volume in which visibility improvement is required for an operational warm fog dispersal system, varies considerably with the engineering application. Therefore, discussion here will be confined to runway clearing for Space Shuttle and aircraft applications. Even in this case the amount of visibility improvement required and the height to which it must be effected depend upon the level of sophistication of the electronic landing aids present along the runway and aboard the aircraft. The least sophisticated systems, called Category I landing systems, require a minimum visibility of 730 m (2400-ft) and a decision height of 60 m (200 ft). The more elaborate Category II systems require visibilities of at least 365 m (1200 ft) and a decision height of 30 m (100 ft). The most sophisticated systems, Category III, are subdivided into three categories. Category III a, b, and c systems have no decision height specification but require minimum visibilities of 215 m (700 ft), 45 m (150 ft), and 0 m, respectively. All major airports in the United States have at least Category I landing systems and several have Category II systems. However, Category III systems are a rarity or operationally nonexistent. Thus, to meet Category II requirements along a typical Shuttle runway (70 m wide by 5 km long) the volume to be modified is approximately 10^7 m^3. Since an ambient wind of order 1 m s^{-1} can refill this volume every minute, any effective fog dispersal system must be able to process tremendous volumes of air.

Promising dispersal techniques investigated in the past include seeding with hygroscopic material such as salt particles; using high voltage wires, charged "bubbles," or charged particle generators to modify the electric field structure; using heaters, burners, and jet engines to evaporate the fog droplets;

using helicopters for mixing dry air downward into the fog; and dropping water from an aircraft in order to remove the fog through coalescence. The thermokinetic technique in which fog droplets are evaporated by undersaturating the air is currently regarded as the best method available. Undersaturation is achieved by either heating the air or mixing it with drier air. This is a very expensive operational method and produces considerable environmental pollution. Although the method has been known for over forty years, it is routinely used at only one airport in the world. The other techniques have the characteristic of being ineffective on a large scale, cost inefficient, producing considerable environmental pollution, or they simply did not work effectively in the configurations tested.

3.0 DETAILED DESCRIPTION OF NEW METHOD

In the proposed new method, large quantities of water, i.e., approximately 6300 liters per second per kilometer of runway (100,000 gallon per minute per 3300 ft), are propelled vertically to a height sometimes in excess of 75 m (250 ft) via a plurality of high capacity nozzles arranged strategically alongside the runway or other area to be cleared. Figure 3-1 is an artist's simplified concept of the system installed along an Orbiter runway.

Since the spray drops are substantially larger than fog droplets and have a terminal velocity one to two orders of magnitude greater, spray drops will overtake and collide with individual fog droplets as they fall toward the ground. When fog and spray drops coalesce upon collision, the fog is partially dissipated. Each spray drop removes several hundred fog droplets before impacting the ground. Thus, the fog is dissipated resulting in a visibility improvement on either side of the water curtain. In the example of a Shuttle or aircraft runway, a water retrieval system may be used to collect the water upon its return to ground and place it into reservoirs for recirculation.

Because fog is nearly always accompanied by a light wind, ≈ 1 m s^{-1} or greater, and the water curtain induces its own air circulation, it is not necessary to have the water spray directly on top of the area to be cleared. The ideal arrangement of the vertically-directed nozzles is in rows parallel to the runway with more active nozzles on the upwind side. In this configuration, the fog is processed through a curtain of water spray created by the water jets. All of the air to be cleared is acted upon directly. The falling water spray induces a downward airflow which causes a circulation of the air on both sides of each curtain. This is important because, as Figure 3-1 illustrates, with water curtains installed on either side and parallel to a runway, there is a convergence of processed air and net upward flow over the center of the runway. Thus, the induced air flow helps process the fog through the curtain sprays, inhibits the entrainment of fog into the cleared volume from above, and impedes movement of the smaller spray drops into the targeted clearing volume.

In this process the removal of fog droplets and concurrent visibility improvement increase in proportion to the quantity of water sprayed. The efficiency and therefore the total water spray requirements for the desired degree of clearing depend upon the size spectra of the spray drops. A simple analysis, assuming a monodisperse water spray, is now presented to show that the optimum spray drop size is between 0.3 mm and 1.0 mm diameter and to illustrate the principles involved. The more complex mathematical formulation which describes this process for a polydisperse spray distribution is presented in Appendix A2.0.

Consider a monodisperse water spray uniformly distributed over a horizontal area A and falling under the influence of gravity. The air motion induced by the falling spray is ignored in this illustration. The total number of drops, N, with radius R sweep out the fog droplets in an effective cross-sectional area $N\pi R^2E$ where E is the collection efficiency of the collector drops for fog droplets. If ΔV is the volume of water dispersed into drops of radius R then

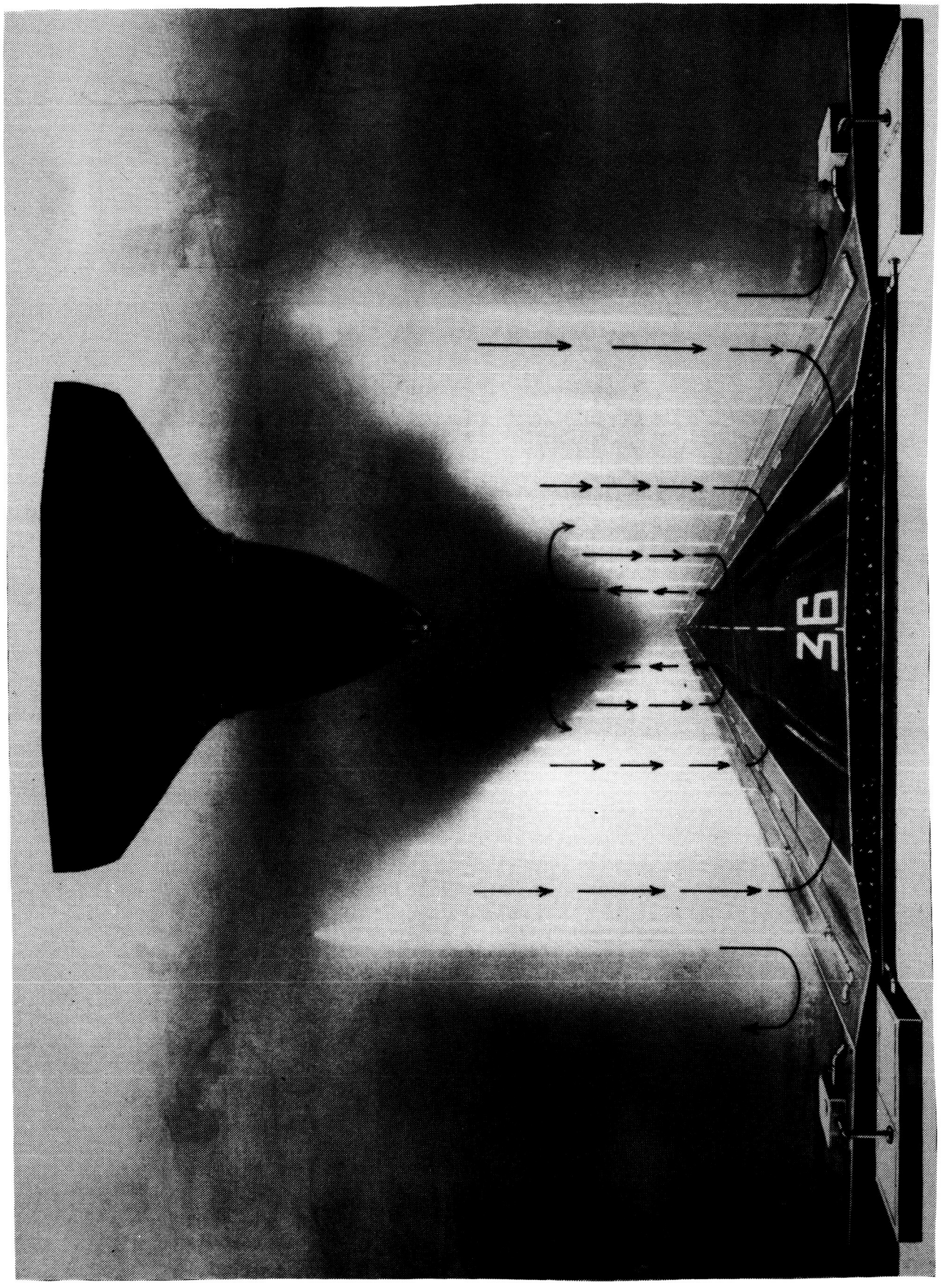

Figure 3-1. Artist's depiction of large volume recyclable water sprays used to clear fog along an Orbiter landing strip. A beneficial air flow is induced by the water spray curtains.

$$N = \frac{\Delta V}{4/3\,\pi R^3} \qquad (3.1)$$

The fraction of fog droplets removed in the curtain of spray is

$$\frac{\Delta n}{n} = \frac{N\pi R^2 E}{A} = \frac{3E\Delta V}{4RA} \quad . \qquad (3.2)$$

This fraction is independent of the concentration n. Continued spraying will result in a logarithmic decrease in concentration, i.e.,

$$n = n_o \exp(-3EV/4RA) \quad , \qquad (3.3)$$

where n_o and n are the initial and final fog droplet concentrations, respectively, and V is the total volume of water sprayed.

If a fog moves at uniform velocity, u, through a spray curtain uniformly distributed along a length, L, and having a total water flow rate, Q, per unit time, then in time, t, a volume, Qt, of water will be delivered on an area, Lut, of the fog. Thus,

$$n = n_o \exp(-3EQt/4RLut) \quad , \qquad (3.4)$$

or

$$n = n_o \exp(-3EQ/4RLu) \quad . \qquad (3.5)$$

Equation (3.5) shows that removal of fog is inversely proportional to the wind speed and directly proportional to the volume flow rate of spray per unit length of curtain (Q/L). Solving equation (3.5) for Q, the water flow rate per unit time, gives

$$Q = \left(\frac{-4RLu}{3E}\right) \ln(n/n_o) \quad . \qquad (3.6)$$

If 90 percent of the fog droplets are removed $n/n_o = 0.1$ and $\ln (n/n_o) = -2.30$. If only 70 percent of the fog droplets are removed $\ln (n/n_o) = -1.20$. Letting L = 1 m, u = 100 m min^{-1} = 1.7 m s^{-1}, and assuming 90 percent removal of fog droplets, this equation reduces to

$$Q = 0.0812\ R/E \ \ (GPM) \quad , \qquad (3.7)$$

where R is the collector drop radius in μm, E is the collection efficiency (fraction) of this collector drop for a fog droplet having radius r (μm), and Q is the water flow rate required in gallons per minute for each meter length of spray curtain. Best available values for the collection efficiency of collector drops for fog size droplets are given in Table 3-1 (see Appendix A3.0).

Using this information and equation (3.7), the volume of curtain water spray required for 90 percent removal of fog droplets per meter length of runway for a fixed cross-wind component of 1.7 m s^{-1} has been computed for various monodisperse water sprays and monodisperse fogs and is given in Table 3-2. For only 70 percent removal of fog droplets, values in Table 3-2 should be halved.

This simple analysis utilizing a monodisperse water spray serves to indicate the primary factors which determine the effectiveness of this technique and provides an estimate of the scale of the required system. The more complete analysis for a polydisperse spray presented in Appendix A2.0 yields the same physical dependencies. In fact, the same equations can be used with the drop size and size-dependent factors replaced by suitable mean values. An analysis, including the effect of the induced air flow, was not within the scope of this study but, in all cases, the effect is to increase the efficiency of the system.

Employing these results to determine the optimum spray size spectra, one wishes to minimize the amount of spray water required while maximizing the visual range. From Table 3-2 alone, it would appear that 50 or 100 μm radius collector drops are optimum for all but the very smallest fog droplets. However, other considerations must be taken into account. The water spray should not be carried by fluctuating winds into the targeted volume where it would reduce the overall effectiveness of the clearing process. For a given wind speed, the larger drops will drift only about one-tenth the distance that the smaller ones will, i.e., 300 μm radius drops fall with a terminal velocity of 2.5 m s^{-1} whereas 50 μm radius drops fall at only 0.26 m s^{-1} (Table 3-2). The drift problem is minimized by the downward air flow induced by the spray curtain. To sustain the beneficial spray induced air circulation and to minimize drift of the spray, it is preferable to work with somewhat larger drops, i.e., 0.3 to 1.0 mm diameter. Still larger drops give lower fog removal efficiencies per volume of water spray but otherwise have no adverse effect if the sprays are recycled.

Recycling of the spray water is another important aspect of the current concept design. In addition to being an important conservation measure, it also ensures that additional fog is not created due to temperature differences between the air and the water spray. Since transient supersaturations result when two volumes of air saturated at different temperatures are mixed, previously unactivated cloud condensation nuclei (CCN) within the fog volume could, under some circumstances, be activated resulting in additional fog. This effect is not likely to be significant in this application because the combined surface area of the existing drops (i.e., spray drops plus fog droplets) is large so that recondensation on them will relieve the supersaturation without formation of additional fog droplets. (As shall be seen later, this is substantiated by the test results.) However, there are valid arguments for maintaining the spray water at the same temperature as the ambient air [6]. In some fog clearing situations, the temperature of the reservoir water before activation of the pumping units may be substantially different from that of the ambient air. By recycling the runoff water, the soil temperature in the runoff area and then the reservoir water itself will approach the ambient wet bulb temperature with a time constant which is site specific. This time can be minimized by reducing the volume of reservoir water and the drainage area. Placing the pump inlet water lines in a location where they pick up the returning runoff water also reduces effects due to initial temperature differences.

TABLE 3-1. COLLECTION EFFICIENCY OF SPRAY DROPS FOR FOG DROPLETS

COLLECTOR DROP		COLLECTION EFFICIENCY (FRACTION)							
TERMINAL VELOCITY (m/sec)	RADIUS (μm)	FOG DROPLET RADIUS (μm)							
		2	2.5	4	5	8	10	15	20
.26	50	.01	.01	.03	.20	.38	.53	.61	.59
.71	100	.01	.04	.32	.48	.65	.70	.69	.65
1.2	150	.01	.14	.41	.55	.68	.70	.66	.61
1.6	200	.04	.18	.45	.57	.68	.69	.63	.57
2.0	250	.06	.21	.46	.58	.67	.67	.60	.54
2.5	300	.08	.23	.47	.58	.66	.66	.58	.51
3.3	400	.10	.24	.47	.58	.64	.63	.54	.48
4.0	500	.12	.24	.47	.58	.62	.61	.51	.48
6.5	1000	.15	.25	.47	.55	.62	.61	.51	.48
8.8	2000	.08	.17	.39	.47	.59	.58	.51	.47
9.2	3000	.03	.10	.29	.38	.53	.55	.49	.47

TABLE 3-2. SPRAY VOLUME REQUIRED FOR FOG REMOVAL BY MONODISPERSE COLLECTOR DROPS

COLLECTOR DROP		GAL OF SPRAY PER 100 m^2 (STATIONARY CLOUD) OR GAL PER MIN PER METER LENGTH OF RUNWAY PER 100m/min AIR SPEED (MOVING CLOUD)							
TERMINAL VELOCITY (m/sec)	RADIUS (μm)	FOG DROPLET RADIUS (μm)							
		2	2.5	4	5	8	10	15	20
.26	50	406	406	135	20	11	8	7	7
.71	100	812	203	25	17	12	12	12	12
1.2	150	1218	87	30	22	18	17	18	20
1.6	200	406	90	36	28	24	24	26	28
2.0	250	338	97	44	35	30	30	34	38
2.5	300	304	106	52	42	37	37	42	48
3.3	400	325	135	69	56	51	52	60	68
4.0	500	338	169	86	70	65	67	80	85
6.5	1000	541	325	173	148	131	133	159	169
8.8	2000	2030	955	416	345	275	280	318	345
9.2	3000	8119	2436	840	641	460	443	497	518

4.0 DETAILED DESCRIPTION OF TEST AND RESULTS

This field test was the initial program to begin development of the recycled water spray fog dispersal technique. It was conducted October 16-25, 1984, at NASA's Marshall Space Flight Center (MSFC), Huntsville, Alabama. Although primary emphasis was placed on determining drop size spectra of water sprays produced by individual commercially available firefighting nozzles, a linear nozzle array was also set up to investigate air flow patterns, to measure the temperature response of the runoff, and to test the fog dispersal concept should a natural fog occur during the two week test period.

4.1 General Set-Up

Fresh water was pumped from a 2 x 10^6 l (500,000 gal) pond near a 37 m high test stand using three mobile firefighting pumping modules developed jointly by NASA/MSFC and the U.S. Navy under an unrelated program [7]. Each module is capable of supporting several high volume flow nozzles. Figure 4-1 illustrates, in simplified form, the fire hose layout and nozzle configuration. Together the three modules supplied 390 l s^{-1} (6200 gpm) of water at 830 kPa (120 psi) to an array of 10 vertically directed 3.5 cm (1 3/8 in.) ID nozzles to form a spray curtain 72-m long, 5-m wide, and 40-m high. Alternately, a single module was used to supply water at pressures up to 1380 kPa (200 psi) to a variety of single nozzles.

Particle Measuring Systems, Inc. (PMS) optical array probes OAP-230X, GBPP-100, and other instrumentation provided and operated under contract by the State University of New York at Albany were used to measure the drop size spectra. More information on these instruments is presented in Appendix A4.0. A smoke generator, furnished by the U.S. Army, and an extensive set of temperature, pressure, and wind measuring instruments were used with the spray curtain to determine both the air flow patterns induced by the water spray and the thermodynamics of the system. Tests were documented with color video, 16 mm cinema, and still photographs. Figures 4-2 and 4-3, photographs of the water spray test area looking toward the north, were taken from atop the 123-m tall Dynamic Test Stand adjacent to this test area. They show the overall features of both the area and the test setup.

To obtain drop spectra measurements, the water jet from a single nozzle was directed vertically and propelled to a height sometimes in excess of 75 m before falling back to the ground as drops. The larger drops (200 μm to 12 mm) were sized along their horizontal dimension as they fell at terminal velocity through the sampling volume of the PMS Ground Based Precipitation Probe (GBPP-100). The other particle probes were equipped with aspirators. The probes and a tipping bucket rain gauge were mounted on an I-beam platform that extended 7.5 m from the test stand (Fig. 4-3). The platform was hinged to the test stand so it could be swung in for easy instrument access. It could also be moved to different heights. The use of the platform prevented undue interference from drop splashing at the ground or on nearby supporting structures. It also prevented ground effects on the air flow from affecting the drop spectra measurements. Care was also taken to insure non-interference between instruments. In general, only two probes and the rain gauge were mounted on the platform at any one time. Spectra measurements were made throughout the main shaft of falling drops when the water jet was directed vertically. They were also made in the curtain of spray which forms when the water jet is arched over the instrument platform from a point as far away as 30 m to one side.

Figure 4-4 is a photograph of a typical single nozzle test as seen looking from east to west. It shows the water jet emanating from a 3.175 cm (1 1/4 in.) ID straight bore Style 489 nozzle operated at 1345 kPa (195 psi) extending to a height of about 60 m before falling to produce a curtain of spray. In this photograph the particle sizing probes are installed 11.5 m above the ground and are located in the

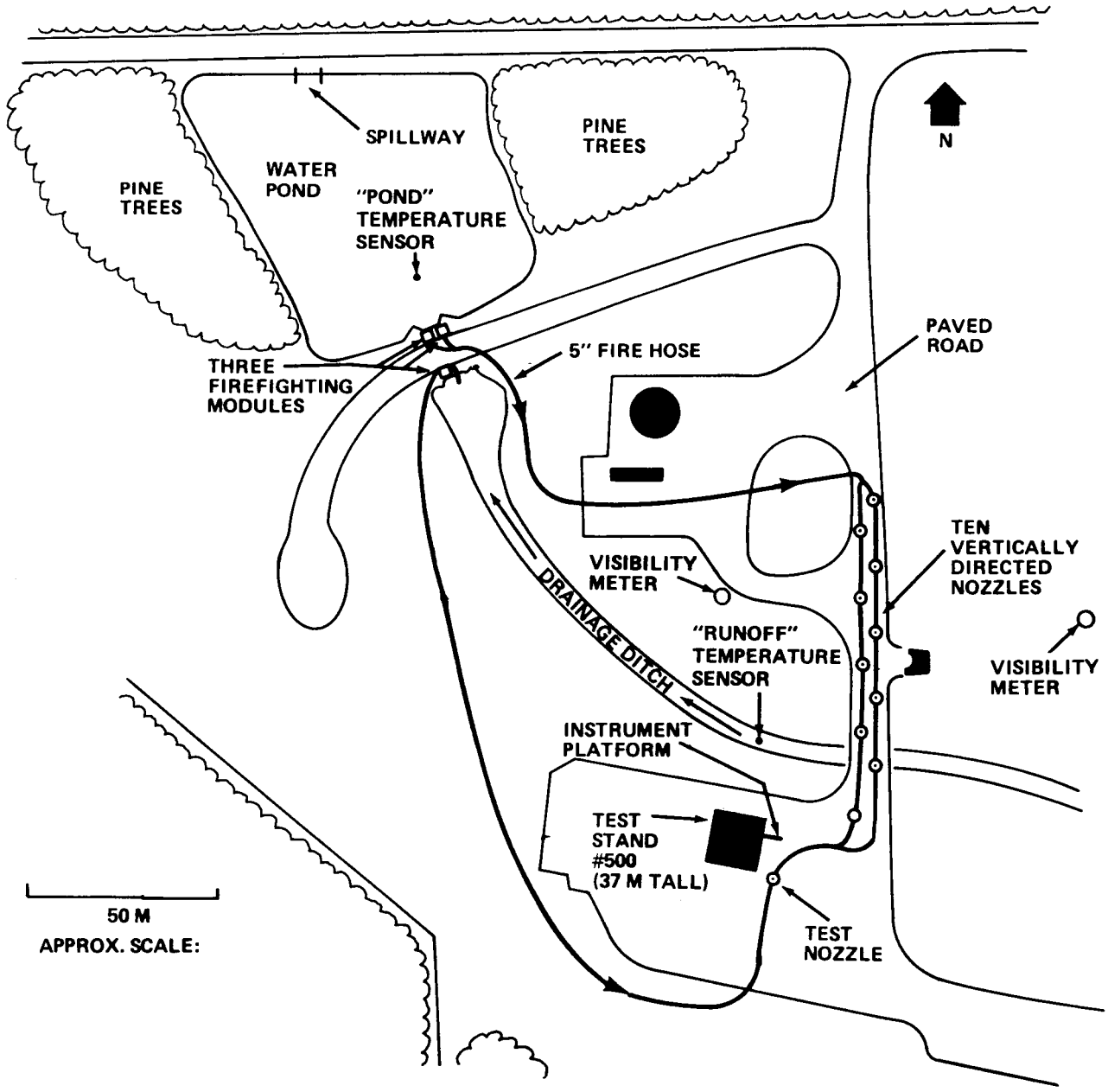

Figure 4-1. Plan view of area used for October 1984 water spray tests including simplified water flow schematic.

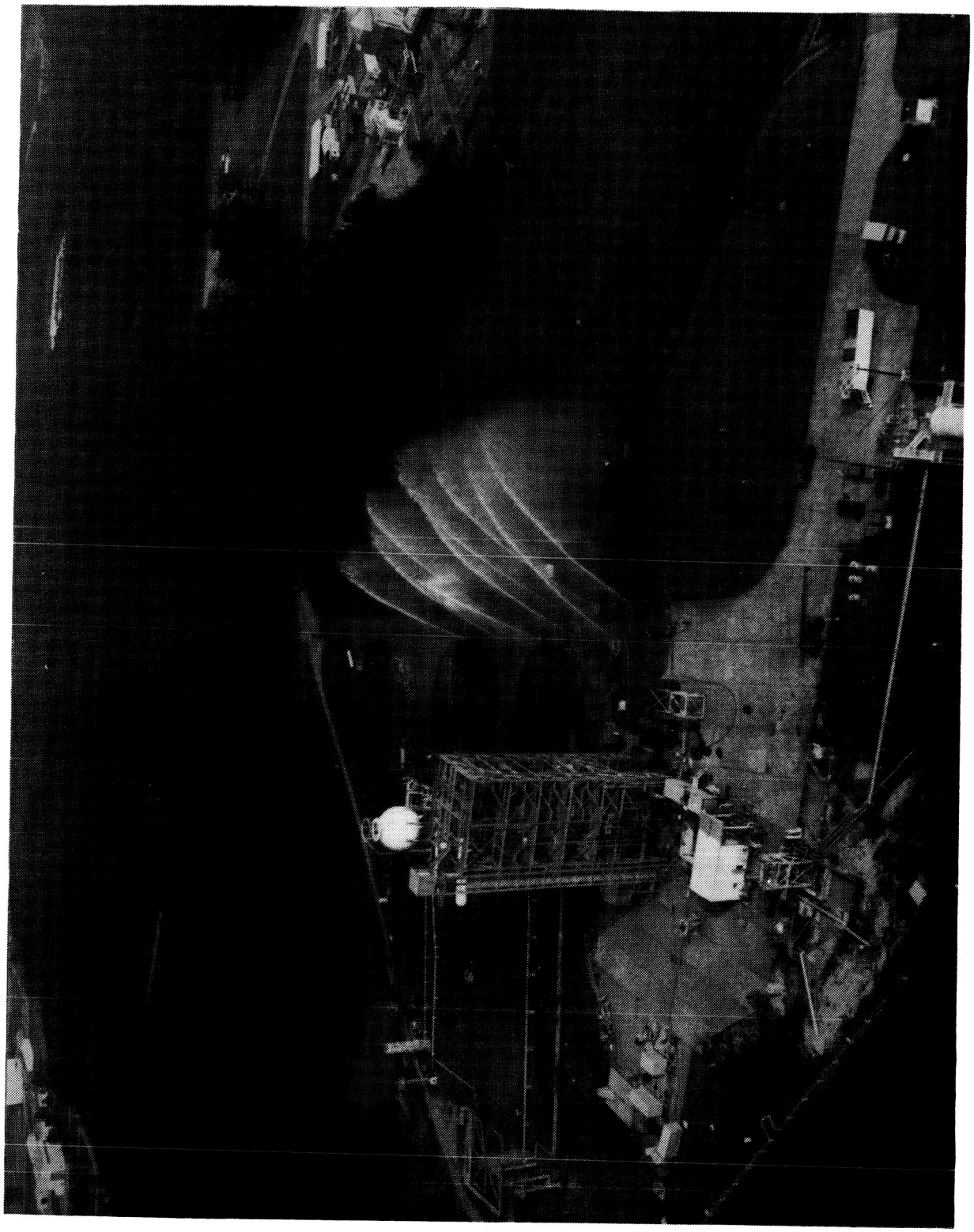

Figure 4-2. Photograph of overall water spray test area taken from atop the 123-m tall Dynamic Test Stand adjacent to this test area.

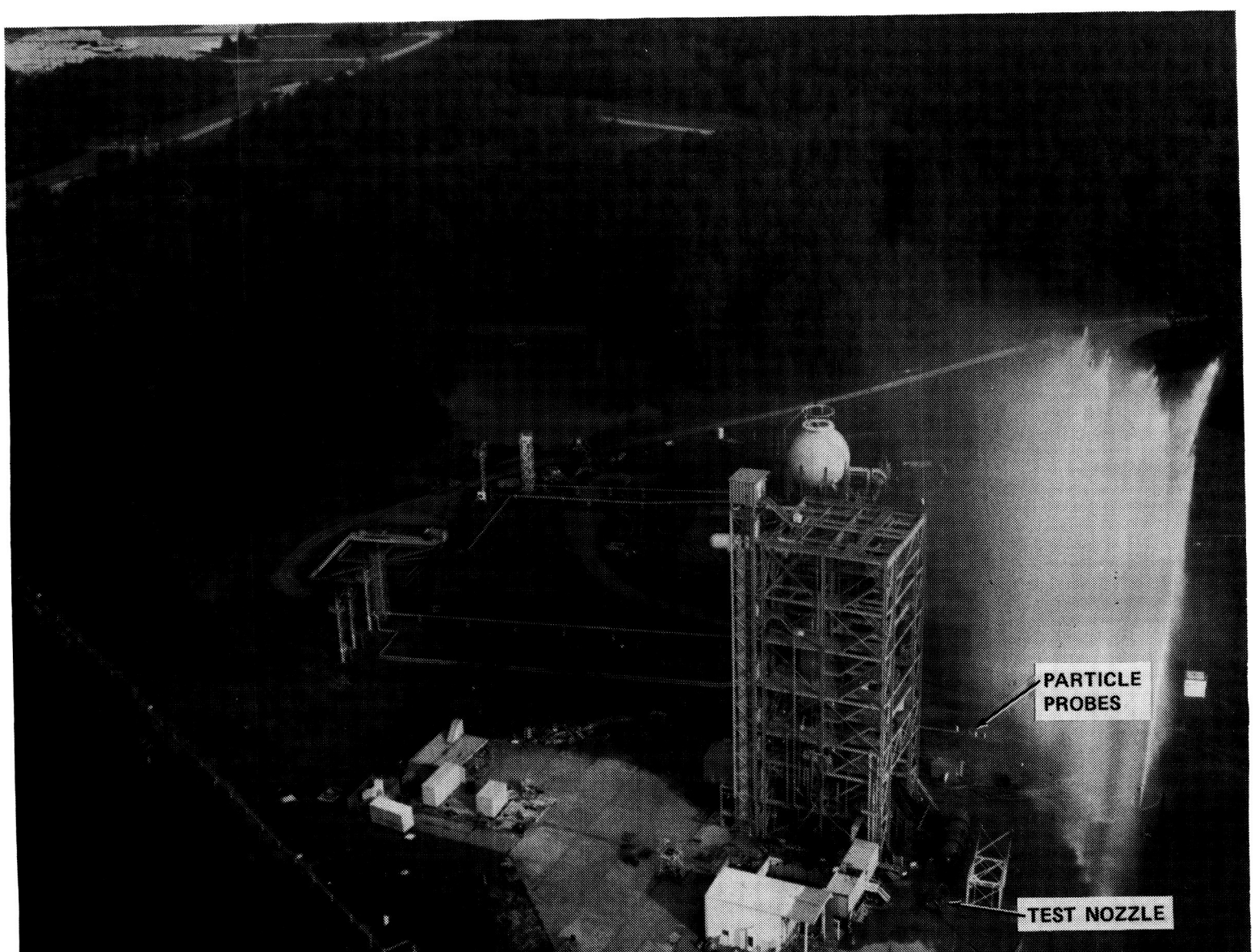

Figure 4-3. Photograph of test area (looking toward the north) gives view of spray curtain from above. Note particle probe platform and test nozzle fixture used in single nozzle tests.

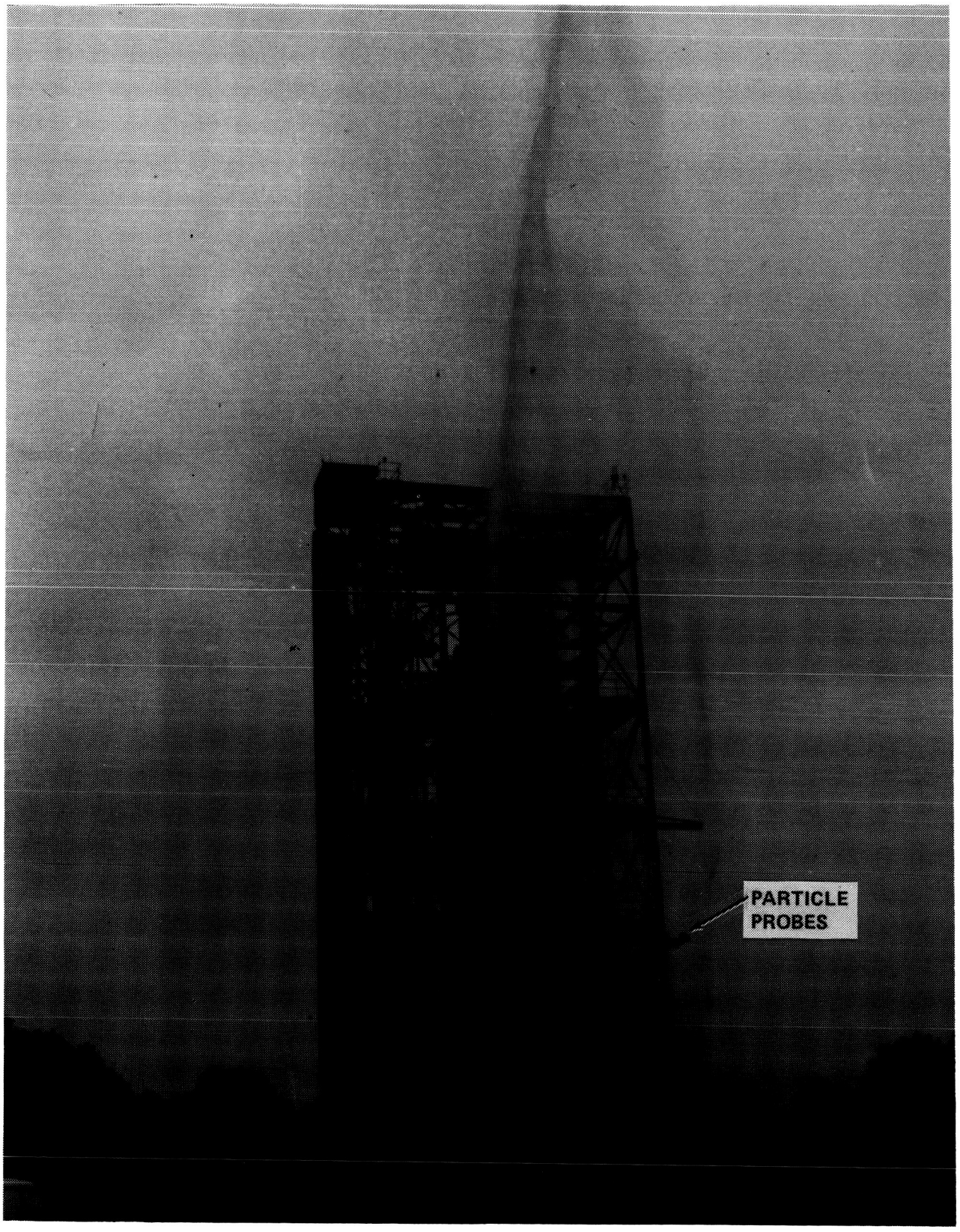

Figure 4-4. Photograph of typical single nozzle test shows water being projected to a height in excess of 60 m.

curtain spray slightly to the left of the main water shaft. Signs on the left-hand foreground corner of the test stand indicate the height above ground of the 7-, 11-, 14-, 17-, 20-, 23-, 26-, 29-, and 34-m levels (to the bottom of each sign). The small building located on the 17-m level of the test stand housed the State University of New York (SUNY) data acquisition hardware. This allowed a standard length data cable to be used from the particle probes to the microprocessor. The trailer to the left of the test stand housed the NASA/MSFC temperature, pressure, and wind recording data acquisition equipment.

4.2 Spray Nozzles Tested

Table 4-1 lists the single nozzles tested, the manufacturer's style number, and the nominal discharge volume at 690 kPa (100 psi). Their physical characteristics are described below and in Figures 4-5 through 4-13. All nozzles tested were manufactured by the Akron Brass Company. Figure 4-5 is a photograph of the Style 417 nozzles. The three sizes shown from right to left are 1 in., 1 1/8 in., and 1 1/4 in. ID. The purpose of the black rubber bumper is to protect the nozzle tip from damage. Figure 4-6 shows a Style 417 nozzle attached to a chrome playpipe. The playpipe is shaped internally to give a gradual transition from a large bore to a small bore. Its use was only required for the smaller nozzles. In operation the nozzle or the playpipe is attached to a discharge pipe, Style 3488, which has full-length stream shaping fins. Figures 4-7 and 4-8 show, respectively, an oblique and end-on view of the discharge pipe with its stream straighteners.

The discharge pipe attaches to either a portable or a fixed monitor which permits the water stream to be pointed in the desired direction by a single operator. The monitor usually has an attached gauge which permits real-time observation of the water pressure. Figure 4-9 shows a portable "Apollo" monitor, Style 3420, with an attached discharge pipe and "Quad Stacked" deluge tip, Style 2499. This is the configuration used for each of the nozzles in the vertically directed array. This monitor which has a single 3 in. waterway with a 2 1/2 in. discharge and two 2 1/2 in. clapper inlets, is designed for pressures up to 1380 kPa (200 psi) and flows up to 75 l s^{-1} (1200 gpm) when truck mounted. The quad stacked deluge tip provides orifice options of 1 3/8 in., 1 1/2 in., 1 3/4 in., and 2 in. ID in one nozzle. The 1 3/8 in. orifice was used exclusively.

A heavier duty 4 in. monitor bolted on a portable trailer was utilized for the single nozzle tests (Fig. 4-3). This permitted large volume flows to be used safely while still allowing considerable freedom in the positioning of the nozzle. For all the tests described in this report, five of the ten pressure gauges in the nozzle array were replaced with pressure transducers. These were Standard Controls Inc. Model 800-30, Type B sealed transducers with an operating range from 0 to 300 psi. The absolute accuracy was better than ±1.5 psi. The output with a resolution of 1 psi was read every 10 sec and recorded digitally on magnetic tape. In addition, both a pressure transducer and a pressure gauge were utilized on the test nozzle monitor.

Figure 4-10 shows three Style 489 plain deluge tip nozzles. From right to left the nozzle orifice is 1 1/4 in., 1 3/4 in., and 2 in. ID. Since these nozzles attach directly to a discharge pipe, no playpipe was required. Figure 4-11 shows one of three combination "fog" and straight stream nozzles which we tested. This particular one, called a "Black Widow," Style 2145, has fixed teeth and is designed for a single fixed flow. It was factory set for 31.5 l s^{-1} (500 gpm) at 690 kPa (100 psi). Figure 4-12 shows a similar nozzle, Style 1750, called a "Turbojet." This nozzle can be manually adjusted to one of four constant flows; 350, 500, 750, or 1000 gpm at 690 kPa. When set in the full "fog" position, a fine spray is produced by spinning turbine teeth. Figure 4-13 shows a third combination "fog" and straight stream nozzle which was tested. This nozzle, Style 5050, called an "Akromatic 1000' also has spinning teeth but is configured a little differently than the Style 1750. It was operated at a setting of 1000 gpm.

TABLE 4-1. LIST OF FIREFIGHTING NOZZLES TESTED AND THEIR NOMINAL VOLUME DISCHARGE

NOZZLES TESTED

TYPE	STYLE NO.	DISCHARGE DIAMETER	DISCHARGE VOLUME AT 100 PSI
PLAIN DELUGE TIP	417	1"	300 gpm
PLAIN DELUGE TIP	489	1 – 1/4"	470 gpm
PLAIN DELUGE TIP	2499	1 – 3/8"	565 gpm
PLAIN DELUGE TIP	489	1 – 3/4"	915 gpm
FIXED TEETH (BLACK WIDOW)	2145	FOG/STRAIGHT STREAM	500 gpm
SPIN TEETH (TURBO JET)	1750	FOG/STRAIGHT STREAM	350 gpm
SPIN TEETH (TURBO JET)	1750	FOG/STRAIGHT STREAM	500 gpm
SPIN TEETH (TURBO JET)	1750	FOG/STRAIGHT STREAM	750 gpm
SPIN TEETH (AKROMATIC 1000)	5050	FOG/STRAIGHT STREAM	1000 gpm

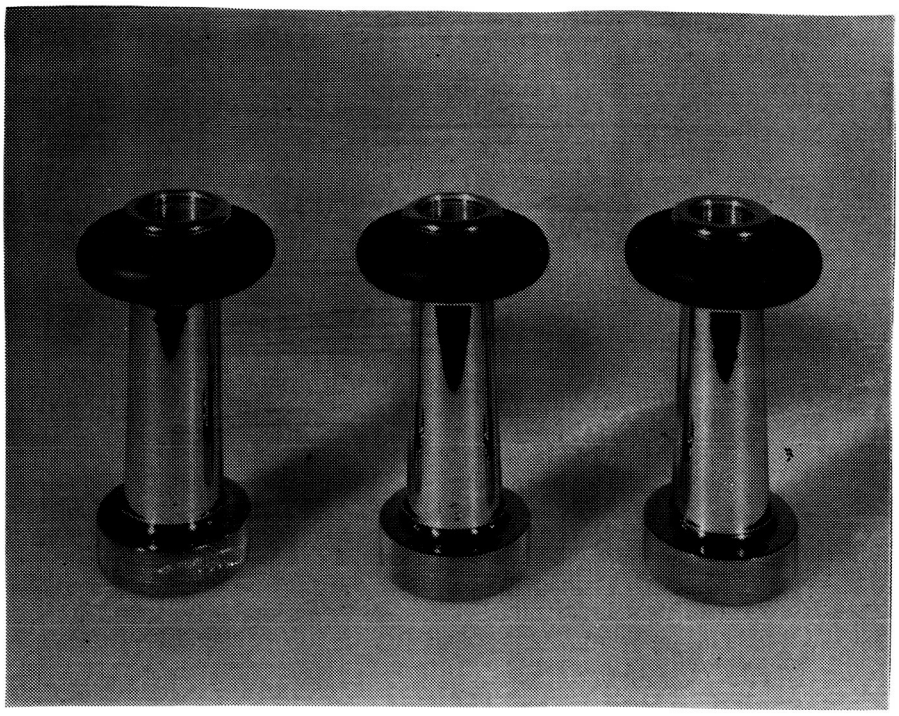

Figure 4-5. Photograph of small bore plain deluge tips (nozzles).

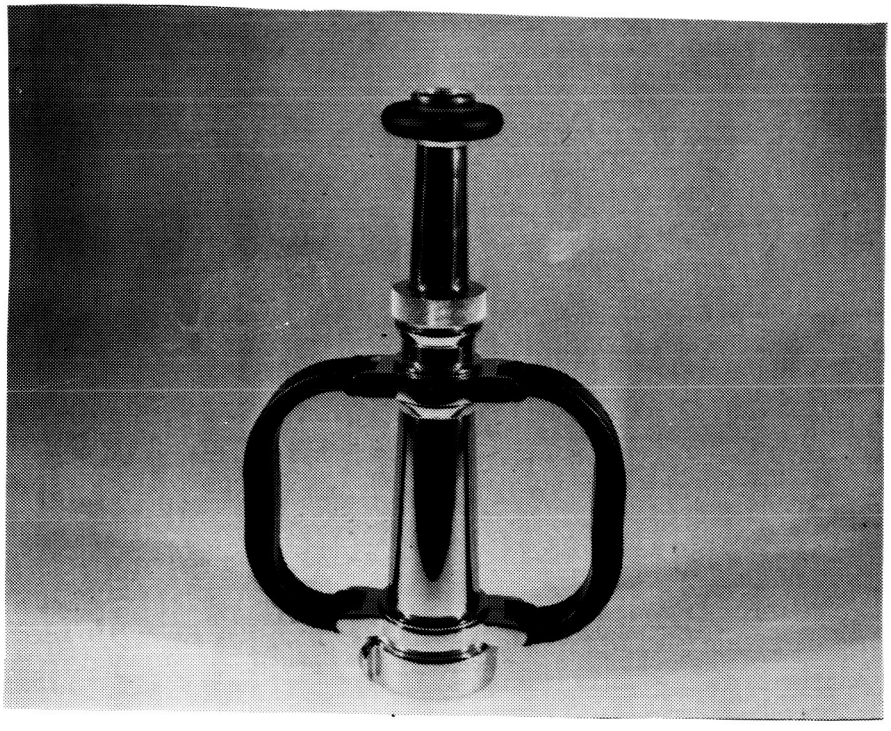

Figure 4-6. Photograph of small bore tip attached to playpipe.

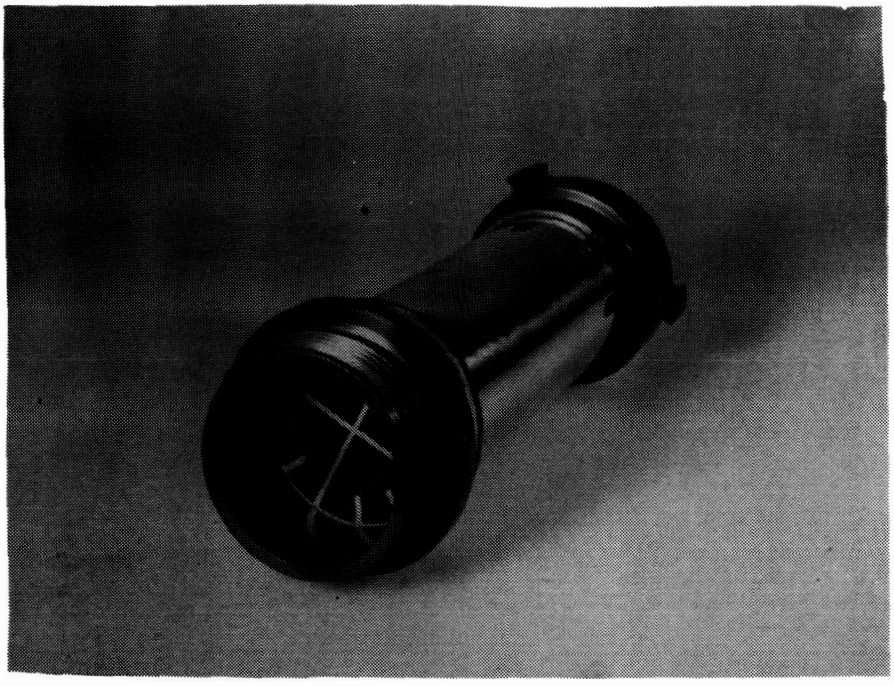

Figure 4-7. Photograph of the discharge pipe which shapes the water stream before entrance to the nozzle.

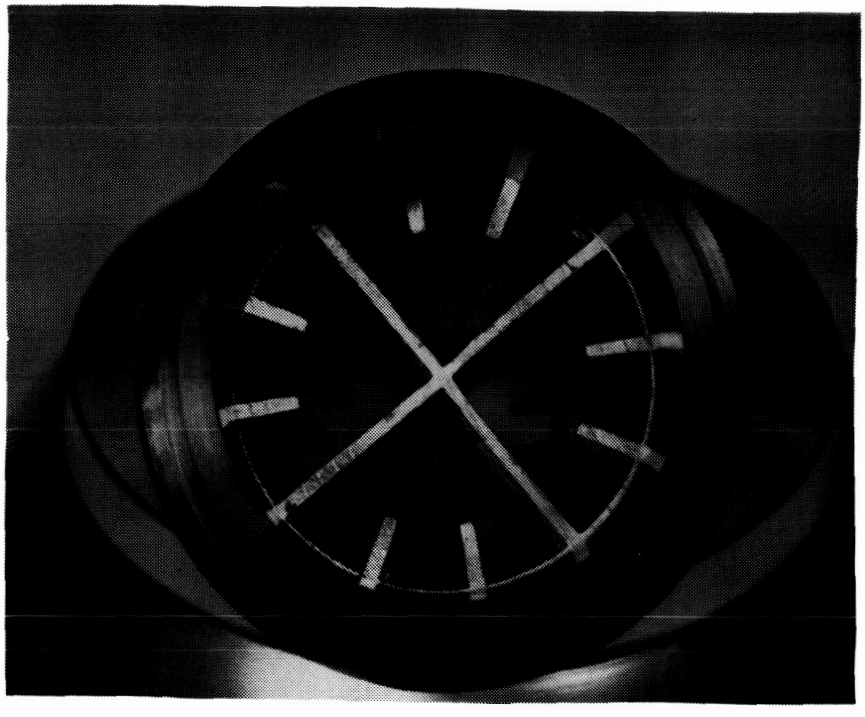

Figure 4-8. End-on photograph of discharge pipe shows stream straightening fins which extend the full length of the pipe.

Figure 4-9. Photograph of "Apollo" monitor with discharge pipe and a Style 2499 "Quad Stacked" nozzle. This is the configuration used for each of the nozzles in the vertically directed array.

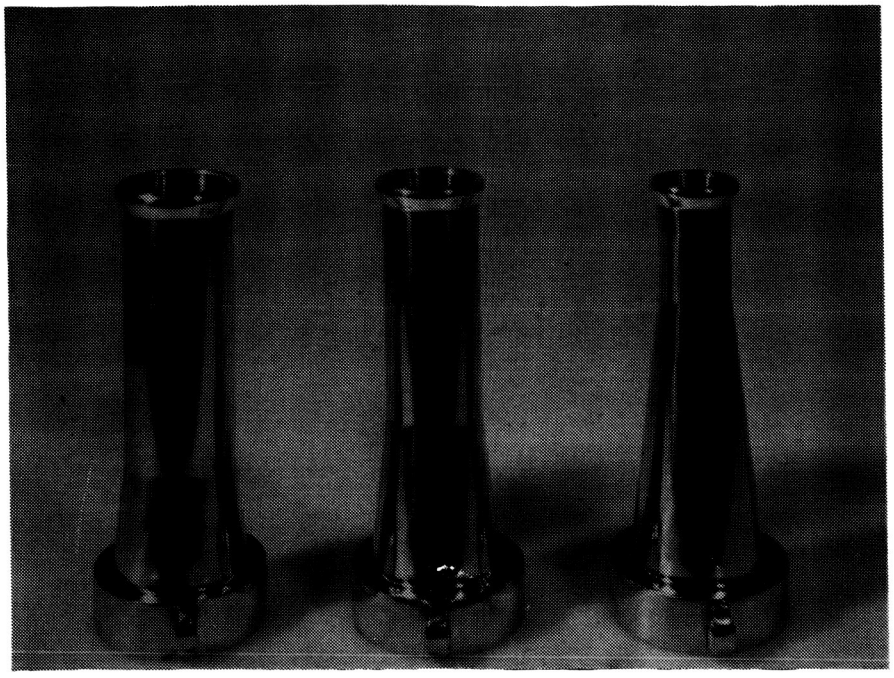

Figure 4-10. Photograph of three different sized Style 489 plain deluge tip nozzles.

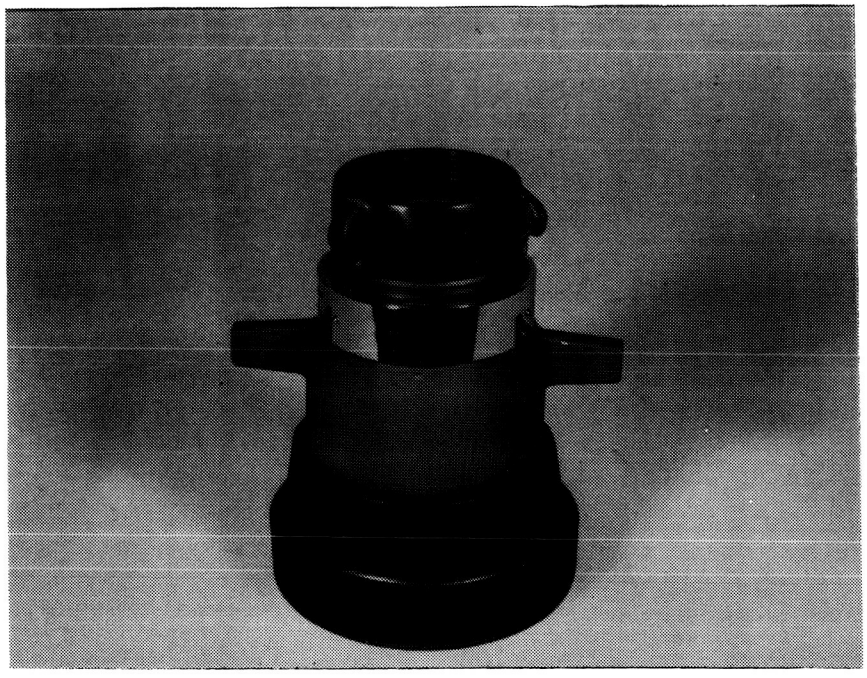

Figure 4-11. Photograph of Style 2145 "Black Widow" fixed teeth nozzle.

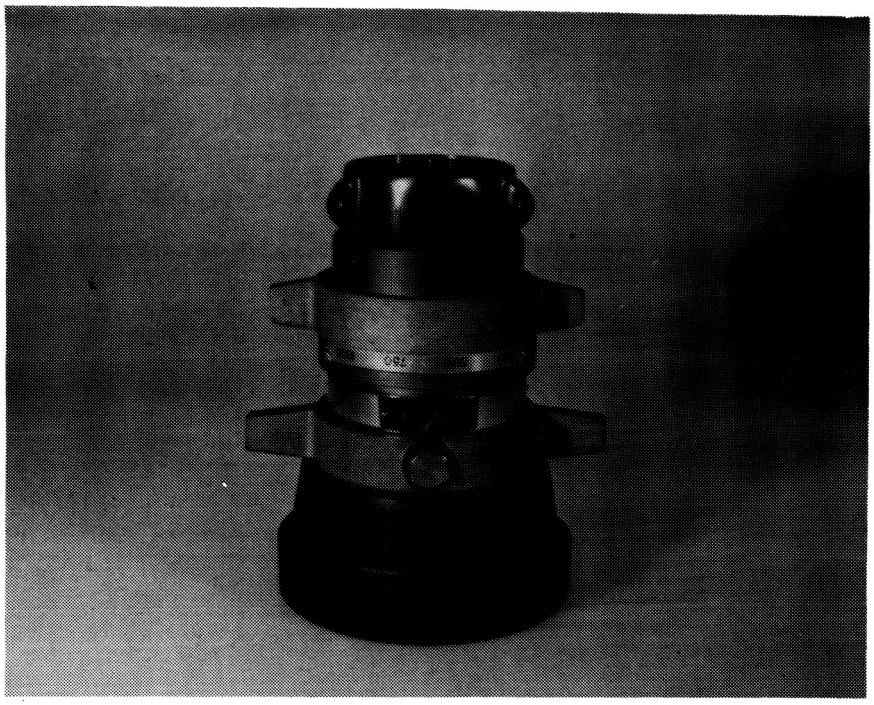

Figure 4-12. Photograph of Style 1750 "Turbojet" spinning teeth nozzle.

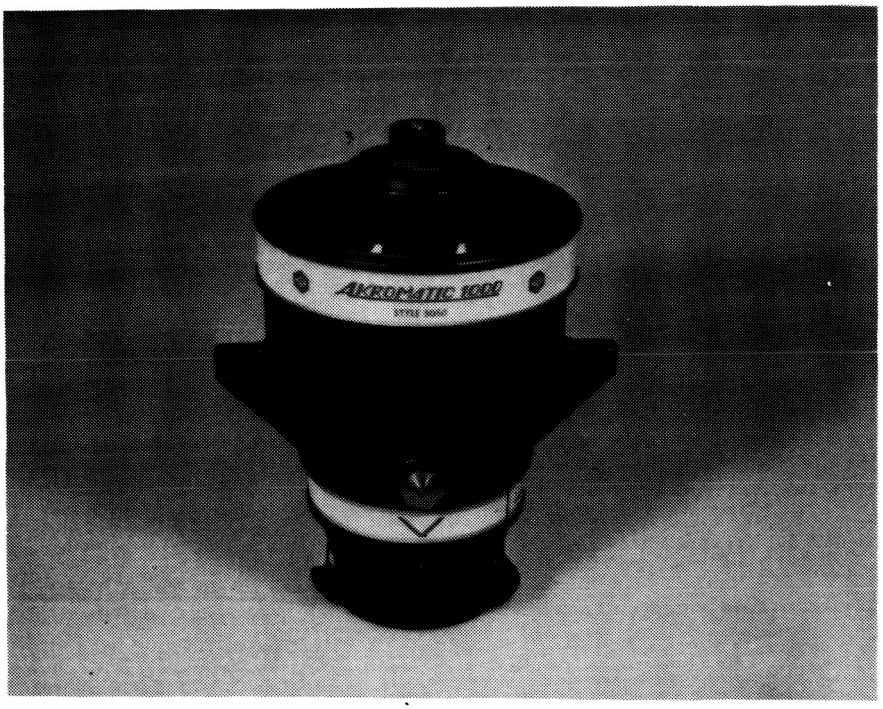

Figure 4-13. Photograph of Style 5050 "Akromatic 1000" spinning teeth nozzle.

4.3 Single Nozzle Test Results

Table 4-2 lists the nozzles, operation parameters, test setup and ambient conditions for the drop spectra measurement data which are presented in this report. Discussion will first be given to the type nozzle used in all the nozzle array tests. Figure 4-14 shows a histogram of the drop spectra obtained from the GBPP particle probe for this Style 2499 "Quad Stacked" (1 3/8 in. ID) nozzle. The same data shown as a cumulative volume plot is presented in Figure 4-15. These and all other plots presented in this report have been corrected for sampling volume edge effects, for the modified sampling volume due to the addition of protective hoods on the GBPP, for the size varying sample volume due to the different terminal fall speeds of the drops, and finally for drop flattening.

An example of the correction calculations required for the GBPP data is given in Appendix A4.0. From Figure 4-14 it can be seen that a substantial number of drops were present at sizes as large as 8.5 mm. In fact, Figure 4-15 clearly shows that the volume median diameter was 4.5 mm, i.e., 50 percent of the total volume was in larger drops. Although drop spectra presented in the format of these two plots is easily interpreted and very useful for specific purposes, this format does not lend itself to presentation of data from both drop probes on the same plot without substantial loss of information. Decade and/or logarithmic plots are more useful for this purpose. Figure 4-16 shows data from both the OAP and GBPP instruments for this nozzle plotted on decade scales. The first y versus x plot shows $dN/dlogD$ (m^{-3}) versus D (mm). This gives information on the drop number concentration as a function of the drop diameter. It is equivalent to plotting Log $dN/dlogD$ (m^{-3}) versus Log D (mm) on Log/Log paper. It should be noted that these are all base ten logarithms. Utilizing the following expression, equation (4.1), this data can readily be transformed to a plot of dN/dD (m^{-3} mm^{-1}) versus D (mm).

$$dN/dD = (1/D)\ (dN/d\mathrm{Log}_{10}D)\ (1/2.302585) \qquad (4.1)$$

The second plot in Figure 4-16 gives information on the surface area of the drops while the third shows how the mass of the total spray is distributed. Using this format, drop spectra from the various nozzles operated at different pressures can all be compared using identically scaled plots. Figures 4-17 to 4-30 present data in this same format for several other nozzles. The nozzle type and operating pressure are specified on each figure.

Drop spectra in these figures as well as in Figure 4-16 were taken in the main shaft of falling drops. The spectral shape of these plots, especially from the plain deluge type nozzles, i.e., Styles 417, 489, and 2499, resembles that for natural rain. This is not surprising since the size distribution, in this case, is primarily determined by aerodynamic breakup as the drops fall through the air toward the ground and not by nozzle peculiar processes. Therefore, it is entirely understandable that the shape of the spectra varies little with nozzle orifice size. Since the magnitude of the ordinate on these plots, number concentration for example, is directly proportional to the volume flow rate of the nozzle and to the extent to which the main shaft of falling drops is centered upon the sampling probes, it varies somewhat from one nozzle to the next. A comparison of drop spectra from the Style 489 (1 1/4 in.ID) nozzle operated over the pressure range 690 kPa (100 psi) to 1380 kPa (200 psi), i.e., Figures 4-18 to 4-22, shows little systematic change with pressure. The spectra at the highest pressure does, however, suggest that increased pressure in this range may slightly decrease the mean drop size. For a given nozzle orifice greater pressures also result in increased projection height up to pressures of about 1380 kPa (200 psi) [8]. Figure 4-31 shows spectra taken in the curtain spray of a Style 489 nozzle (1 3/4 in. ID) outside the main shaft of falling drops. In this case the test nozzle was located approximately 25 m to the south of the I-beam platform and the water jet was arched over the instrument platform at a height of about 35 m. Even in this case there is not a marked change in the drop spectra from that observed in the main shaft of falling drops, i.e., Figure 4-23.

TABLE 4-2. TABULATION OF THE NOZZLES, OPERATION PARAMETERS, TEST SETUP AND AMBIENT CONDITIONS FOR THE DROP SPECTRA MEASUREMENT DATA WHICH ARE PRESENTED IN THIS REPORT

NOZZLE	PRESSURE (psi)	FLOW (gpm)	DATE	TIME (cst)	AMBIENT COMDITIONS				COMMENTS
					WIND (38 m)		TEMP (Celsius)	RELATIVE HUMIDITY (%)	
					SPEED (m/s)	DIRECT (degs)			
1 3/8" PLAIN DELUGE.....(STYLE 2499)	125	630	84/10/25	12:10:53	1.5	170	26	75	USED IN ALL ARRAY TESTS
1" PLAIN DELUGE.....(STYLE 417)	145	360	84/10/23	13:29:25	2.5	320	20	100	RAIN/DRIZZLE
1 1/4" PLAIN DELUGE.....(STYLE 489)	100	465	84/10/23	17:32:27	1.5	40	18	100	
	120	510	84/10/23	17:22:55	2.5	60	18	100	
	145	560	84/10/23	17:39:47	1.5	30	18	100	
	175	620	84/10/23	17:48:09	1.0	20	18	100	
	200	660	84/10/23	17:08:13	2.0	90	18	100	
1 3/4" PLAIN DELUGE.....(STYLE 489)	165	1150	84/10/24	12:32:33	1.0	330	18.5	100	
FIXED TEETH "BLACK WIDOW".....(STYLE 2145)	195	<(500)>	84/10/19	13:14:15	3.0	240	26	75	PROBE PLATFORM AT 19 METERS
SPIN TEETH "TURBOJET".....(STYLE 1750) (SET 25 DEG OFF FULL FOG)	115	<(350)>	84/10/22	18:10:43	1.0	100	20.5	100	OVERCAST SKIES ALL DAY
	145	<(350)>	84/10/22	17:25:57	0.5	130	21	100	
	165	<(350)>	84/10/22	18:15:23	0.5	110	20.5	100	
	195	<(350)>	84/10/22	17:44:03	0.5	90	20.5	100	
SPIN TEETH "TURBOJET".....(STYLE 1750) (SET 25 DEG OFF FULL FOG)	175	<(500)>	84/10/23	09:50:34	1.5	90	18	100	
SPIN TEETH "TURBOJET".....(STYLE 1750) (SET 25 DEG OFF FULL FOG)	185	<(750)>	84/10/23	12:02:41	2.0	170	20	100	RAIN/DRIZZLE
1 3/4" PLAIN DELUGE.....(STYLE 489)	150	1120	84/10/24	14:47:21	2.0	320	20	100	CURTAIN SPRAY
(TWO) 1 1/4" PLAIN DELUGE.....(STYLE 489)	190	635/ea	84/10/24	16:06:28	1.0	0	22	95	INTERACTION OF WATER JETS
SPIN TEETH "AKROMATIC 1000".....(STYLE 5050) (SET 25 DEG OFF FULL FOG)	145	<(1000)>	84/10/23	13:12:00	3.5	320	20	100	SPRAY NOT HIGH ENOUGH

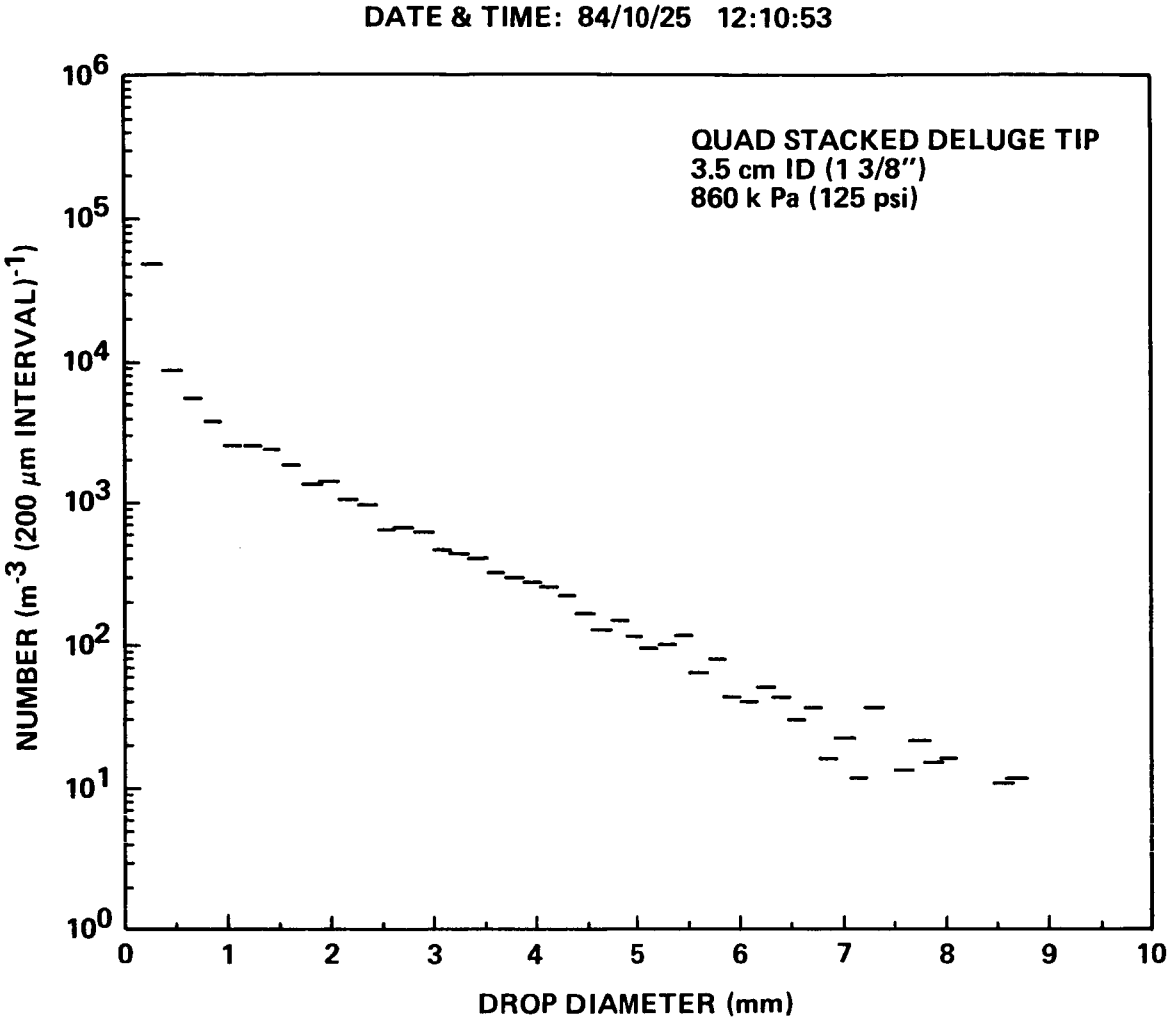

Figure 4-14. Histogram of the drop spectra from the Style 2499 "Quad Stacked" nozzle used to form the spray curtain.

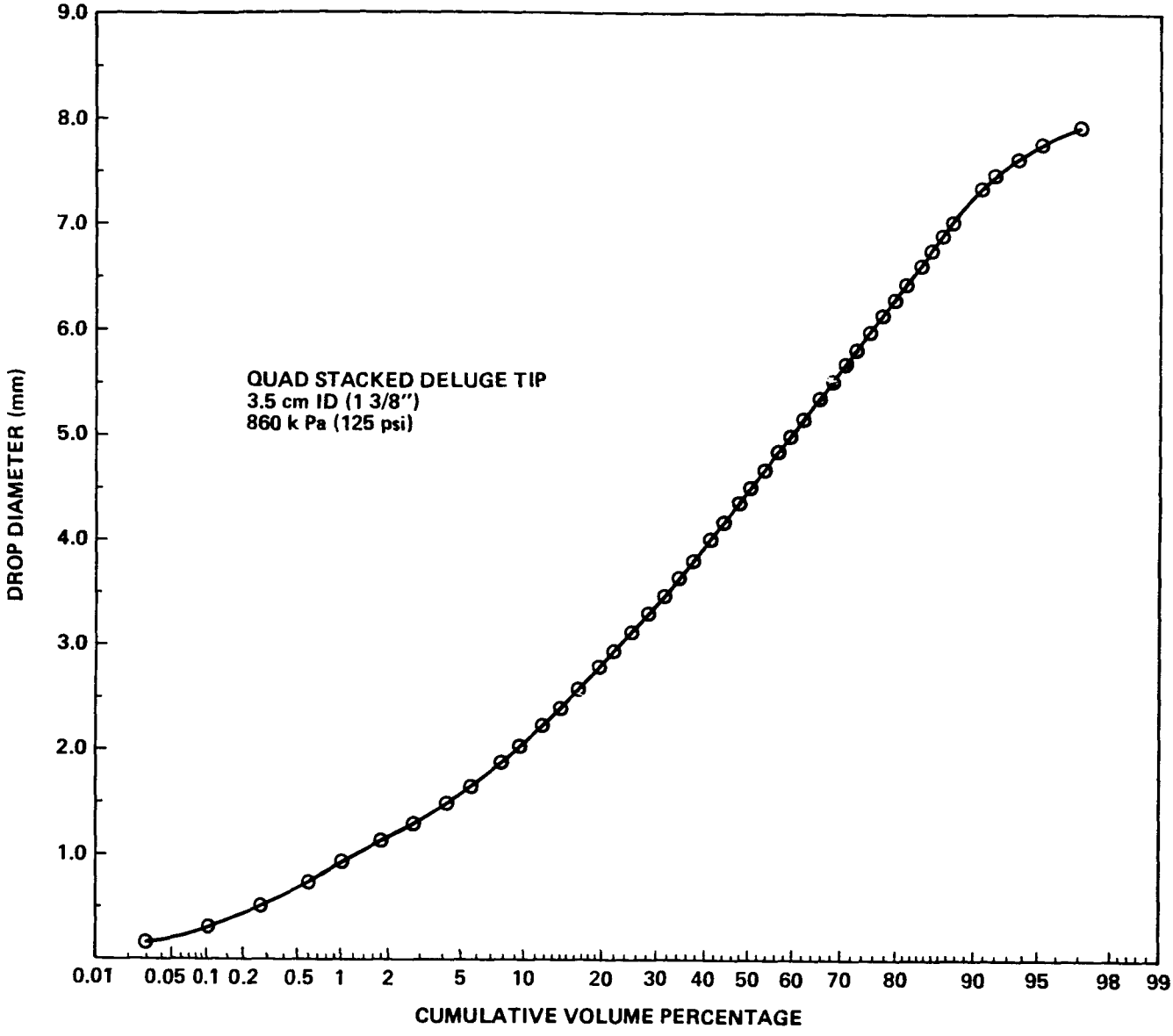

Figure 4-15. Cumulative volume plot of drop spectra from the Style 2499 "Quad Stacked" nozzle used to form the spray curtain (same data as shown in Figure 4-14).

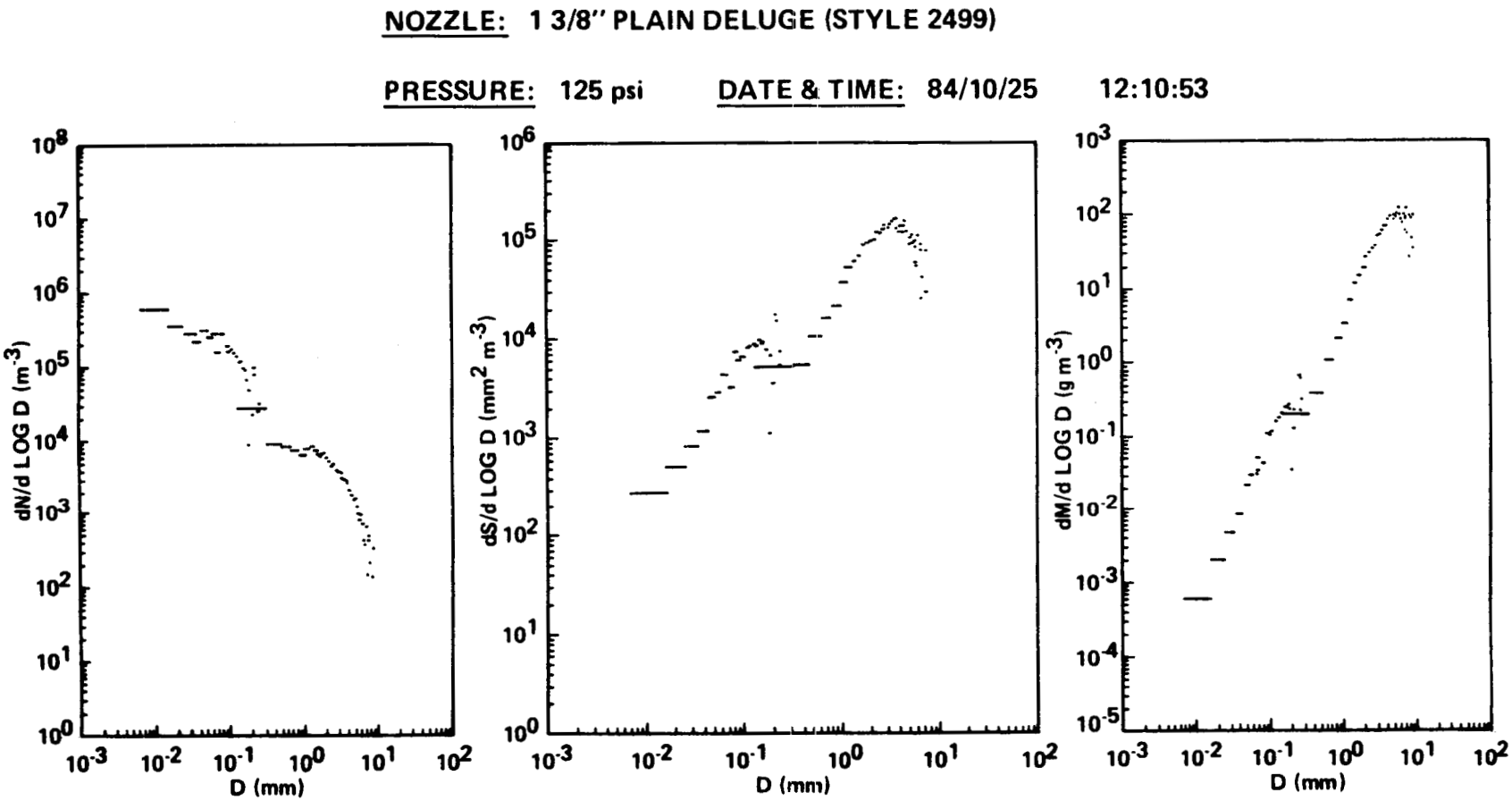

Figure 4-16. Representative distributions of spray from the Style 2499 "Quad Stacked" plain deluge 1 3/8 in. ID nozzle operated at 125 psi. Each nozzle in the vertically directed array was of this type.

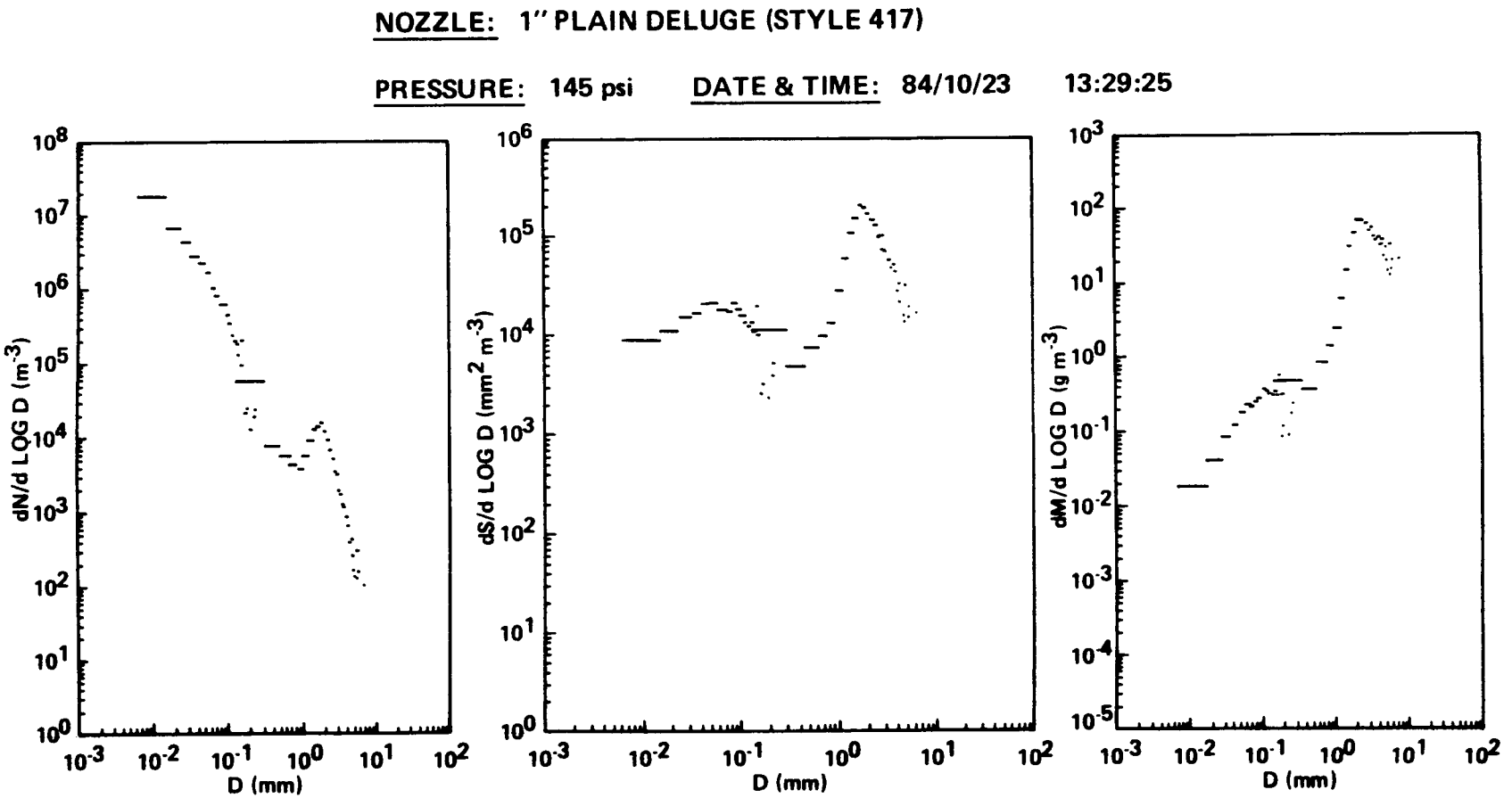

Figure 4-17. Representative distributions of spray from a Style 417 plain deluge 1 in. ID nozzle operated at 145 psi.

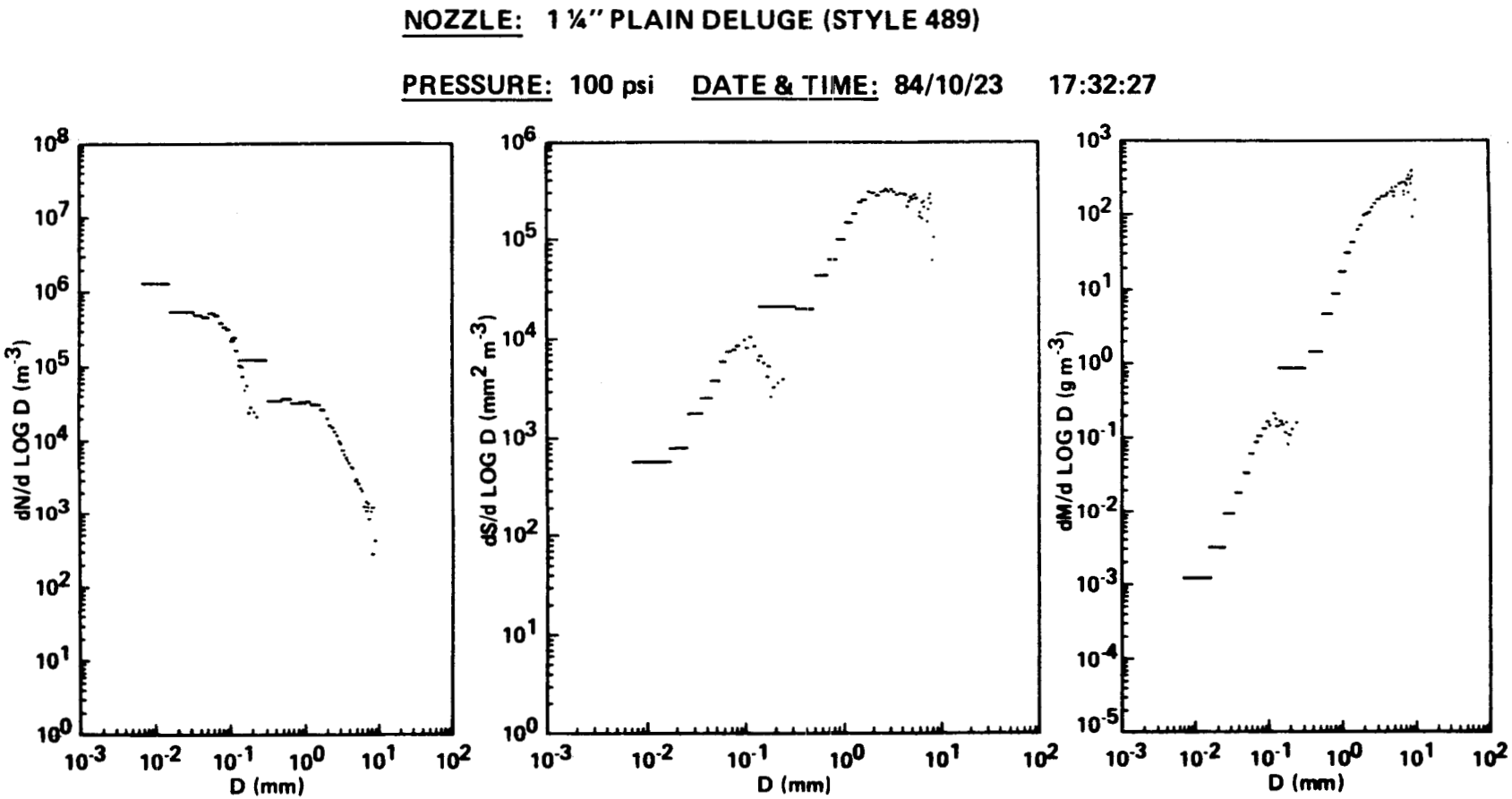

Figure 4-18. Representative distributions of spray from a Style 489 plain deluge 1 1/4 in. ID nozzle operated at 100 psi.

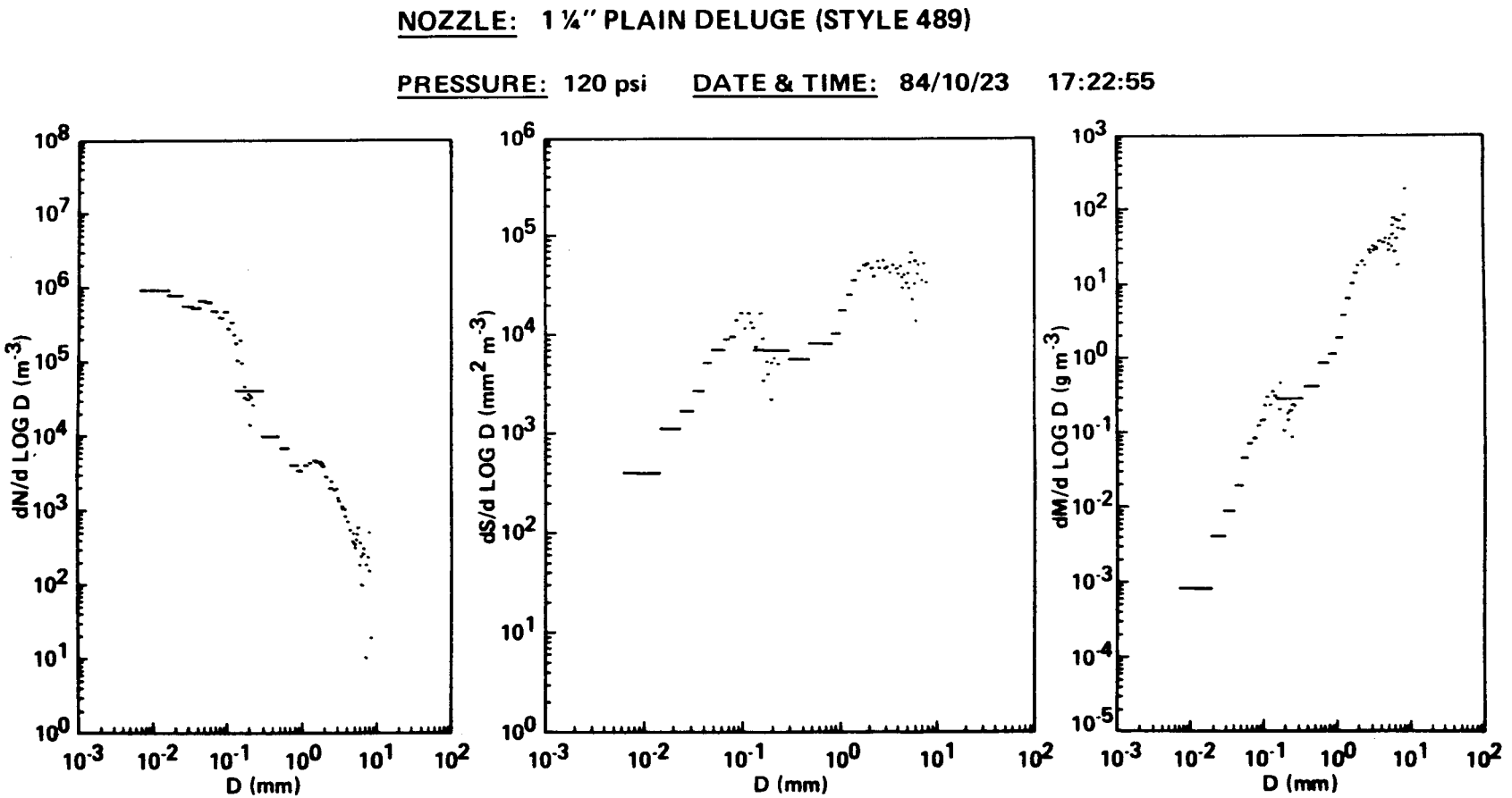

Figure 4-19. Representative distributions of spray from a Style 489 plain deluge 1 1/4 in. ID nozzle operated at 120 psi.

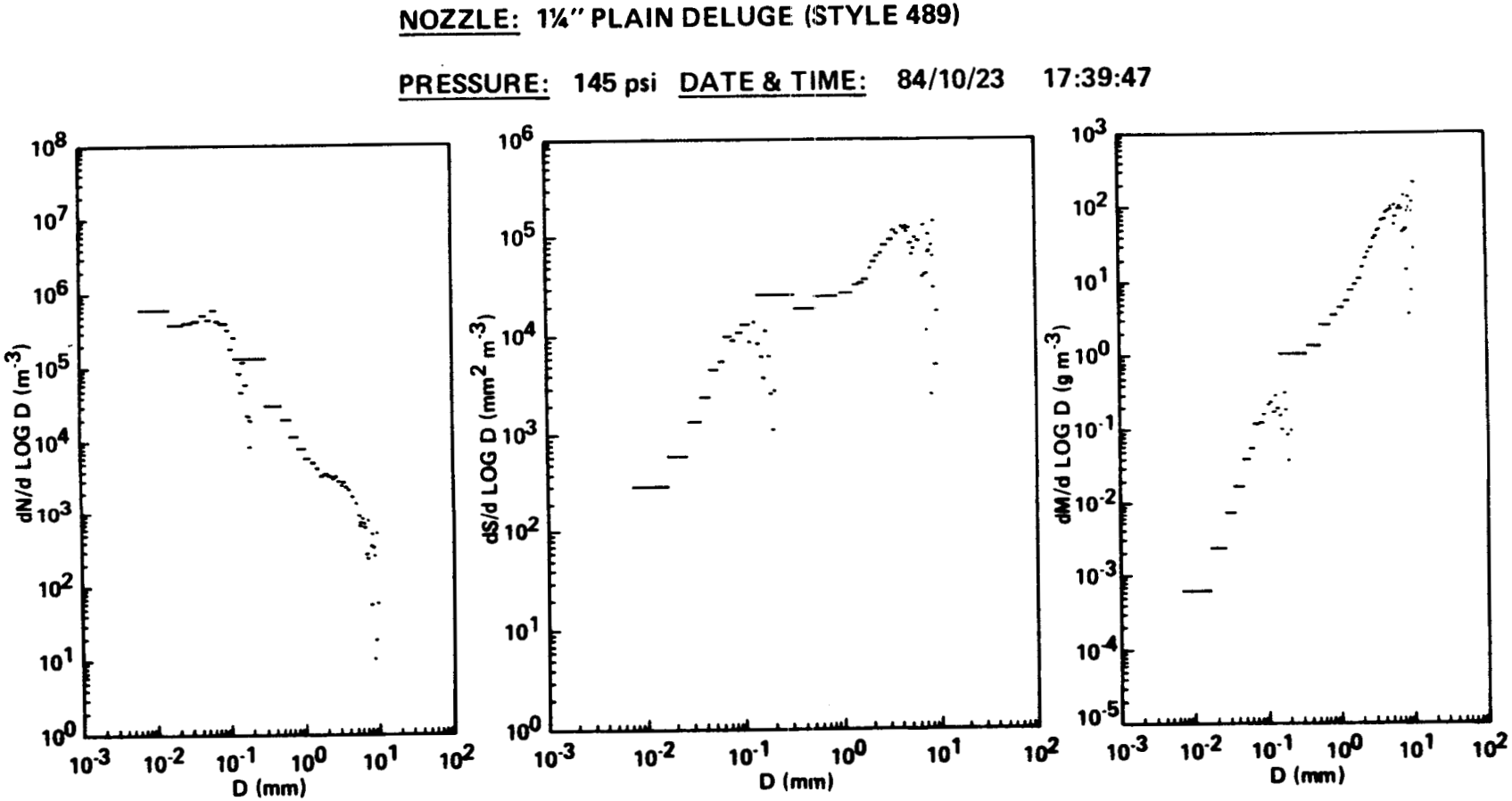

Figure 4-20. Representative distributions of spray from a Style 489 plain deluge 1 1/4 in. ID nozzle operated at 145 psi.

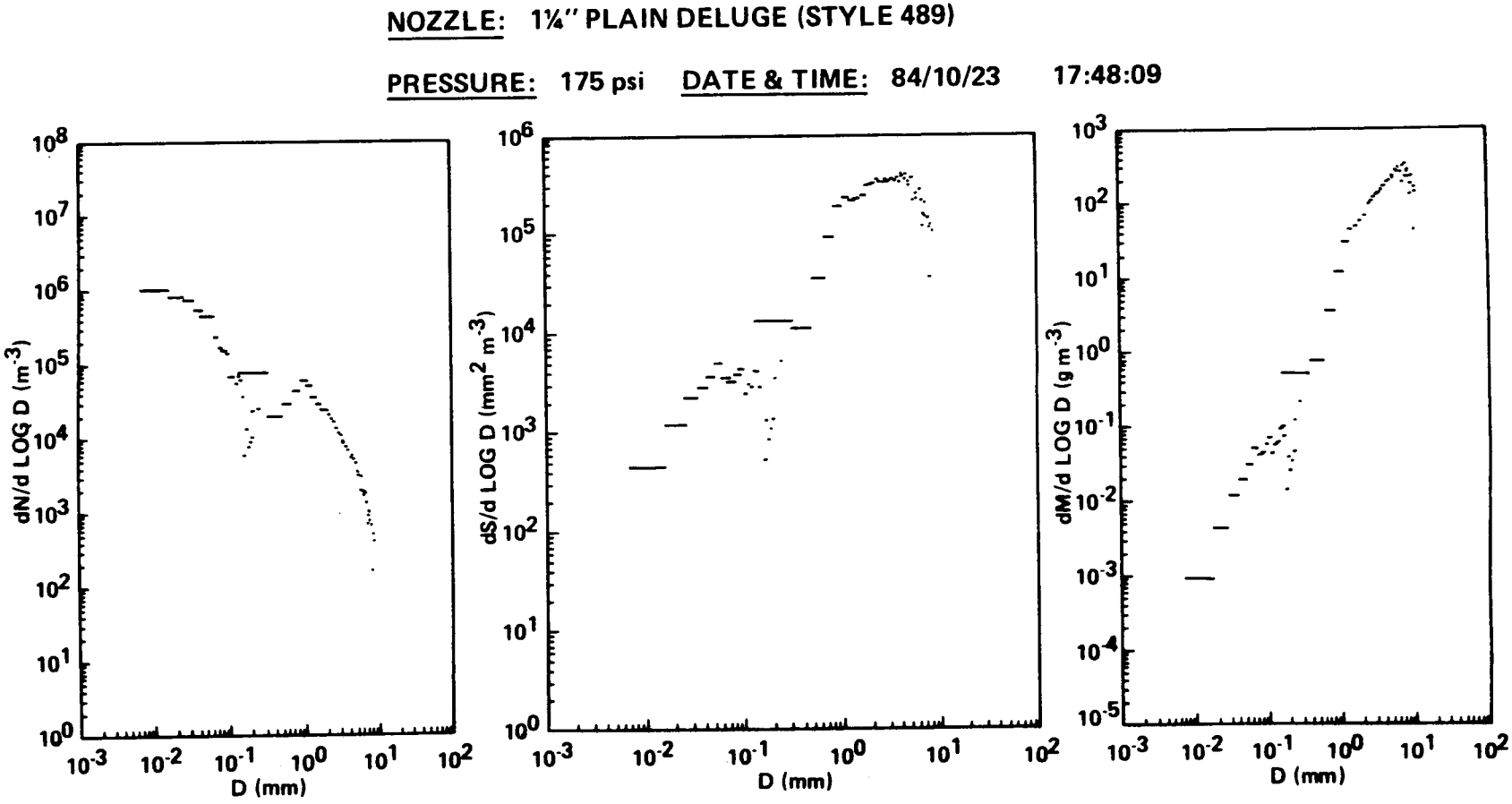

Figure 4-21. Representative distributions of spray from a Style 489 plain deluge 1 1/4 in. ID nozzle operated at 175 psi.

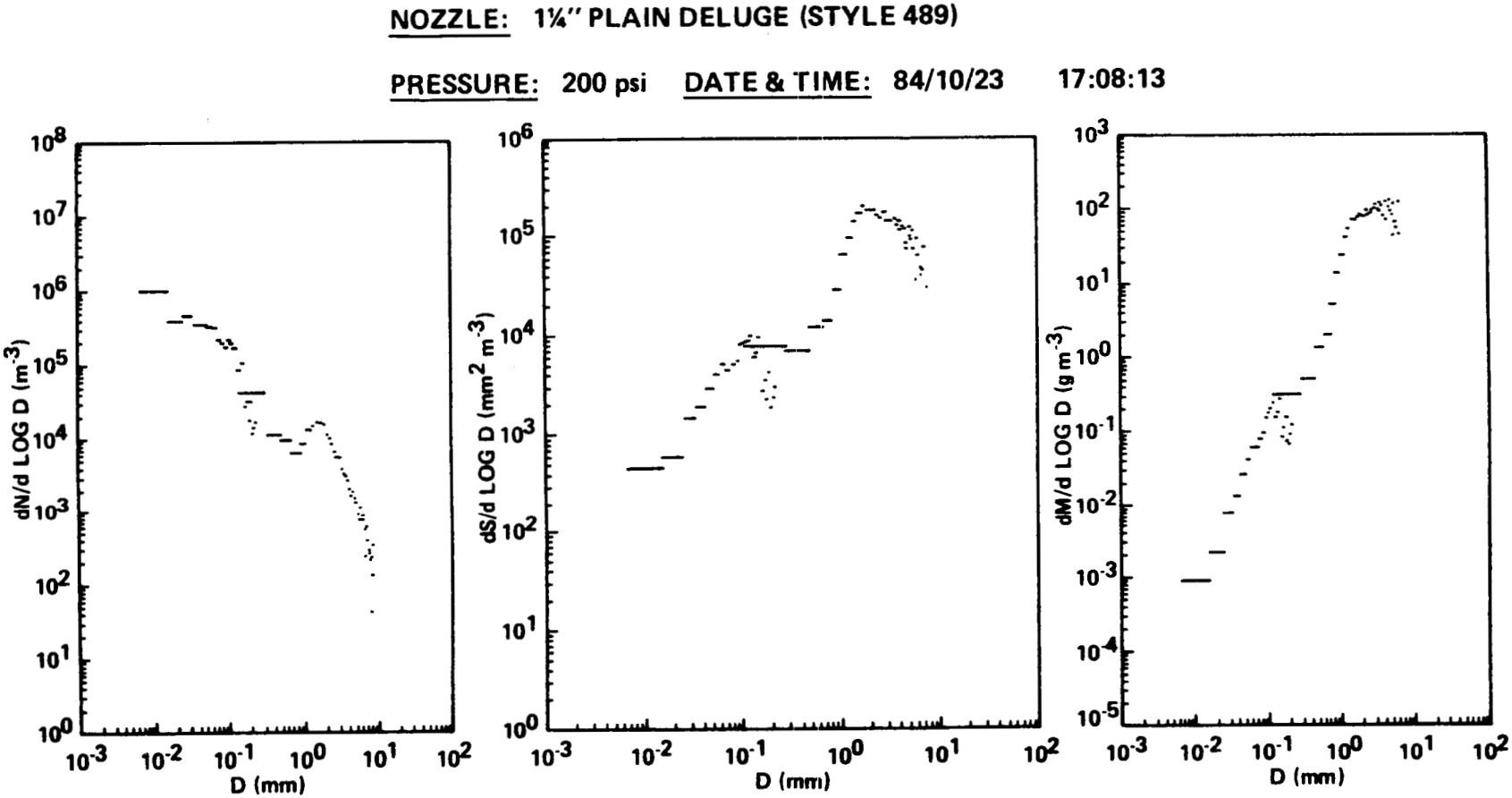

Figure 4-22. Representative distributions of spray from a Style 489 plain deluge 1 1/4 in. ID nozzle operated at 200 psi.

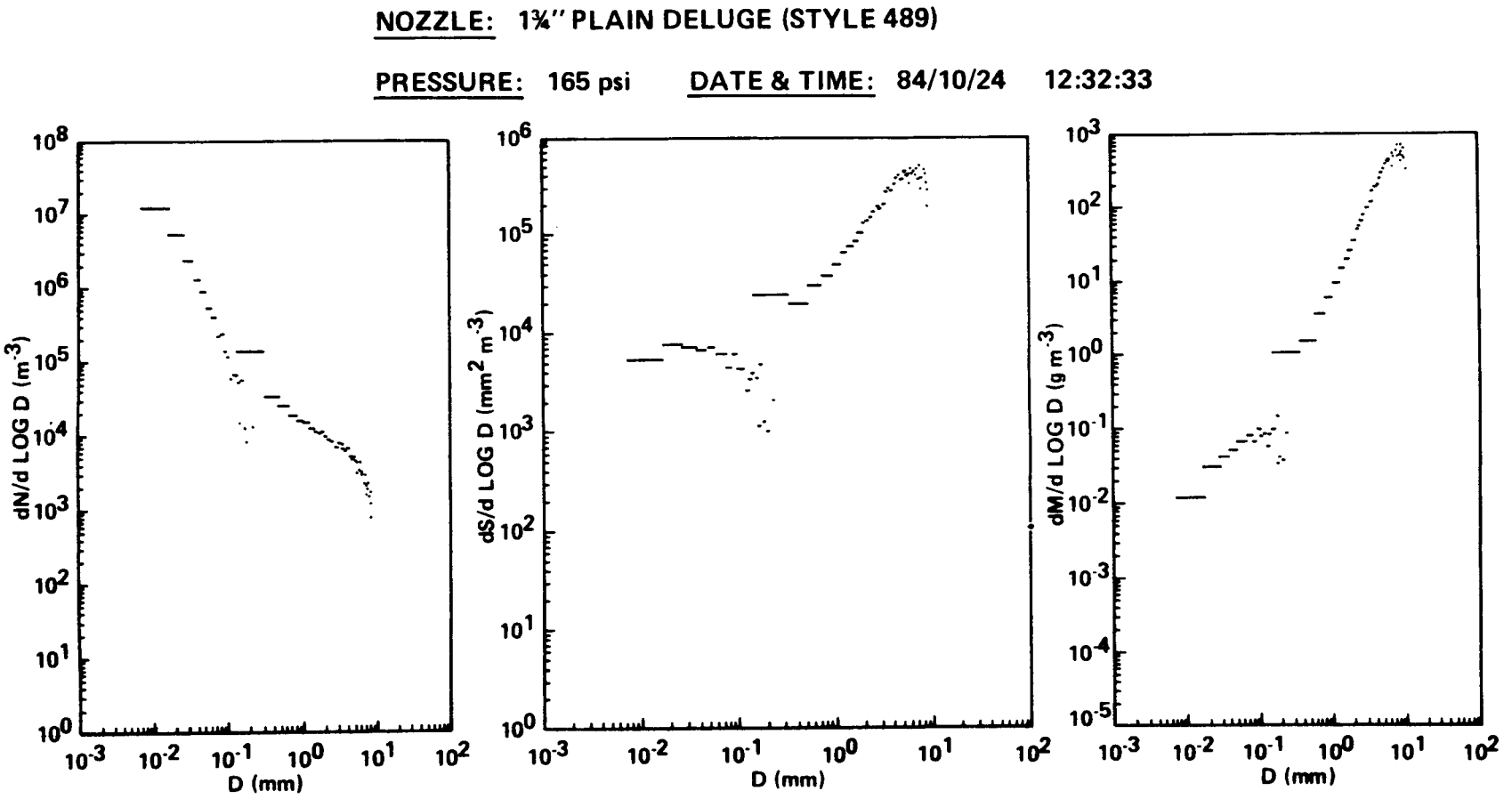

Figure 4-23. Representative distributions of spray from a Style 489 plain deluge 1 3/4 in. ID nozzle operated at 165 psi.

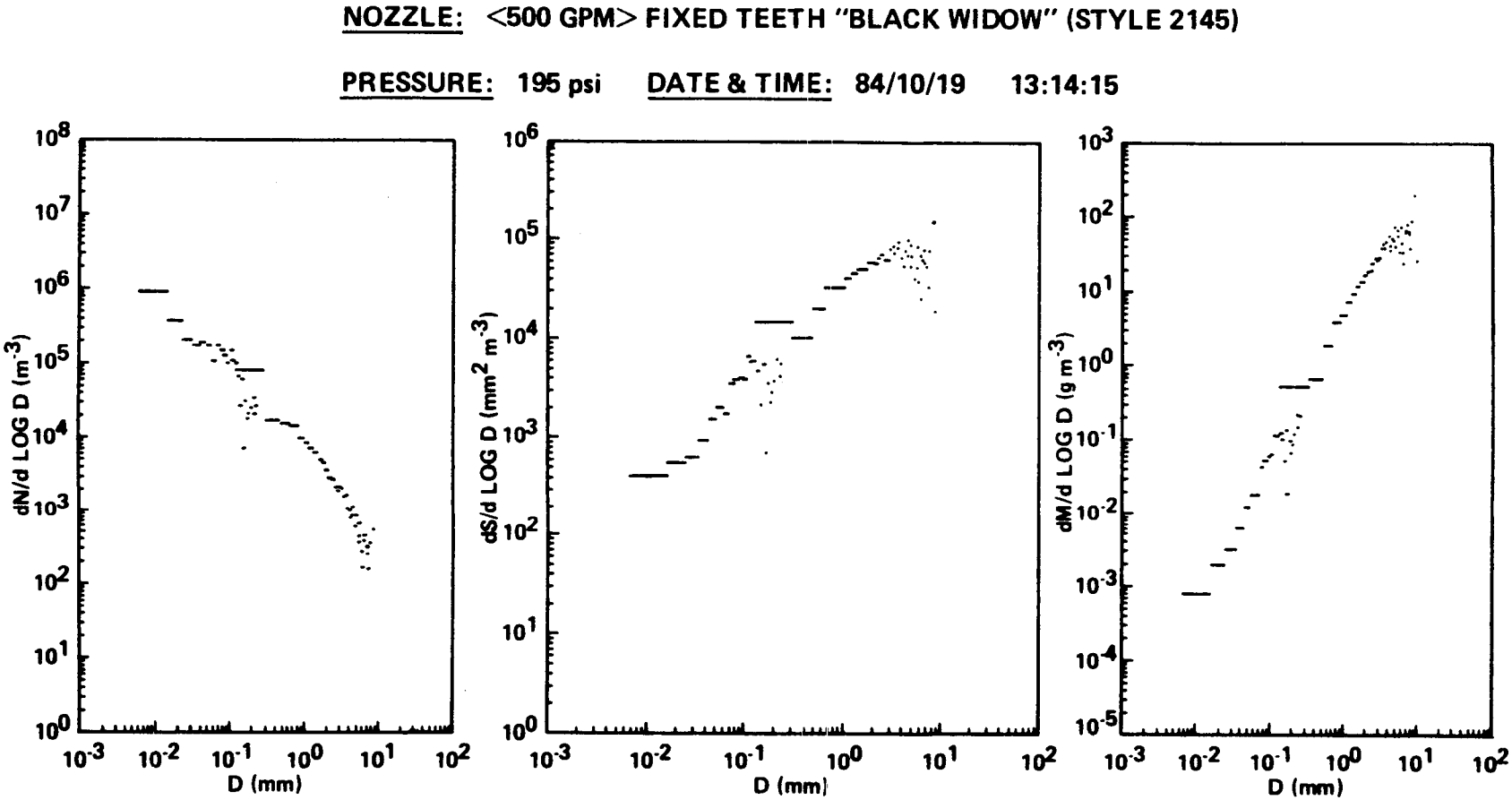

Figure 4-24. Representative distributions of spray from a Style 2145 "Black Widow" (500 gpm) fog nozzle operated at 195 psi.

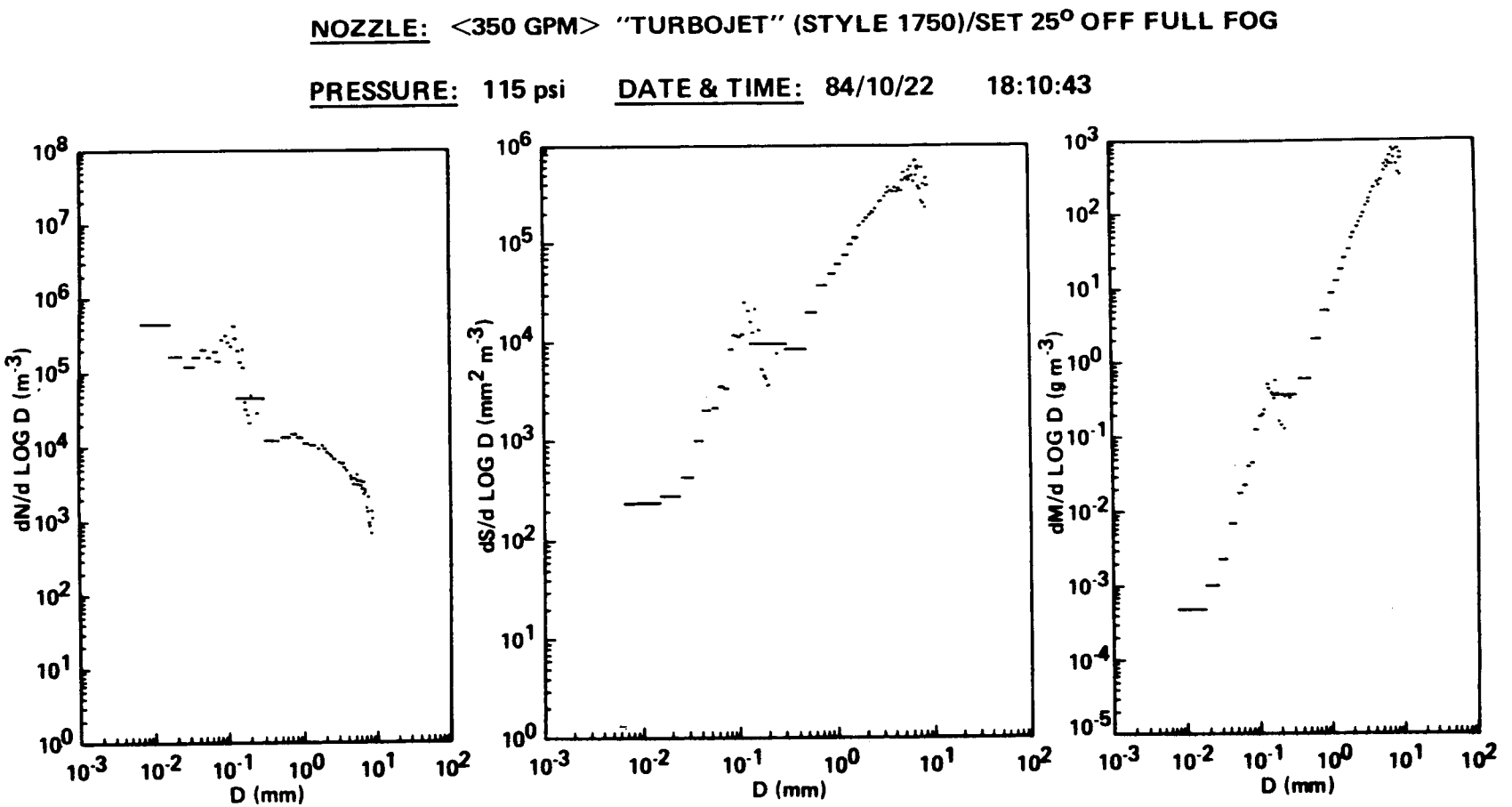

Figure 4-25. Representative distributions of spray from a Style 1750 "Turbojet" (350 gpm) fog nozzle operated at 115 psi.

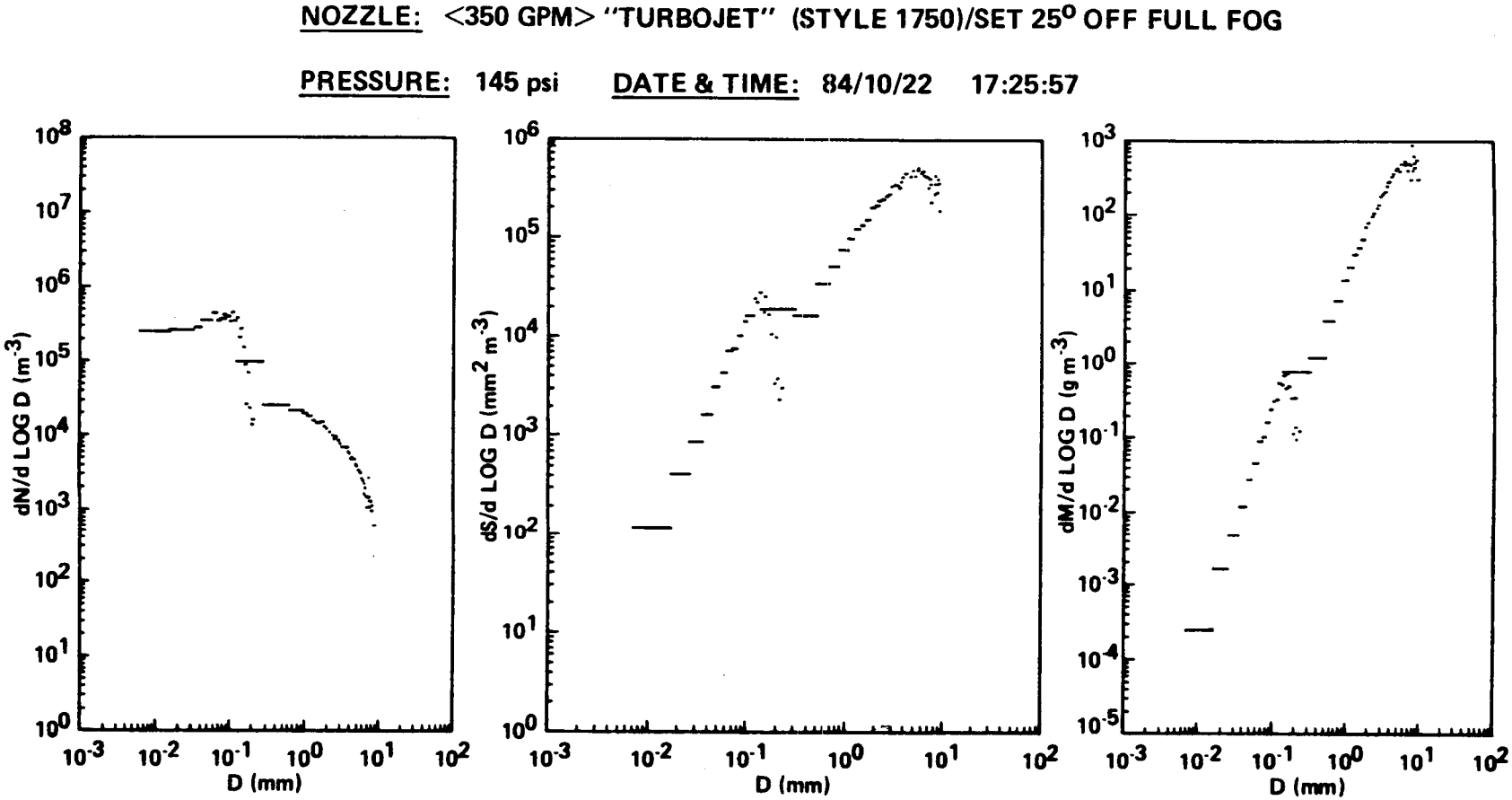

Figure 4-26. Representative distributions of spray from a Style 1750 "Turbojet" (350 gpm) fog nozzle operated at 145 psi.

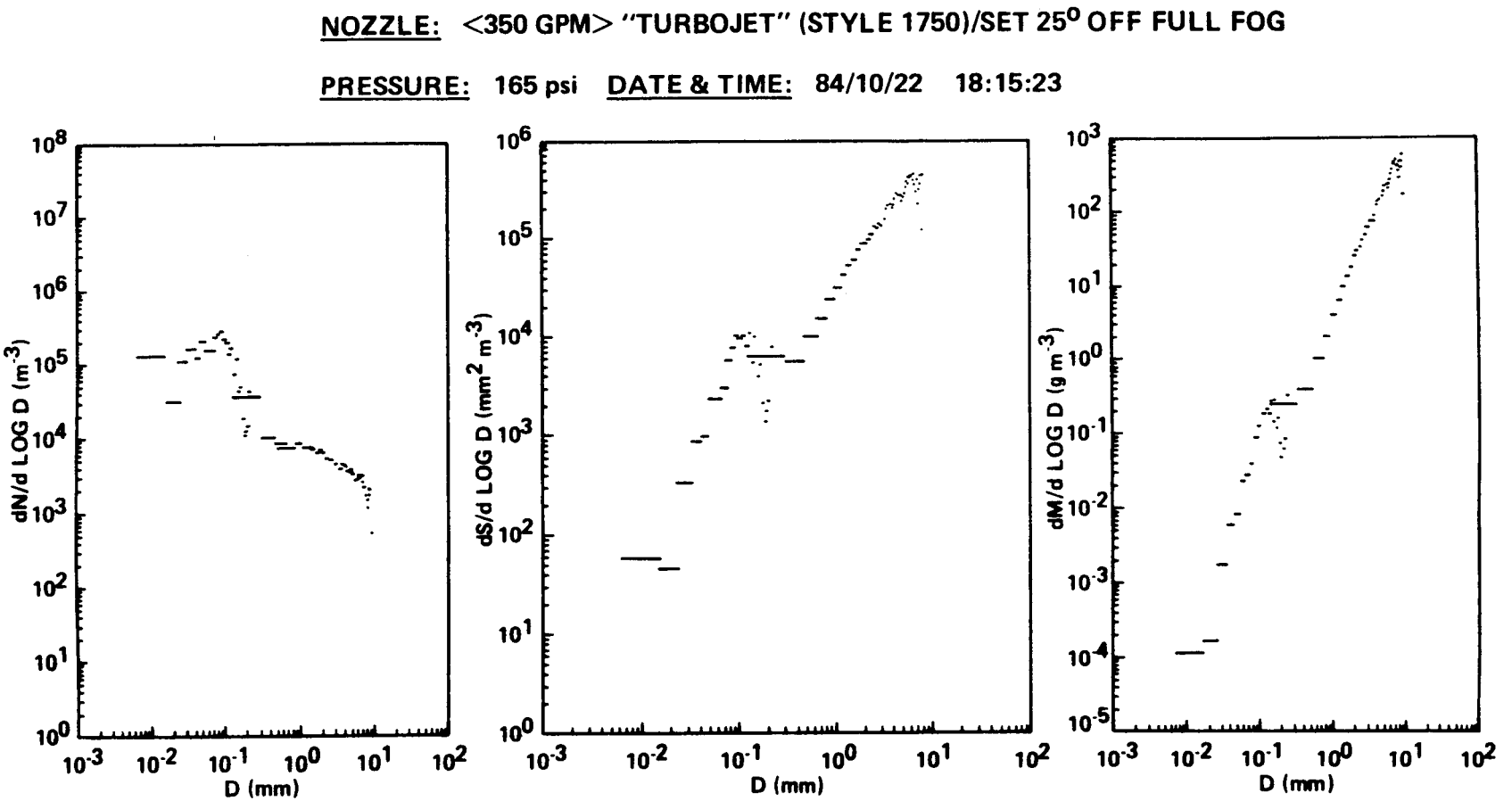

Figure 4-27. Representative distributions of spray from a Style 1750 "Turbojet" (350 gpm) fog nozzle operated at 165 psi.

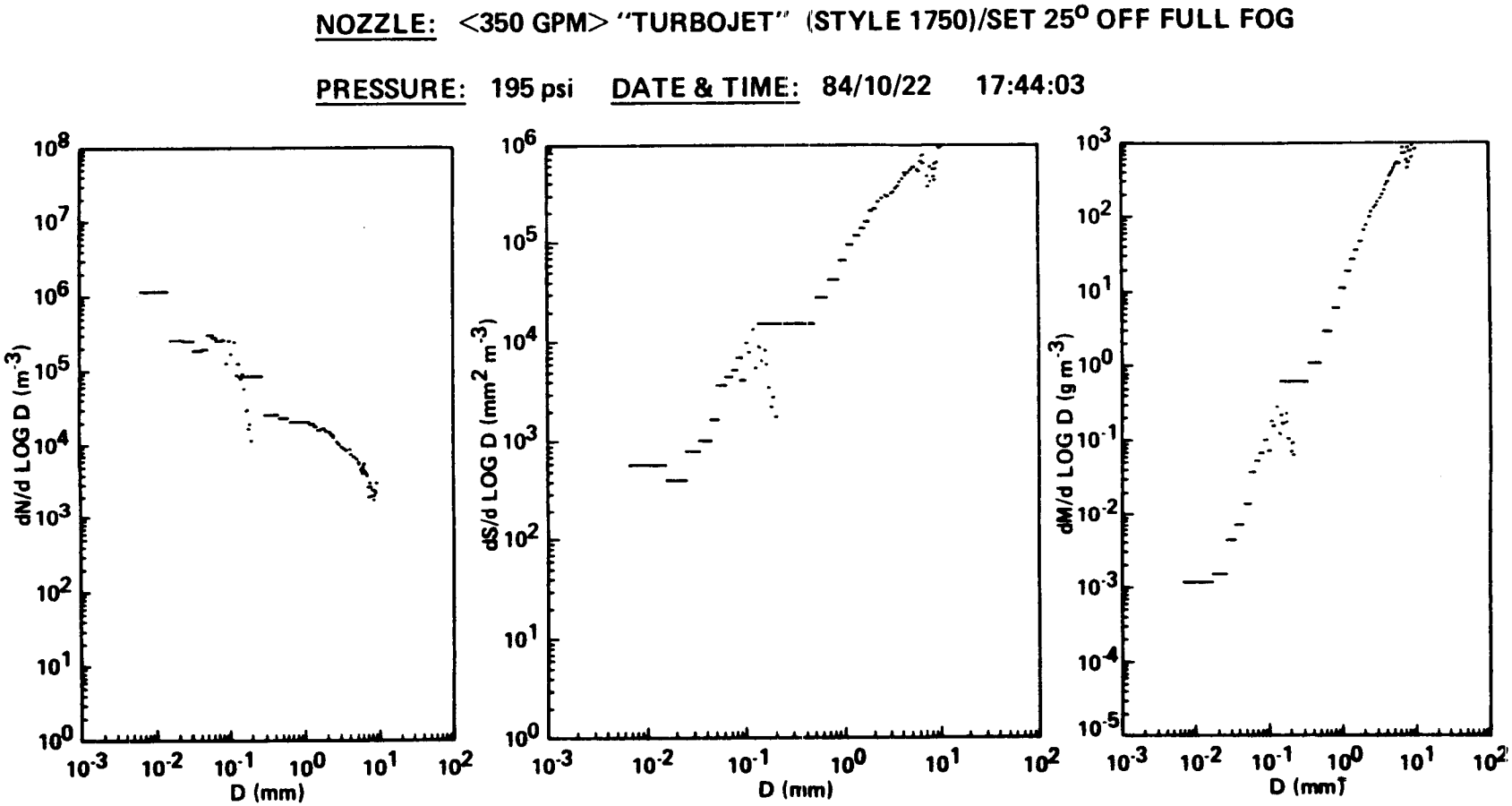

Figure 4-28. Representative distributions of spray from a Style 1750 "Turbojet" (350 gpm) fog nozzle operated at 195 psi.

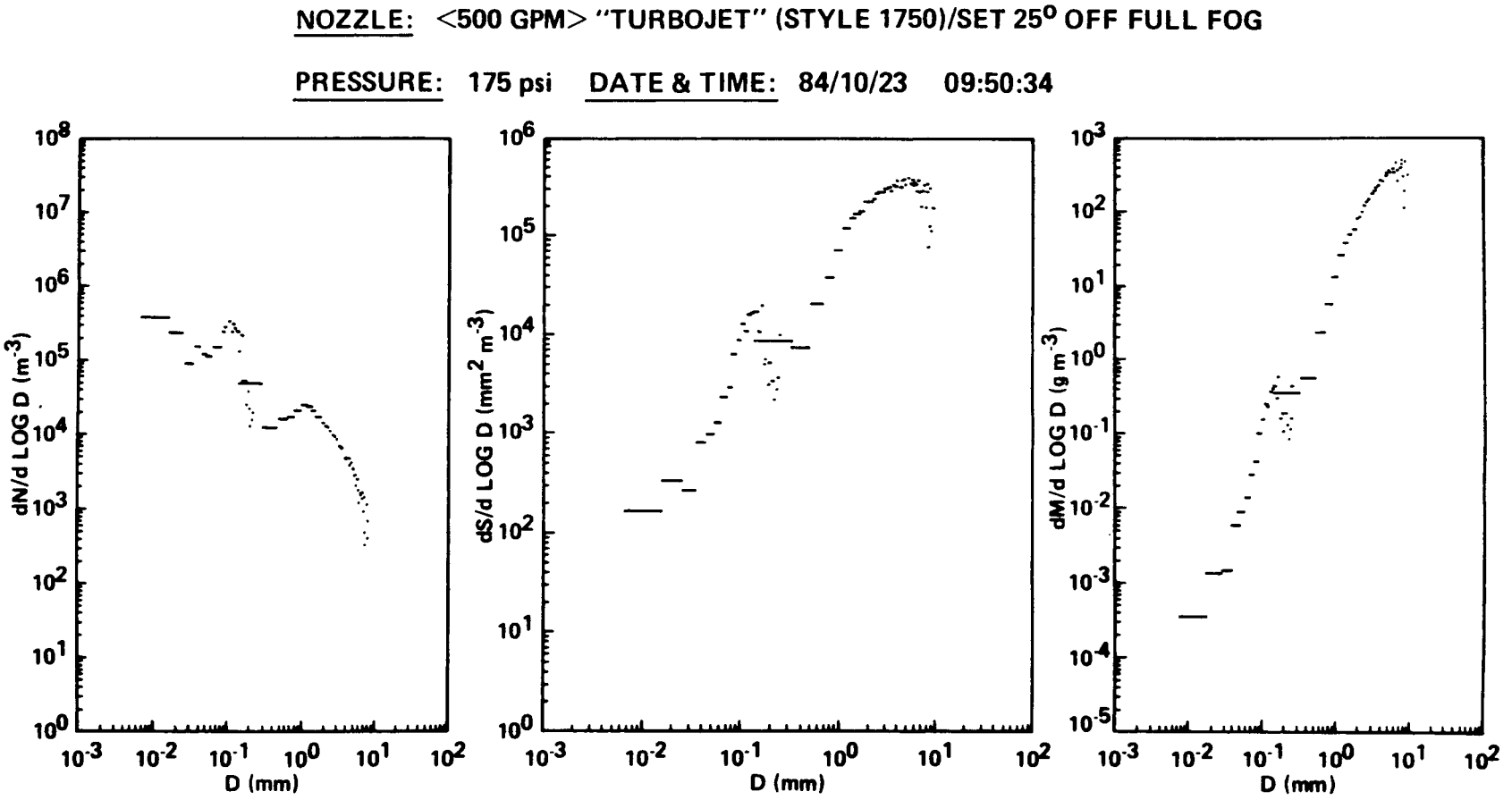

Figure 4-29. Representative distributions of spray from a Style 1750 "Turbojet" (500 gpm) fog nozzle operated at 175 psi.

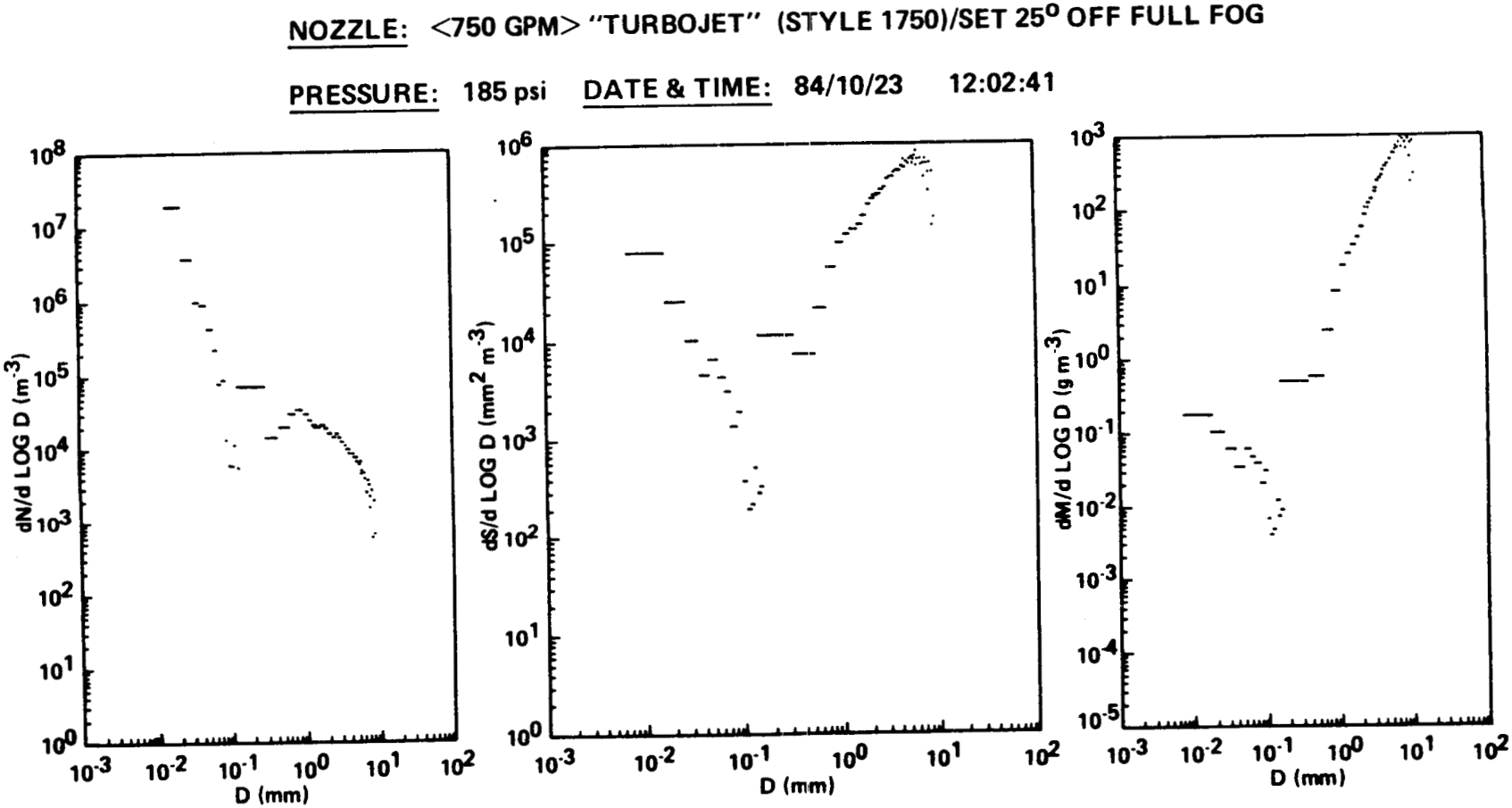

Figure 4-30. Representative distributions of spray from a Style 1750 "Turbojet" (750 gpm) fog nozzle operated at 185 psi.

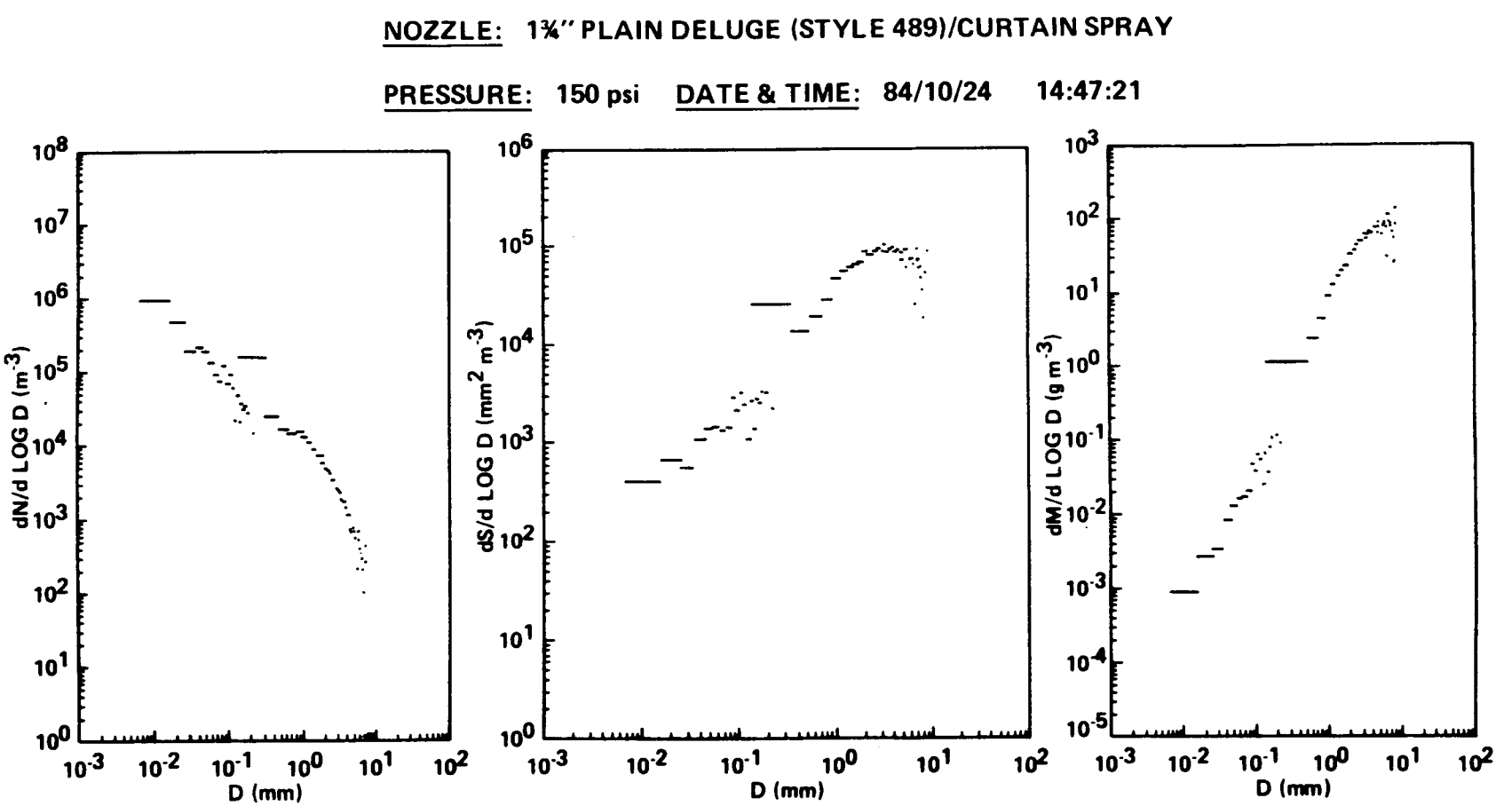

Figure 4-31. Representative distributions of "curtain spray" from a Style 489 plain deluge 1 3/4 in. ID nozzle operated at 150 psi.

It should be noted that the spectra in both Figure 4-17 and 4-30 are complicated by natural drizzle/rain which occurred at midday, October 23, 1984, the date and time of these two tests. Comparison with spectra taken of the natural drizzle when the sprays were off show that, although the mass of water in the natural rain was essentially negligible compared to the spray, it had a clearly discernible impact on the spectra of drops smaller than 200 μm diameter.

The drop spectra from all the nozzles show an apparent bimodal structure. However, the large drop mode in spectra from the combination "fog" and straight stream nozzles, Figures 4-24 through 4-30, show a narrower size distribution than the spectra from the plain deluge nozzles. This is most likely due to the difference in physical mechanisms through which the drops are formed. For the plain deluge nozzles, the primary drop forming mechanism is aerodynamic breakup. In the case of the "fog" nozzles, a large percentage of the drops are formed by mechanical breakup at the nozzle. This is why it is very difficult to propel these sprays to significant heights. That is, since the spray has a very large surface-to-mass ratio, air drag on the drops is very high. In the case of the Style 5050 "Akromatic 1000" nozzle, the sprays were not projected high enough to obtain meaningful drop spectra.

In an attempt to decrease the mean size of the spray drops while maintaining the maximum possible spray height, water jets from two 1 1/4 in. ID nozzles were impacted together above the drop sizing instrumentation as in Figure 4-32. It was anticipated that this would result in enhanced drop breakup and hence a spray spectra having a mean size smaller than that from a single 1 1/4 in. ID nozzle. Figure 4-33 presents the drop spectra which resulted from this water jet interaction. Comparison with Figures 4-21 and 4-22 indicates that a significant improvement in drop spectra over that from single nozzles operated at comparable pressures was not achieved by this technique. It was also observed that since the cross section of the water streams was small and projected distance was large, moderate wind fluctuations caused the streams to interact intermittently. Response time was such that it would be extremely difficult to maintain the interaction even with a feedback control system pointing the nozzles. Therefore, use of this technique operationally would at best produce interaction of the water streams only in the mean.

4.4 Temperature Measurements

A total of ten calibrated Thermometrics high precision thermistors were used to record the temperature of the pond, the water entering the pump, the water at the nozzles, the water spray, the concrete at depths of 2.5 cm and 10 cm in the spray area, the runoff water, and the air at heights of 1.5 m, 10 m, and 38 m. Their output was recorded digitally at 10-s intervals with an overall absolute accuracy of 0.2°C. These measurements were made to provide a data base on the thermal response of the total air/spray/reservoir/ground system when the nozzle array was activated. An excellent illustration occurred on the morning of October 24 during the natural fog event. The thermal data associated with that case is presented in Figure 4-34.

Temperatures are plotted in Figure 4-34 for the pond, the inlet water for the gray (2500 gpm) pumping module, a nozzle within the array, the runoff water, and the ambient air. The temperature scale is on the left-hand side of the figure. Periodic operation of the nozzle array is indicated by sharp changes in the lower plot labeled "ARRAY PRESSURE." The pressure scale is on the right-hand side of the figure. Consider first the curve labeled "NOZZLE." Before activation of the pumps the thermistor attached to the outer wall of the empty aluminum nozzle registered the same temperature as the ambient air. When the pumps and the nozzle array were activated, the nozzle filled with water and the temperature soon registered much warmer than the ambient air. The pond water was about 4°C warmer than the air. The runoff water temperature was initially about 1°C warmer than the pond water. This was due to the

Figure 4-32. Photograph of interacting water jets from two 1 1/4 in. ID plain deluge nozzles operated at 190 psi.

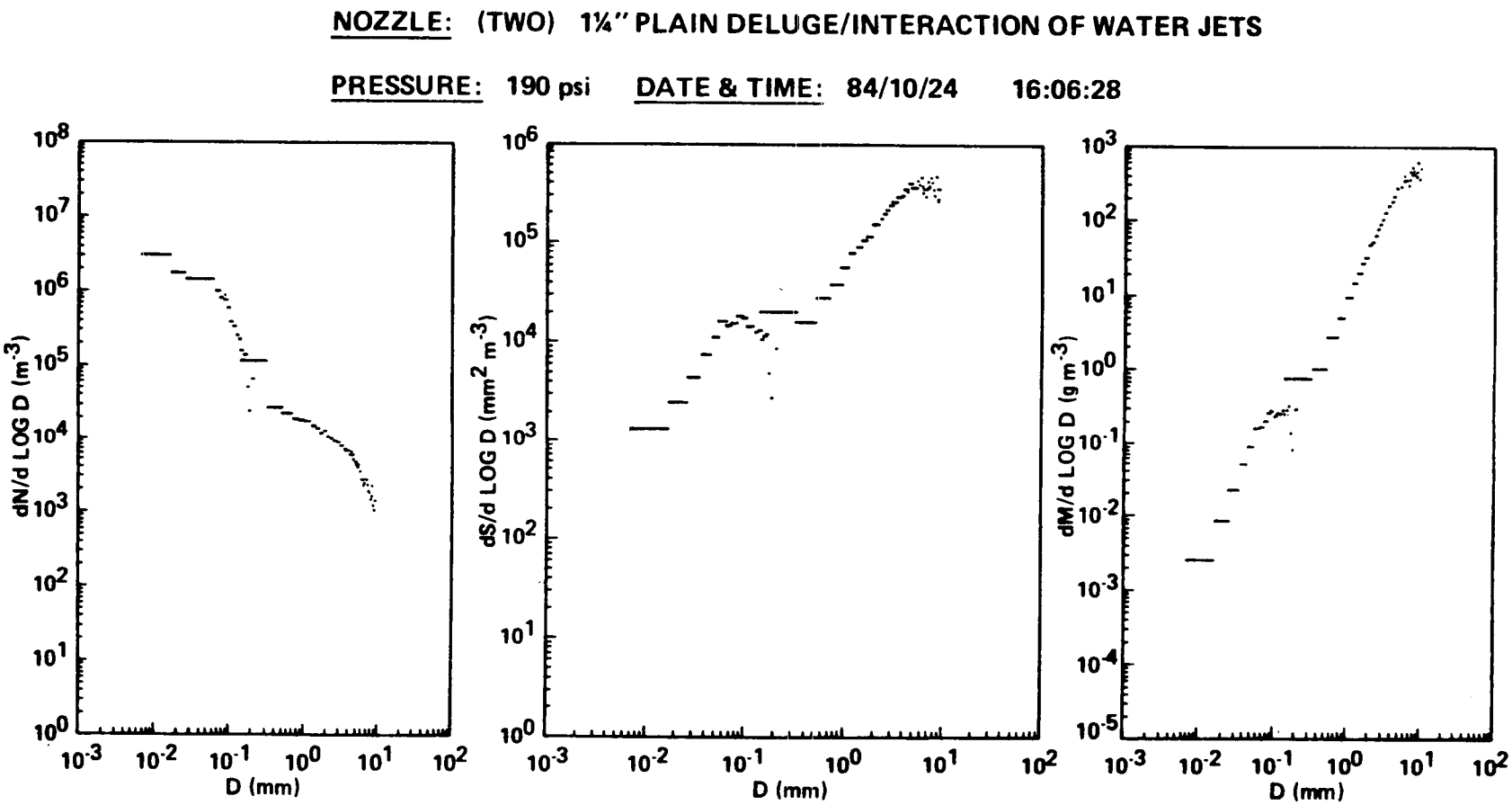

Figure 4-33. Representative distributions of spray from interaction of two 1 1/4 in. ID plain deluge nozzles operated at 190 psi.

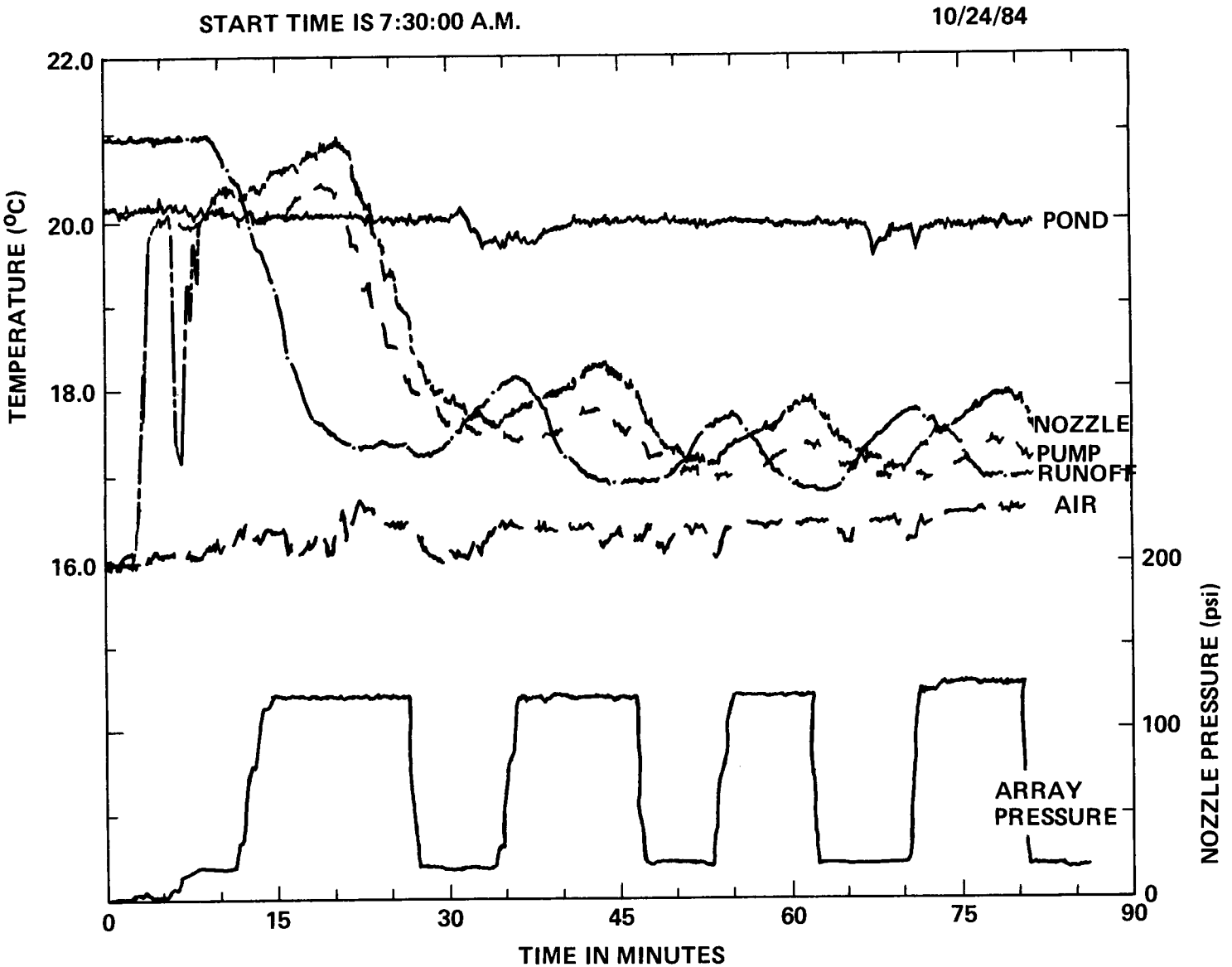

Figure 4-34. Thermal data and nozzle array pressure data for the natural fog case which occurred the morning of October 24, 1984.

fact that the runoff measurement was made in the drainage ditch (Fig. 4-1) which had a residual flow from another test area of approximately 5 l s^{-1} (75 gpm). The runoff temperature as well as the pond temperature was measured 10 cm below the surface of the water to minimize solar heating effects. Of course this early in the morning these effects were small anyway. Due to the location of the pond temperature sensor (Fig. 4-1) and the large volume of the pond, this sensor reading changed very little until the water spray was turned off. The excess water in the drainage ditch then flowed into the pond past the sensor resulting in sharp short term changes as seen in Figure 4-34. Since the spray water was dispersed as drops which approached thermal equilibrium with the cool ambient air as they fell toward the ground (see Appendix A6.0), the runoff water and then the nozzle and pump temperatures decreased quite rapidly. Due to the spacing of the sensors and the on/off cycling time of the nozzle array, the runoff temperature was fortuitously out of phase with the nozzle temperature. Each time the nozzle array was reactivated, warm pond water was drawn into the system resulting in a temperature increase in the recycled water. The relatively short times of continuous operation of the pumps and the fact that a warm residual flow was always mixing with the recycled water did not permit the runoff and pump inlet temperatures to reach the cooler air temperature. However, they did approach within about 0.4°C of the ambient air temperature. The nozzle temperature was always a few tenths of a degree Celsius warmer than the pump inlet temperature primarily due to frictional heating in the pump. Based on other measurements, the amount of heating which occurred as the water passed through the pump is given in Figure 4-35 as a function of test nozzle pressure. The water temperature increase ranged from 0.4°C at 340 kPa (50 psi) to 0.65°C at 1380 kPa (200 psi). If required operationally, the impact of this temperature increase could be minimized by utilizing good heat exchange between the water lines from pumps to nozzles and the returning runoff water.

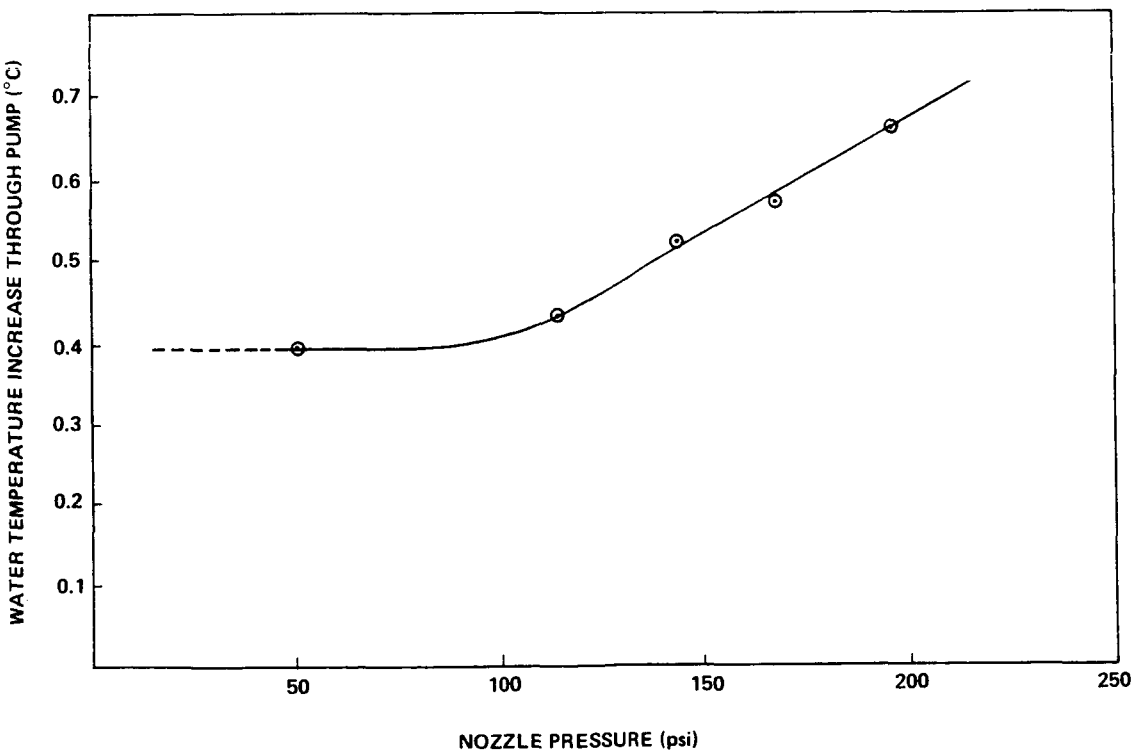

Figure 4-35. The frictional heating of the water which occurs as it passes through the pumps is directly proportional to the operating pressure.

Data taken early the morning of October 23 when the concrete was initially 2°C warmer than the air is presented in Figure 4-36. The thermal response of the concrete pad at a depth of 2.5 cm and of the runoff water following activation of the water spray on this morning is illustrated. It had been raining so the initial temperatures of the pond and runoff water were nearly identical. Note that within 30 min of operation the runoff temperature was within 0.5°C of the ambient air temperature despite the fact that heat was still being transferred from the concrete pad to the runoff water. The concrete pad temperature at a depth of 2.5 cm decreased almost linearly but at a slow rate as one would anticipate due to the low thermal conductivity of concrete. Unfortunately, the sensor in the concrete pad at 10 cm depth gave unreliable data on this day.

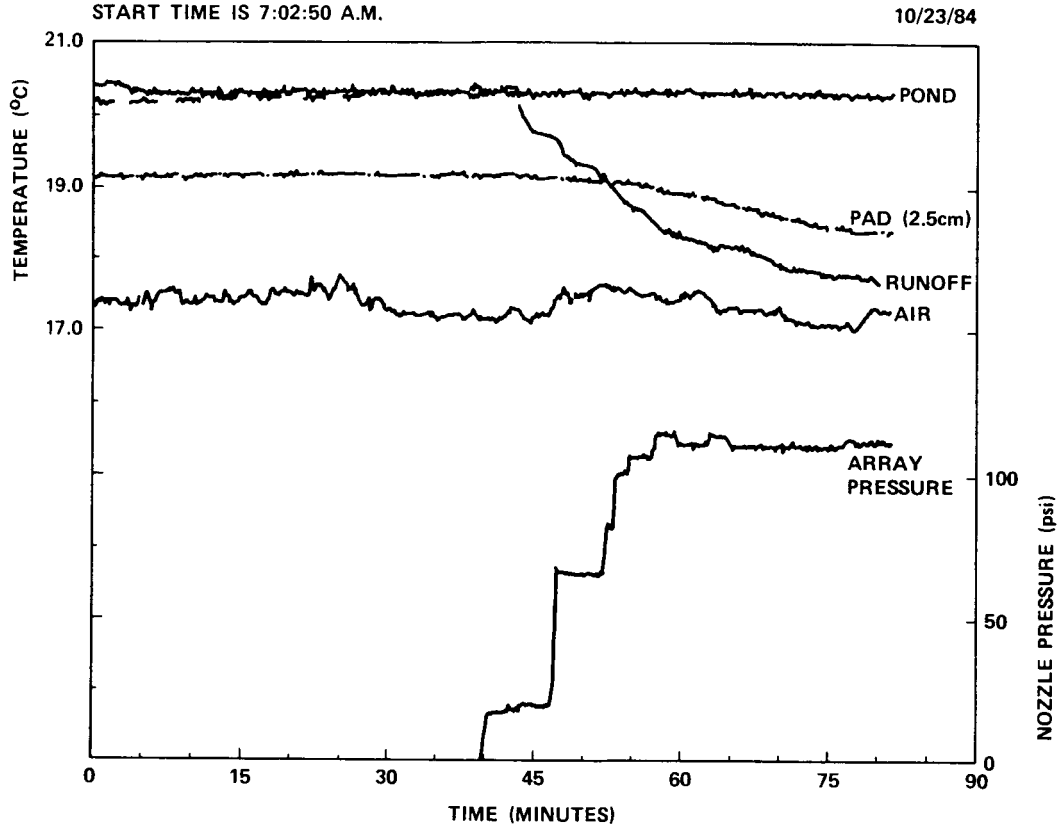

Figure 4-36. Thermal data and nozzle array pressure data taken early the morning of October 23, 1984, when the concrete was initially 2°C warmer than the air.

4.5 Air Flow Measurement

Investigation of the air flow pattern in the vicinity of the spray curtain was performed using smoke from a U.S. Army Model XM49 mechanical smoke generator as a tracer and a handheld anemometer to make quantitative measurements of the flow along the ground at various distances on either side of the curtain. Ambient wind speed and direction were measured with cup anemometers and wind vanes fixed to the test stand. The lower instruments were mounted on a platform which extended from the SE corner of the stand at a height of 10 m. When the array of nozzles was operated, the measurements from these instruments were dominated by the spray induced air flow. The upper instruments were mounted at the top on the NW corner at a height of 38 m, above the influence of the spray curtain.

The smoke and anemometer measurements yielded the air flow pattern illustrated schematically in Figure 4-37. Due to aerodynamic drag, the falling water spray produces a downdraft and outflow from the curtain. Outflows of order 3 m s^{-1} were measured both upwind and downwind of the curtain, for 0 to 2 m s^{-1} ambient surface winds. The downward air flow in and adjacent to the spray curtain is very important, as shall be seen later, because even the smallest droplets in the spray spectra tend to be carried to the ground rather than drift very far downwind, away from the curtain.

4.6 Natural Fog Dispersal

A dense natural fog occurred on one occasion during the test period giving the authors the opportunity to demonstrate the fog dispersal concept. On the morning of October 23, 1984, the ambient wind was from the NNW (~300 deg) at about 1 m s^{-1}. The ten vertically directed 3.5 cm (1 3/8 in.) ID nozzles in the 72 m (235 ft) long array were operated simultaneously at a pressure of 830 kPa (120 psi) projecting a water spray of approximately 390 liter per second (6200 gpm) to a height in excess of 40 m (130 ft). Despite the fact that the water temperature was initially 4°C warmer than the air temperature (Fig. 4-34) and that the water spray spectra was far from ideal (Fig. 4-16), the visibility in the area downwind of the water spray curtain measurably improved almost immediately. Figure 4-38 is a plot of visual range (km) versus time obtained from a Wright and Wright Fog-15 forward scatter visibility meter located 55 m (180 ft) downwind (east) of the water spray curtain at a height of 2 m. Its location can be seen on Figure 4-1. The time periods when the water sprays were on are indicated with horizontal bars along the abscissa. Note that at 7:40 am, just before the sprays were first turned on, the visual range was approximately 100 m. Within less than 2 min after start-up the visual range increased to more than 250 m. The visual range increased (decreased) by a factor of between two and three each of the four times the water spray was turned on (off).

Droplet spectra (fog and spray combined) were measured in the spray curtain outflow approximately 20 m from the spray curtain at the 11-m level of the test stand. The size range 2 to 47 μm was measured with a Particle Measuring Systems (PMS) Forward Scattering Spectrometer Probe (FSSP-100) operated at a 1-min sampling rate. The size range 10 to 300 μm was measured with the PMS Optical Array Probe (OAP-230x) which was also operated at a 1-min sampling rate. The OAP was mounted on the I-beam platform but the platform was swung in against the test stand structure. The FSSP was located inside the (open frame) test stand structure, about 5 m from the edge. This resulted in a partial shielding of the FSSP so that for drops larger than 20 μm it measured lower concentration than the OAP.

Figure 4-39 shows three selected FSSP channels (small, medium, and large droplets) of droplet spectra plotted as number concentration (dN/dD) versus time. These data and extinction values computed from all 15 channels of FSSP spectra at 1-min intervals (Fig. 4-40) show a strikingly similar spray on/spray off response to that obtained with the eastern most visibility meter (Fig. 4-38). These results vividly demonstrate the influence of the spray curtain on the fog droplet population. The magnitude of the visual range is quite different in the two figures, but this is only because drops larger than 20 μm were under counted and those over 47 μm, above the range of the FSSP, were excluded entirely from the extinction calculation (Fig. 4-40).

Figure 4-41 shows samples of complete spectra for both the FSSP and OAP taken in the area of the spray curtain outflow during the natural fog event. The spectra on the left were taken at 8:02 am with the spray off while those on the right were taken at 8:09 am with the spray on. Visual range computed from OAP data alone (Fig. 4-42) compares quite well with that measured by the eastern most visibility meter. (The FSSP data need not be considered since it was found to contribute less than 5 percent to all visual ranges calculated for this day.) For example, the visual range computed from the

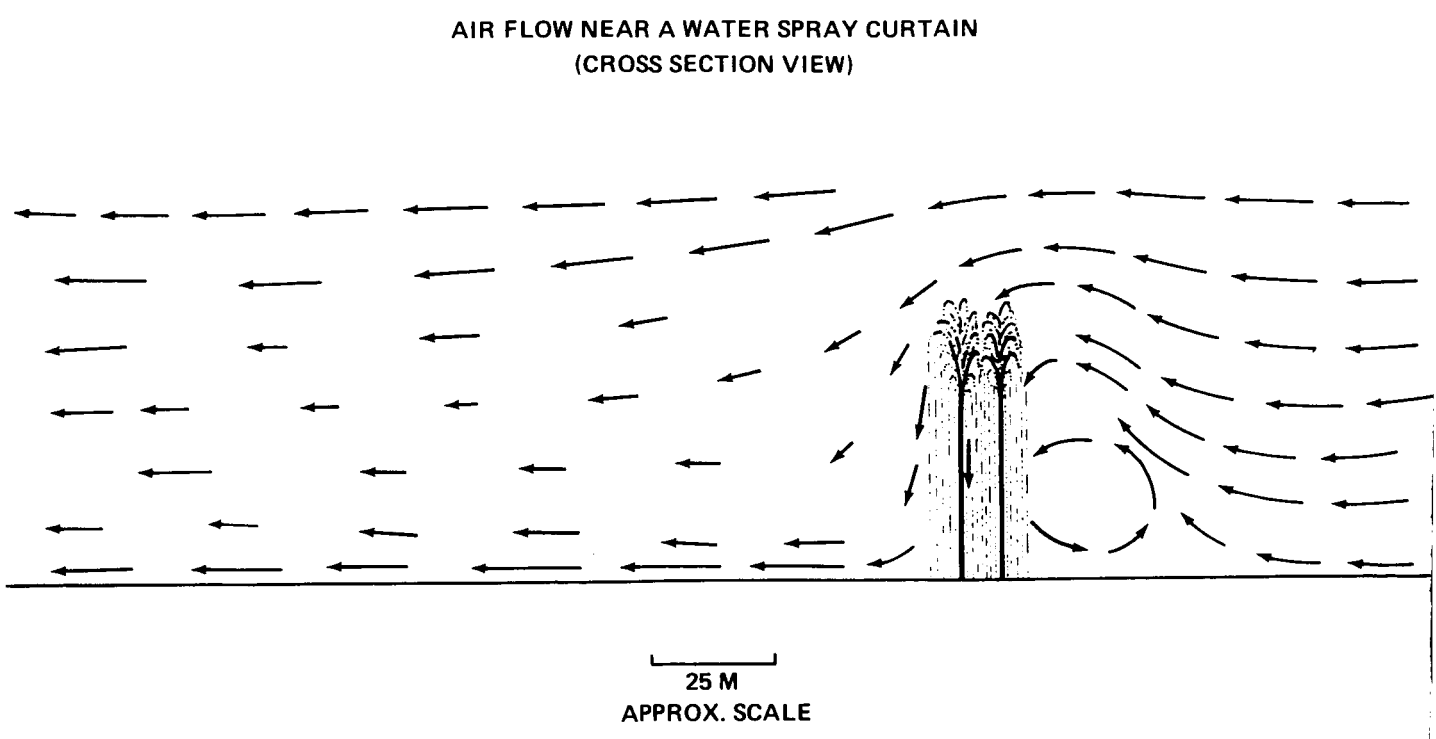

Figure 4-37. Schematic illustration of air flow pattern induced by the water spray curtain. The flow increases the time the fog is in the spray and tends to limit horizontal dispersion of the spray itself.

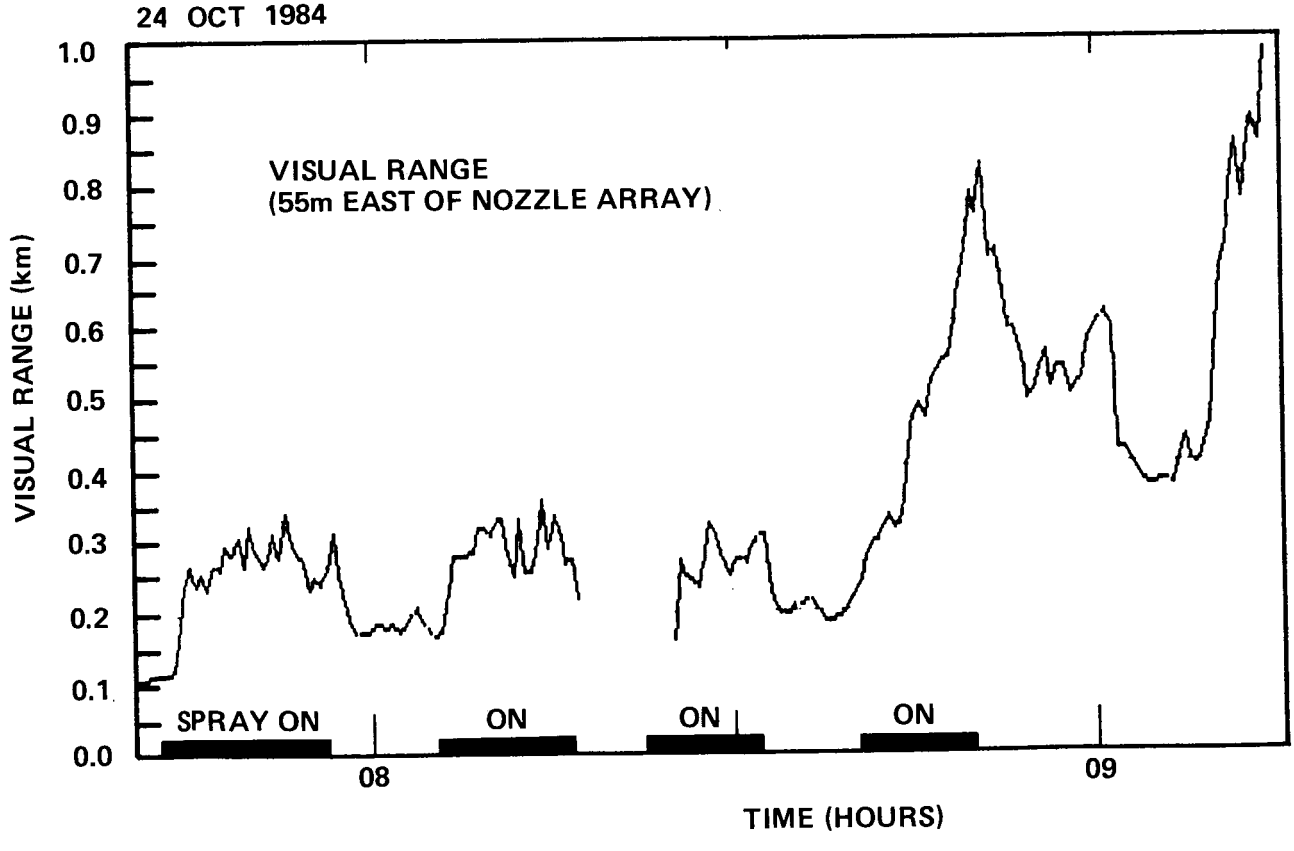

Figure 4-38. Visual range improvement in response to water spray fog dispersal. Measurement was made in natural fog approximately 55 m from the spray curtain at a height of 2 m.

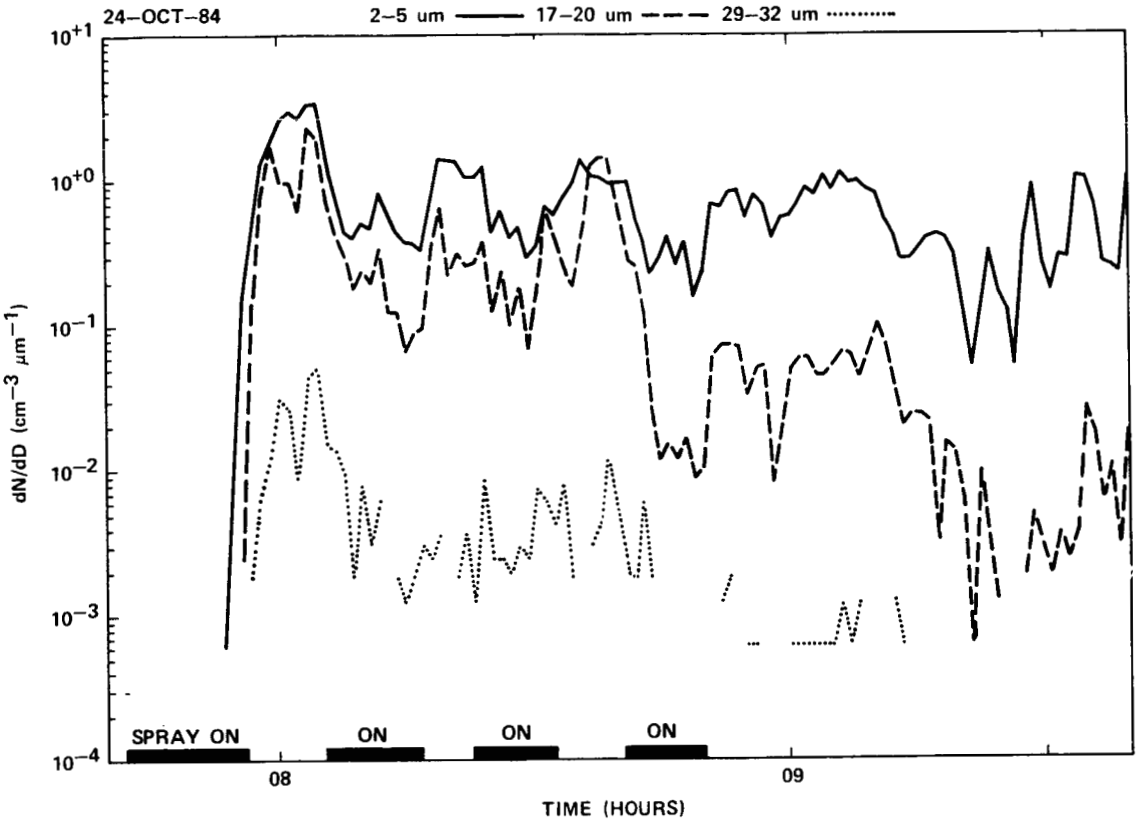

Figure 4-39. Number concentration of droplets measured in the spray curtain outflow while dispersing natural fog. Three of the fifteen channels of a FSSP located at a height of 11 m are displayed as a function of time.

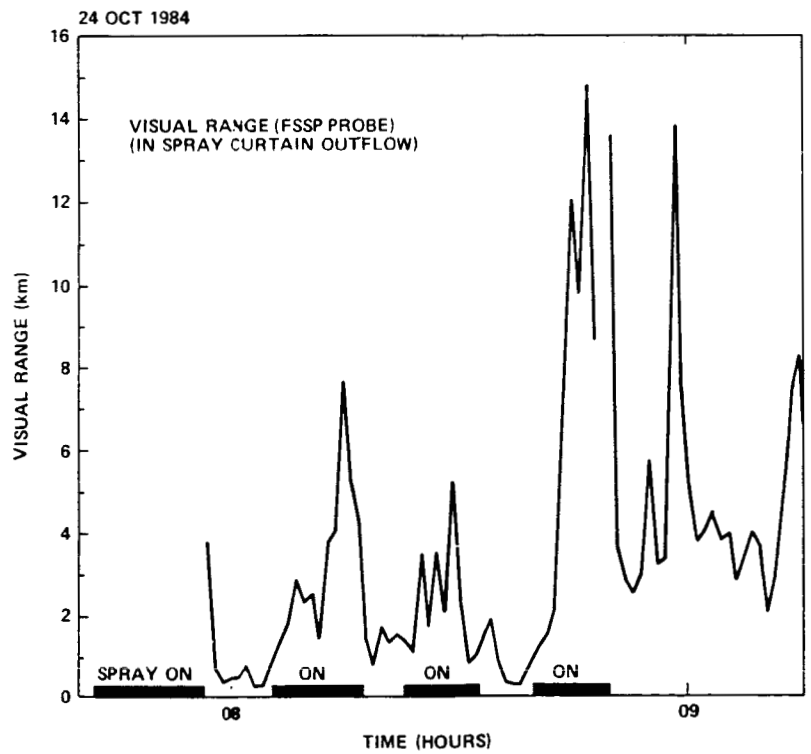

Figure 4-40. Visual range computed from all fifteen channels of a FSSP located in the spray curtain outflow during dispersal of natural fog.

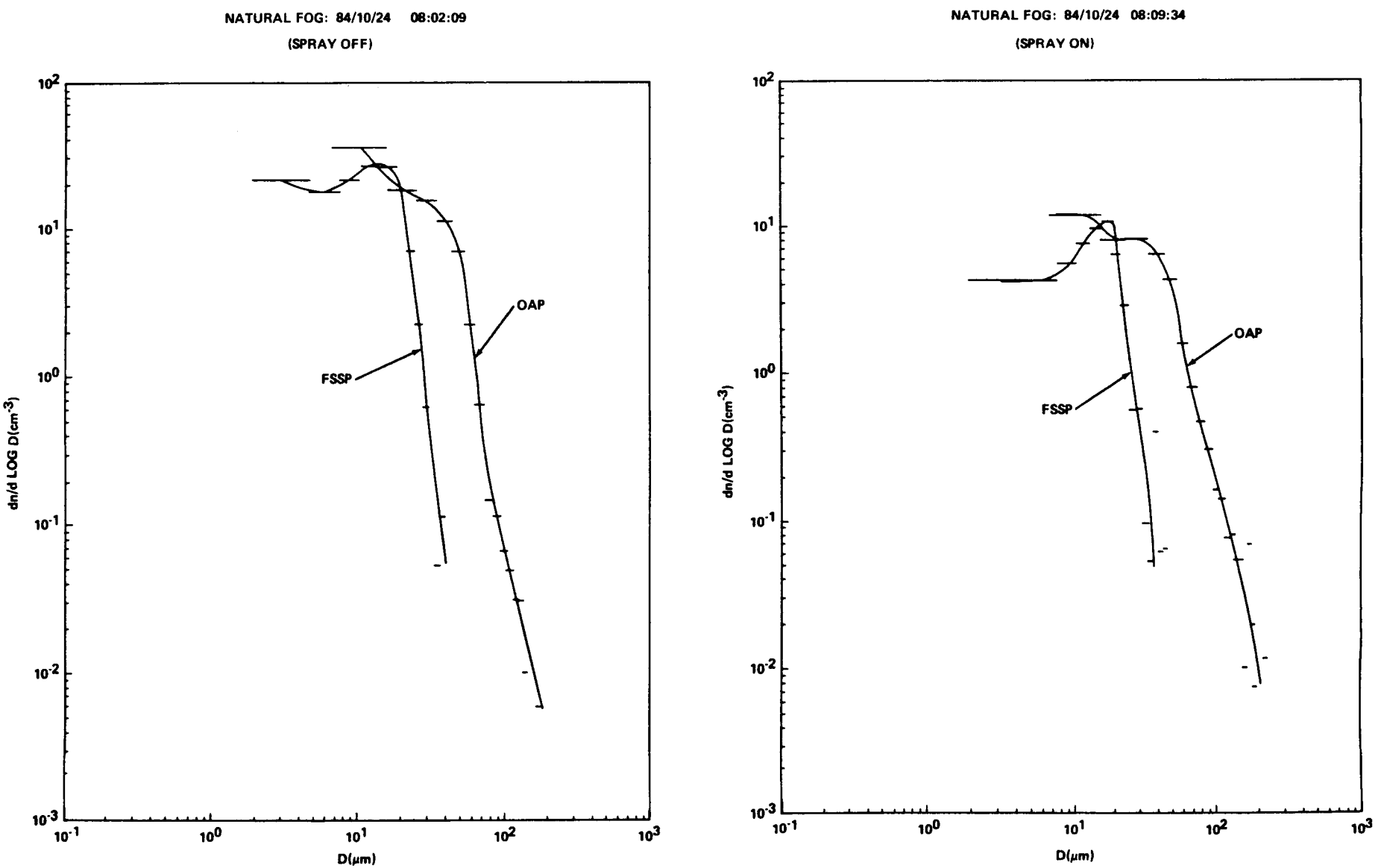

Figure 4-41. Histograms of fog droplet number concentration measured in the spray curtain outflow with both a FSSP and an OAP at a height of 11 m. Spray curtain off (left). Spray curtain on (right).

OAP data in Figure 4-41 is 250 m with the spray off (8:02 am) and 430 m with the spray on (8.09 am). The visual range from the visibility meter east of the curtain was about 190 m with the spray off and about 320 m with it on. Unfortunately, the other visibility meter did not operate properly on this occasion. This agreement is certainly as good as can be expected considering the differences in measurement method and location of the instruments, as well as, the natural variability of the fog.

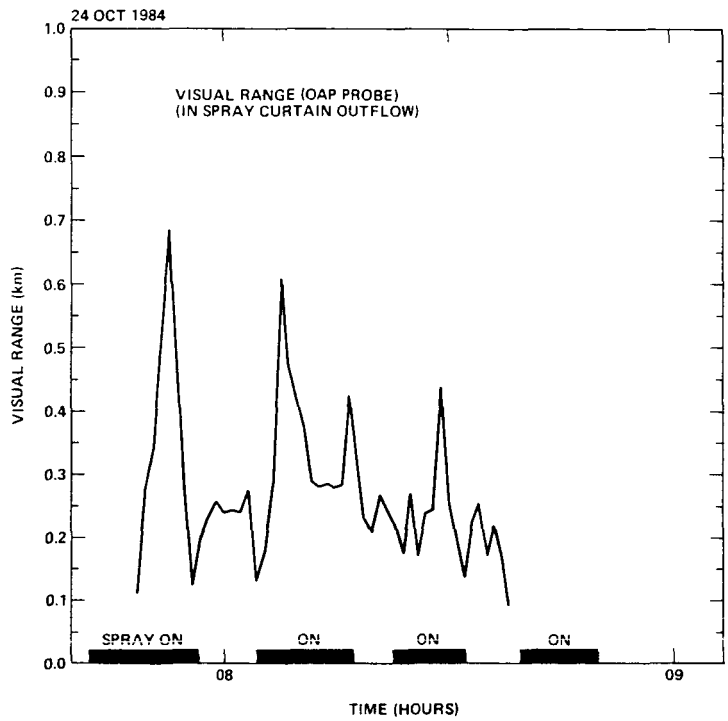

Figure 4-42. Visual range computed from all channels of the OAP-230x located in the spray curtain outflow during dispersal of natural fog.

5.0 ANALYSIS

5.1 Model and Measurements Compared

A numerical model based on the mathematical formulation presented in Appendix A2.0 was developed for evaluating the time dependent washout of fog. In this section the model is used to develop an understanding of the measured field results. A copy of the Fortran computer code and a brief explanation of the critical variables, steps, and equations is given in Appendix A5.0. The model computes the depletion of a specified (initial) fog droplet distribution by an exponential spray drop distribution. The model output gives the fog distribution (size and mass spectra) and visual range at time increments appropriate for washout in the spray curtain. The model can also be used to calculate the visual range for a measured fog or spray drop size distribution (no washout included).

An exponential spray drop distribution for the model was developed by fitting the measured spectra from the 1 3/8 in. ID "Quad Stacked" nozzle (Fig. 4-14). This nozzle was utilized in all the spray curtain tests. In this figure there are about 1000 drops m^{-3} per 0.2 mm interval at D = 2.3 mm and 10 drops m^{-3} per 0.2 mm interval at D = 8.5 mm. Using these two points the exponential distribution function, $dN/dD = -a \exp(-bD)$, fits the measured spectra very well over the range D = 1 to 8 mm when a = 0.2760 cm^{-4} and b = 7.428 cm^{-1}. Using this distribution along with the measured "spray off" fog droplet spectra (Fig. 4-41), the clearing process was modeled as a function of time (see Fig. A8-1, untreated spray).

Figure 5-1 shows both the OAP measured fog spectra of Figure 4-41 and a calculated spectrum after 0.82 sec of washout plotted on an expanded 7 to 100 μm range. The measured spray off (8:02 am) distribution is the upper histogram (heavy lines) and the measured spray on (8:09 am) distribution is the lower histogram (dashed lines). The model result (dotted lines) at the same visual range (430 m) as the spray on distribution was computed for washout of the mean droplet sizes for each size class. The calculated washout result is in good agreement for concentration and visual range with the spray on distribution from 20 to 60 μm (with compensating offsets above and below this range). At sizes larger than about 65 μm the spray is contributing significantly to the spray on droplet spectra. Fortunately, these very large droplets do not greatly affect the visual range of the spray on spectrum (about 11 percent for $D > 67$ μm). The washout calculation results in a slope similar to the spray off distribution. This is another indication that the shallower slope of the measured spray on distribution, even for $D < 67$ μm, is not a result of washout but is due to large droplets supplied by the spray.

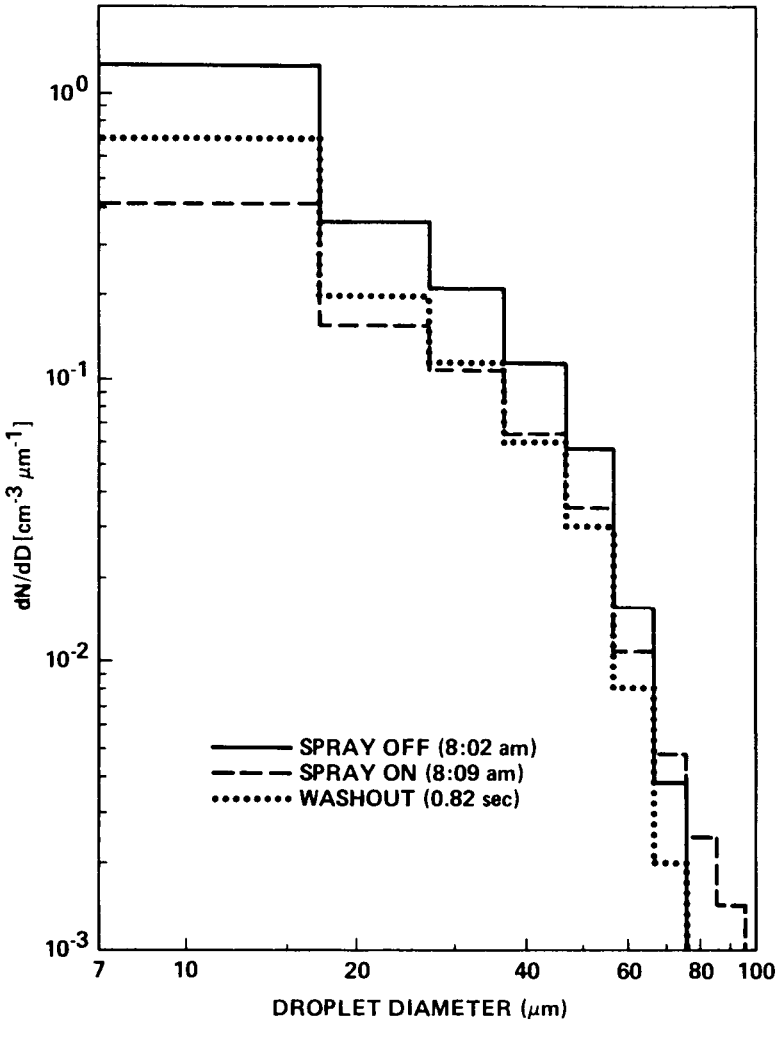

Figure 5-1. Comparison of fog droplet distributions in the size range that contributes to 95 percent of the visual range. Measured spectra are shown at two times during the October 24, 1984, fog episode: SPRAY OFF at 08:02 and SPRAY ON at 08:09. The washout spectrum was calculated for 0.82 sec of washout using a model initialized with the measured SPRAY OFF distribution. [The model distribution has the same visual range (430 m) as the SPRAY ON distribution.]

We can attempt to separate the washout effect from other changes in the spectrum produced by the spray by considering the washout time required for the concentration of droplets in each category to agree with the "spray on" distribution. Table 5-1 shows the washout time for agreement in concentration as a function of category. One expects the processing time, the time the air actually dwells in the curtain, to be at least 1 sec. Thus, the times less than 1 sec inferred by Table 5-1 are too short. They imply the addition of drops larger than 30 μm from the spray. The fact that the calculated visual range agrees with the measured value after only 0.82 sec of washout of the "spray off" spectrum verifies the same conclusion, the visual range was partially reduced by the spray itself. However, in spite of the droplets from the spray, washout produces a significant reduction in net concentration of the most important droplet sizes (20 to 60 μm) with a corresponding increase in visual range.

TABLE 5-1. CALCULATION OF WASHOUT TIME, BASED ON THE MEAN CATEGORY DIAMETER, REQUIRED TO REDUCE THE "SPRAY OFF" DISTRIBUTION TO THE SAME CONCENTRATION AS THE "SPRAY ON" DISTRIBUTION

D (μm)	12.1	22.0	31.9	41.8	51.7	61.5
t (sec)	1.67	1.30	0.96	0.83	0.70	0.50

As a further example of the effect of drops from the spray curtain on the visual range, the data from October 18, 1984, when the system was operated under windy conditions, can be examined. On this date the spray from the array of nozzles was being projected to a height in excess of 40 m. The wind was from the east at 5 m s^{-1} and the relative humidity was 80 percent. Throughout this one-half hour spray curtain test, 11:30 am to noon, the visual range at the west (downwind) meter varied from 140 m to 2500 m but was typically about 1000 m. This instrument was only 30 m from the curtain so it is to be expected that drops as large as 2 mm could be carried this far by wind gusts resulting in the 140 m minimum visual range. However, the fog clearing effect extends well beyond 30 m from the curtain and 5 m s^{-1} winds are near the upper limit of fog conditions of interest. Thus, the potential for degradation of the visual range by drops blown from the spray does not appear overly serious, although additional study is clearly required.

5.2 Removal Efficiency

Using the exponential spray drop distribution developed above, it is possible to determine the "effective" mean size (i.e., the equivalent monodisperse spray size) of the curtain spray drops used in this field test. Equation A2.8 from Appendix A2.0 gives the fog droplet removal rate in terms of the volume flow rate of a polydisperse spray drop spectra. Using the standard terminal velocity relation,

$$U = 965 \text{ cm s}^{-1} - 1030 \text{ cm s}^{-1} \exp[-(6 \text{ cm}^{-1}) D] \quad ,$$

where D is the diameter of the drop expressed in cm and using the value of b = 7.428 cm^{-1} from the exponential spray drop distribution, equation A2.8 reduces to

$$n = n_o \exp(-3.38 E'Q/Lu) \quad . \tag{5.1}$$

Equating n with the result for a monodisperse spray, equation 3.5, gives

$$n_o \exp[-(3/4)(EQ/RLu)] = n_o \exp[-3.38\ (E'Q/Lu)] \quad ,$$

or

$$R = 0.222\ E/E' \quad .$$

Since R and E denote equivalent means for polydisperse washout and E′ is the integral mean collection efficiency, then $E/E' \sim 1$ and the effective drop size for this measured spectra is R = 2.2 mm. This, as was seen in Section 3.0 (Table 3-2) means the spray drop size used in the MSFC fog dispersal demonstration was much larger than optimum. Tremendous potential exists for improving the spray drop spectra thus increasing the fog washout rate and clearing achieved.

Prior to this field test it was recognized that factors such as growth of previously unactivated haze particles or the drift of spray drops into the cleared volume could adversely affect the overall efficiency of the fog removal process. Since a supersaturation results any time two volumes of air saturated at different temperatures are mixed, a large water/air temperature difference is a potential mechanism for the creation of additional fog. However, in these field tests natural fog was cleared (Fig. 4-38) even though this temperature difference was initially large, 4°C. Although a complete analysis of the problem was beyond the scope of this project, the test results (Fig. 4-34) show that recycling the water works rapidly and effectively to reduce these temperature differences. It now appears that the effect is not as critical as was previously believed. Furthermore, it appears probable, for reasons discussed below, that the large volume water sprays may even be effective in clearing fog for cases where recycling is not feasible.

The capability to clear fog with high volume sprays even when the water/air temperature difference is large apparently results from two facts; the smaller spray drops along with the fog droplets rapidly approach thermal equilibrium with the surrounding air and the diffusive water vapor sink of these drops is large. These two factors cause transient supersaturations to be relieved before the air is processed out of the curtain. Appendix A6.0 discusses the thermal response of the water spray and gives the formulation for the thermal relaxation time constant of a drop falling through stationary air. Clearly, spray drops as large as 2.0 mm diameter have sufficient time to approach within at least 95 percent of thermal equilibrium on a single pass through the curtain if they are sprayed as high as 40 m.

If the larger, faster falling spray drops have insufficient time to achieve thermal equilibrium, then small drops and large drops at the same height will have different temperatures. The warmer drops will serve as sources and cooler ones as sinks of water vapor. Net transfer of water vapor will occur between them as depicted in Figure A6-1. Since the mass growth or evaporation rate of a drop is directly proportional to the drop radius, the vapor sink or source represented by the fog and spray drops is given by the product of the drop radius (or diameter) and the drop concentration in that size class. Figure 5-2 is a plot of linear D · (dN/d Log D) versus drop diameter for the nozzle array and for the October 24, 1984, natural fog. The spray spectra was obtained with the GBPP and OAP-230x particle probes while the fog spectra (8:02 am) was obtained with the OAP-230x and FSSP probes. Since the ordinate on this plot is linear and the abscissa is (d Log D) the area under the curve is directly proportional to the instantaneous sink or source of the corresponding drop spectra. From comparison of the areas under the two curves it is clear that the diffusive water vapor sink represented by the fog droplets is much greater than that represented by the spray drops. Thus, the fog droplets and small spray drops are very effective in limiting the transient supersaturation which might otherwise exist in the spray curtain.

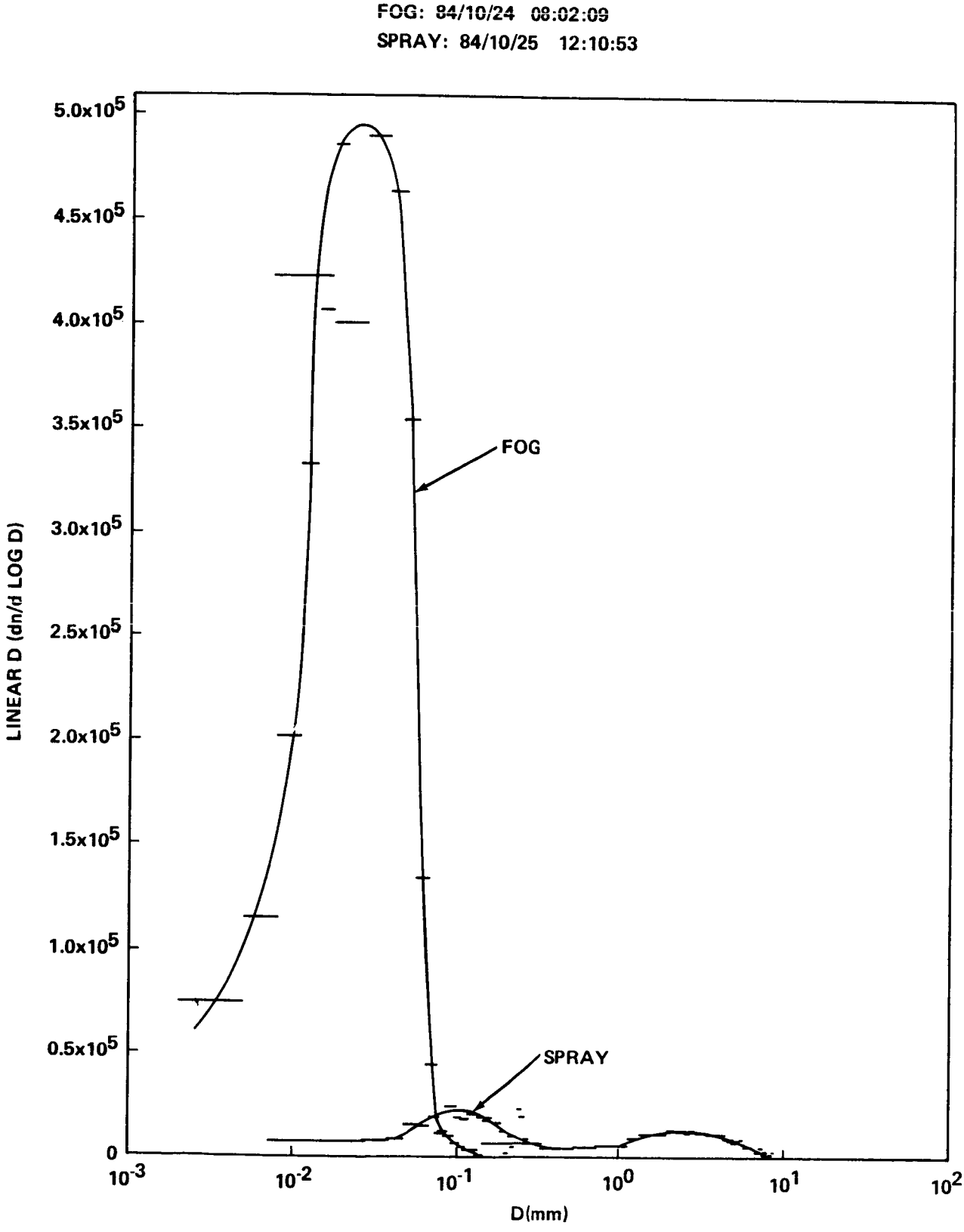

Figure 5-2. The diffusive water vapor sink represented by the fog droplets is much greater than that represented by spray drops.

It is interesting to note that in the case of a large water/air temperature difference the amount of water evaporated from the large water spray drops before they achieve thermal equilibrium exceeds the total volume of water contained in the fog droplets. Of course, both these amounts are small compared to either the total volume of water being sprayed or the amount of water present as vapor in the saturated air. Appendix A7.0 gives quantitative values for the volume of water partitioned as vapor, spray, and fog for a typical case. Thus, the process of recondensation and subsequent fallout deals with a small change in a large quantity. As seen above a sufficient vapor sink exists to relieve transient supersaturations which might otherwise tend to form. This beneficial effect can be slightly enhanced by reducing the relative amount of spray in the large size drops as discussed later in this report.

In considering the efficiency of any fog removal process, a very important consideration is the relative rate with which fog refills or reforms in the cleared volume, compared to the removal rate. The volume may refill by either advection or vertical mixing. Reformation may occur because the clearing method removes the fog droplets but not the fog forming mechanism. The residual supersaturation may cause in situ growth on the remaining small droplets or previously unactivated aerosol. The large volume recycled spray method averts the refilling problem by operating continuously and by creating its own local air flows of a magnitude comparable to the flows found in most natural fogs. Thus, it partially controls the advection and mixing into the cleared region. The method works even in the higher wind cases. Higher wind speeds do, however, require greater spray rate for the same amount of clearing since the time the fog laden air spends in the spray curtain is reduced. They also increase the potential for advecting spray drops into the cleared volume which might limit the visual range achievable. Figure 5-3 is a plot of linear (dS/d Log D) versus drop diameter for both the natural fog (spray off case: 8:02 am) and the spray spectra from a single nozzle like that used in the spray curtain. Since the extinction factor (Fig. A1-1) is essentially constant over this size range, the visual range for a given spectra is proportional to the surface area of the drops. The area under the fog curve on Figure 5-3 corresponds to a visual range of 250 m. The area under the spray curve for drops smaller than 200 μm corresponds to a visual range of 2000 m. However, it should be recognized that due to the nature of the experimental setup used to characterize the single nozzles some of the smaller spray drops may have been carried away by the wind and therefore may not be accurately accounted for on this plot. The ambient wind speed was 2 m s^{-1} at the time this particular single nozzle was characterized. From Figure 5-3 it would appear that even if the small diameter spray concentration in the curtain was quadruple the value given here, advection of spray drops smaller than 100 μm diameter into the cleared volume, would not be a big problem. However, at the higher wind speeds if drops as large as 2 mm diameter were carried into the cleared volume, severe restrictions would be placed on the maximum clearing achievable. As noted earlier, this effect was observed during the October 18, 1984, tests near the spray curtain.

An important aspect of this method relative to the potential for reformation of fog in the cleared volume is the fact that the spray curtain acts directly on all the air that is cleared. As the air exits a spray curtain and moves into the cleared volume, it is usually well-mixed, isothermal to the height of the curtain, and saturated at the ambient wet bulb temperature. This is important because in an advection fog, turbulent transport and advection generally control the production of supersaturation, S_v. If liquid water is removed from the fog by some physical mechanism there is usually less surface area to serve as a sink for the excess water vapor and the supersaturation rises. If (S_{v-1}) rises sufficiently (perhaps only 0.05 percent) unactivated haze particles may be activated, forming new cloud droplets and bringing the fog droplet population back to near original levels. However, in the case of the high volume recycled water spray method the supersaturation instabilities are removed in the spray curtain. Therefore, in situ formation of fog in the cleared volume is less likely.

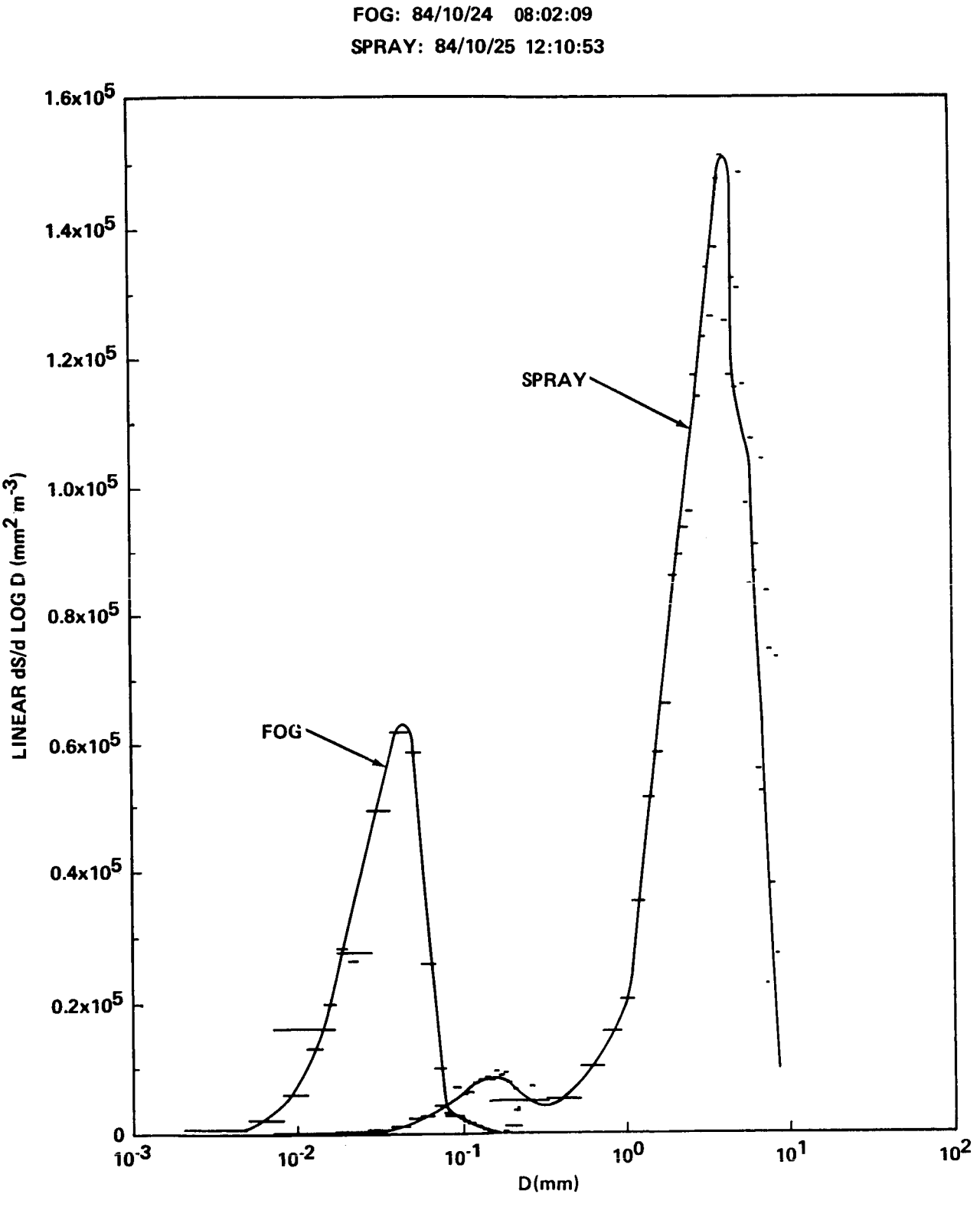

Figure 5-3. Surface area of the spray drops and fog droplets as a function of size for the nozzle array and for the natural fog. Visual range is proportional to the drop surface area.

5.3 Potential Improvements

Several potential improvements can be made to increase the fog clearing efficiency for a given spray rate. The first possibility is to reduce the mean drop size of the spray. Although improvement in nozzle design to maintain maximum projection height while maximizing the quantity of water in the drop size range 0.3 mm to 1.0 mm is a possibility, it does not appear very feasible at this time. A more promising possibility involves interspersing nozzles which produce smaller size drops with their accompanying penalty in projection height within a straight stream nozzle array. Since the air circulation induced by the water spray curtain processes the fog down through the spray, it does not matter whether the fog is removed high or low in the curtain as long as it is removed before leaving the curtain. Another promising possibility for decreasing the spray drop size is to reduce the liquid surface tension through the addition of a surfactant. Appendix A8.0 addresses this possibility. The net result is that halving the surface tension, through the addition of a small quantity of long chain alcohol for example, reduces the mean drop size, increases the fog washout and more than doubles the visibility improvement achieved for a given spray rate.

Increasing the collection efficiency of spray drops for fog droplets through electrical charging of the sprays is still another possibility for improving the fog washout. However, this introduces potentially disruptive electric fields along the runway. It has been shown (personal communication, Dr. Michael H. Smith, University of Manchester Institute of Science and Technology, Manchester, U.K., 1985) that collection efficiencies of highly charged (charged to several tenths of the Rayleigh bursting value) spray size drops for fog size droplets may approach the value 20 due to dipole, not Coulomb, forces; so that neutral fog droplets are swept out efficiently. Oppositely charging adjacent nozzles could minimize the net electric field while still maintaining the enhanced collection efficiencies.

A somewhat different but complementary approach to improving the clearing efficiency involves the air flow near the spray curtain. The spacing and water flow rate of the nozzles within the array should be optimized to give maximum projection height, a uniform spray curtain, and optimum induced air circulation. This will enhance processing of fog through the spray while minimizing entrainment into the cleared volume. Computational Fluid Dynamics (CFD) computer codes could be used to investigate these effects. Tracer smoke and variations on the nozzle arrangement in a large field test could be used experimentally to verify the numerical results.

6.0 DISCUSSION OF OPERATIONAL FEASIBILITY OF METHOD

The energy requirement for the large volume water spray method is nearly an order of magnitude less than that required to operate a thermokinetic system. For example, it has been calculated [1] that to raise Category III landing conditions to minimum Category II via the thermokinetic technique (assuming a total clearing length of 2 km) would require 20 jet engines each rated at approximately 10,000 lb thrust at sea level and each consuming 1,000 gallon per hour of jet fuel (JET-A). Therefore, a total of 20,000 gallon per hour of fuel would be required for the thermokinetic technique. By way of comparison the small pumping modules (2500 gpm) used in our water spray tests each required less than 40 gallon per hour of diesel fuel [7]. Larger pumping units would, of course, be more efficient as well as more cost effective. Using the lower efficiency value and assuming a total water requirement of 200,000 gpm to clear 2 km of runway, the requirement would be 3200 gallon per hour of the lower grade fuel, about 15 percent of the amount required for a thermokinetic system.

Although water pumps which will each supply 50,000 gpm at a pressure of 150 psi are commercially available, at the present time they are not as cost effective as 20,000 gpm units. The current (1985) price of a single new 20,000 gpm pumping unit with an electric driver is approximately $100,000. The same pump with a diesel driver costs approximately $300,000. In addition to being less expensive to purchase, the electric driven pumps have other important advantages over the diesel driven units. For example, they require less maintenance and they do not emit engine exhaust pollution in the operation area. The disadvantages are that an electric substation and transmission lines would be required for their operation and the system would be inoperable in the event of an electrical power outage.

The total one time cost of installing a thermokinetic system utilizing used jet engines at an assumed cost of 15 percent of their new price was estimated at $5 million (1975 U.S. dollars) [1]. Although a detailed cost analysis has not been performed for the large volume water spray method, its one time installation cost, even assuming all new hardware, should be considerably less than that for a thermokinetic system. Moreover, pumps and electric motors are much simpler to operate and maintain than jet engines. Coupled with the smaller fuel requirement, the annual operating costs should also be much less than encountered with a thermokinetic system.

The FAA report [1] showed that Los Angeles International Airport (LAX) would derive the highest benefit from the installation and operation of a thermokinetic fog dispersal system, although such a system could be cost effective at a few other major U.S. airports as well. The large volume water spray method should, therefore, also be cost effective at these same airports. Reluctance to install an operational system at LAX has been due in part to the considerable environmental air pollution which a thermokinetic system would introduce. As already noted, the water spray system circumvents this problem through the use of electric drivers for the pumps. In fact, the water spray technique actually cleans the air because pollutants in the fog are removed with the fog drops. The system has other advantages as well. When required by changes in wind direction, water can be redistributed to other parts of the runway perimeter by simple valving whereas redistribution of heat from the fixed position jet engines is more difficult. Perhaps the most important side benefit of the technique is the considerable emergency fire extinguishing capability it provides along the runway.

A diverted landing of the Space Shuttle to an alternate site due, for instance, to fog at the primary site, results in a five to seven day schedule slip for the next mission. Since a diverted landing from the primary KSC site to Edwards AFB, California, costs $1,800,000 (personal communication, Mr. Sam Beddingfield, Deputy Director, Shuttle Projects Management, Kennedy Space Center, Florida, 1985) and a launch delay costs approximately $500,000 per day, it is easily seen that an effective operational fog dispersal system could pay for itself in one or two fog events. Based on climatology data (NASA TM 82473, 1982, p. 4.30) the probability of precipitation or fog resulting in visibility less than 0.8 km (0.5 mile) is given by month and hour for the Kennedy Space Center (KSC), Florida, in Figure 6-1 and Vandenberg AFB (VAFB), California, in Figure 6-2. The afternoon incidence of low visibility at KSC is due to precipitation. Most other low visibility occurrences represented on both figures are due to warm fog. Note that the maximum probability of fog at KSC occurs in the winter months. Even at its maximum the fog probability for a given hour is less than 10 percent. In contrast the frequency of fog peaks in the summer months at VAFB and has a maximum probability in excess of 60 percent during the early morning hours of July and August.

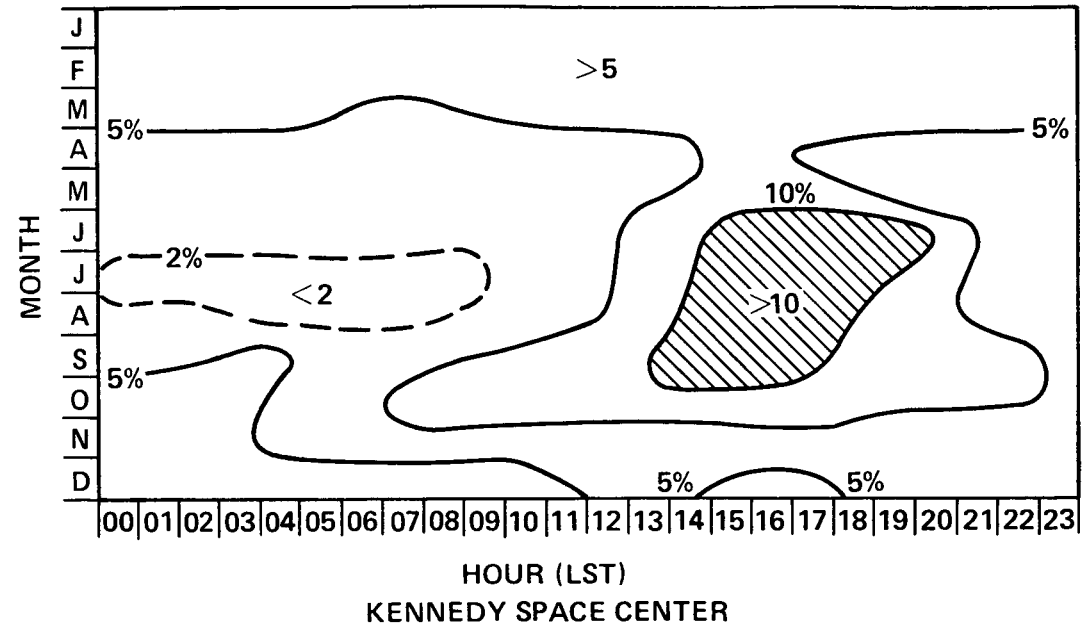

Figure 6-1. Probability of precipitation or fog at KSC with visibility < 0.8 km (0.5 mi.).

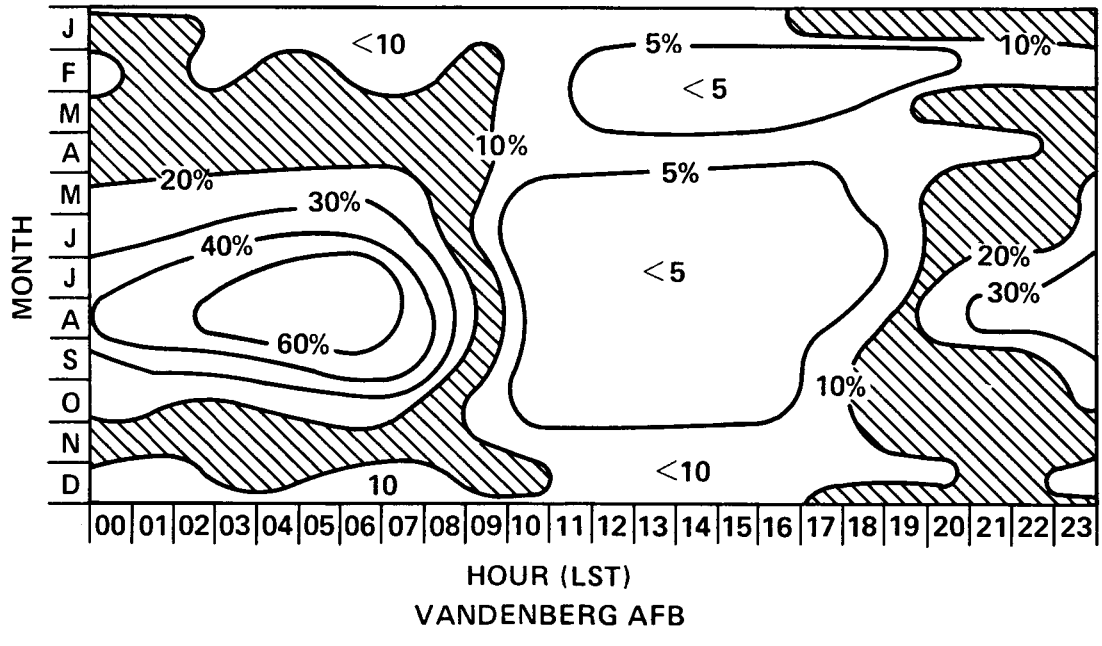

Figure 6-2. Probability of precipitation or fog at VAFB with visibility < 0.8 km (0.5 mi.).

7.0 CONCLUSIONS AND NEXT STEP RECOMMENDATIONS

The limited field test results reported in this document indicate that it is feasible to develop a large volume recycled water spray technique for warm fog dispersal. The technique was actually demonstrated in a natural fog situation. Utilizing measured spray drop spectra and natural fog droplet spectra obtained during these tests, the mathematical formulation for the fog droplet removal rate by a polydisperse spray distribution gives numerical results which confirm the field test observations. These results coupled with the anticipated system improvements indicate that the proposed technique will be feasible for large scale commercial use.

Several system design refinements to improve the efficiency of the technique can and should be explored further. Promising methods of reducing the mean spray drop size and thereby improving the fog removal efficiency include addition of a surfactant to reduce the surface tension and interspersing nozzles which produce smaller drops at a penalty in projection height within the array. When reducing the mean spray drop size it is important that a balance be achieved between the maximum fog sweepout for a fixed spray rate and the potential for the smallest spray drops to drift into the cleared volume. We have shown analytically that a factor of two reduction in surface tension should yield about a factor of two increase in visibility over an untreated spray. It remains to be shown experimentally that such a reduction in surface tension does in fact give smaller drops without substantially decreasing the projection height of the spray.

Analytical studies using Computational Fluid Dynamics (CFD) computer codes to investigate the effect of nozzle spacing and water flow rate on induced air circulation and thus the clearing efficiency should also be conducted. However, full characterization and verification of the technique under various natural fog conditions on a scale useful to Shuttle landing operations depends upon a large field test. If such a test is undertaken, the other agencies, such as the Air Force, Army, Navy, and FAA, which have an interest in fog dispersal or basic fog research, should be invited to actively participate. Considerable time (~18 months) would be required to prepare for such a test. The test should be conducted during the season of high fog probability (usually sometime between July and October for most suitable U.S. sites) at a high probability site to maximize test opportunities. Sufficient time to complete required system design refinements should be allowed between the Authority To Proceed (ATP) date and the test. A preliminary fog dispersal project outline is given in Appendix A9.0.

APPENDICES

A1.0 MIE EXTINCTION COEFFICIENT AND VISUAL RANGE

Mie scattering theory takes into account the size, shape, dielectric constant, and absorptivity of the scatterers. If the particle size is larger than or even the same order of magnitude as the wavelength of electromagnetic energy being scattered, then the special Rayleigh scattering case is inappropriate and the more general Mie theory must be used. This is the case for light scattering by fog droplets. The total extinction coefficient, σ, (sometimes called the extinction or attenuation coefficient) is composed of extinction due to both scattering and absorption.

$$\sigma = \sigma_{Scatt} + \sigma_{Absorp} \quad . \tag{A1.1}$$

For visible wavelengths, however, the index of refraction for water is approximately $1.33 + 10^{-8}$ i where i is the complex root. Since the complex portion of the refractive index is so small, absorption is very low and extinction is almost entirely due to scattering. Another simplification results from the fact that particles having the same ratio of particle circumference to wavelength have the same scattering properties. This ratio, α, given by

$$\alpha = \frac{2\pi r}{\lambda} \quad , \tag{A1.2}$$

is called the particle size parameter.

Although a single fog droplet has a cross-section πr^2, its extinction capability is higher than what would be expected from its geometric cross-section. In fact, its effective cross-section is higher by a factor K (or Q_S) called the extinction factor (or scattering efficiency or scattering area coefficient). The extinction cross-section (or scattering cross-section) for each droplet is then $K\pi r^2$ and the total cross-section is

$$\sigma = \pi \sum_{i=1}^{M} (K_i N_i r_i^2) \quad , \tag{A1.3}$$

where N is the fog droplet number concentration, r is the droplet radius, and the summation, Σ, is taken over all fog droplets. Figure A1.1 is a plot of the extinction factor K for scattering particles of refractive index 1.33 (water droplets) versus the particle size parameter, α, or alternatively against the particle radius, r, for three separate wavelengths of visible light ranging from the blue part of the spectrum (λ = 0.450 μm) to the red (λ = 0.650 μm). In the case of fog and visible wavelengths, the droplet size is usually sufficiently large, i.e., $r > 2$ μm, that $K \sim 2$ is a reasonable approximation. If this simplification is valid, the extinction coefficient can be expressed as

$$\sigma \sim 2\pi N \bar{r}^2 \quad , \tag{A1.4}$$

where $\bar{r}$ is the mean droplet radius. This is known as Trabert's formula.

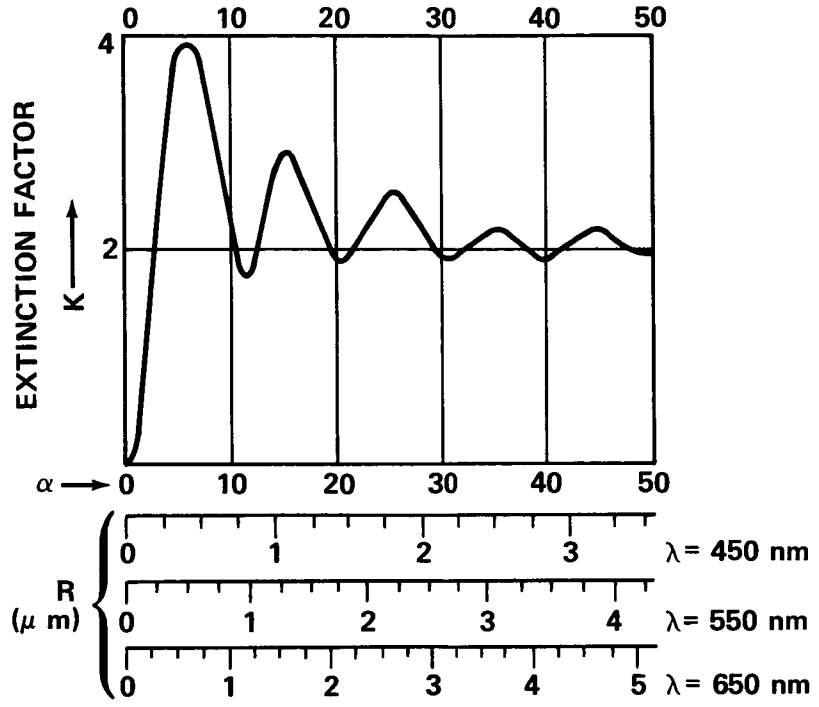

Figure A1-1. Plot of the extinction factor K for scattering particles of refractive index n = 1.33 (water drops).

The visual range, V_R, of objects seen against the horizon sky through an atmosphere having an extinction coefficient σ is

$$V_R = \frac{1}{\sigma} \ln(1/\epsilon) \quad , \tag{A1.5}$$

where $\epsilon = (B_h - B_o/B_h)$ is the threshold of contrast, B_h is the brightness of the background horizon and B_o is the brightness of the object. Since ϵ is dependent upon the visual acuity of the human eye, the actual value of this threshold will vary from observer to observer. Various laboratory and field experiments have yielded values of ϵ ranging from 0.008 to 0.06. For calculations of the meteorological visual range, $\epsilon = 0.02$ has been adopted as standard. Therefore, the standard visual range is given by

$$V_R = \frac{3.912}{\sigma} = \frac{3.912}{\pi \sum_{i=1}^{M} (K_i N_i r_i^2)} \quad . \tag{A1.6}$$

Since the liquid water content, LWC, of the fog is approximately given by

$$LWC \sim 4/3\ \pi\ N\ \bar{r}^3 \quad , \tag{A1.7}$$

and the density of water is assumed to be 1.0 g cm^{-3}, the simplified but sometimes useful formula for the standard visual range can be expressed using Trabert's formula as

$$V_R \sim \frac{3.912}{2\pi N \bar{r}^2} \sim \frac{2.61\ \bar{r}}{LWC} \quad . \tag{A1-8}$$

If the mean droplet radius, $\bar{r}$, is expressed in μm and the liquid water content, LWC, is given in g m^{-3}, the computed visual range has the units of meters. A similar relationship can be obtained relating V_R (m) to N (m^{-3}) and LWC (g m^{-3}):

$$V_R = 1.62\ N^{-1/3}\ LWC^{-2/3} \quad . \tag{A1.9}$$

It is important to keep in mind that equations (A1.4), (A1.7), (A1.8), and (A1.9) are approximate formulae, assuming as they do that all the droplets are of equal size. For a dense fog the liquid water content is approximately 0.2 g m^{-3} or greater. Using this value and a selection of mean droplet radii, some illustrative values for the droplet number concentration, the extinction coefficient, and the visual range have been computed and tabulated in Table A1-1.

TABLE A1-1. COMPUTED PROPERTIES FOR CONSTRUCT FOGS
(ASSUMES LWC = 0.2 g m^{-3})

	$\bar{r}$ (μm)				
	2.5	5	10	20	30
N (cm^{-3})	3060	380	48	6	1.8
σ (m^{-1})	0.12	0.056	0.030	0.015	0.010
V_R (m)	33	65	130	260	390

A2.0 FOG DROPLET REMOVAL BY A POLYDISPERSE SPRAY

The removal of fog droplets in a spray curtain is analogous to an aerosol washout problem. This problem has been discussed elsewhere in the literature (e.g., Beard [11]). Following Beard's formulation, the rate of loss of fog droplets to a polydisperse spray distribution can be determined from

$$\frac{dn}{dt} = -\left(\frac{\pi}{4}\right) n \int E\, U\, D^2\, N\, dD \quad , \tag{A2.1}$$

where n is the number per unit volume of fog droplets (assumed to have one characteristic size), E is the collection efficiency, U the terminal fall speed of the spray drops, D their diameter, and N the number of spray drops in the size interval dD. With the assumption of an exponential spray drop distribution [$N = dN'/dD = a \exp(-bD)$], and a standard terminal fall speed relation [$U = \gamma - \alpha \exp(-\beta D)$], the fractional loss of droplets [$F_D = (1/n)\, dn/dt$] is given by

$$F_D = -\left(\frac{\pi}{4}\right) \int E\, [\gamma - \alpha \exp(-\beta D)]\; D^2\, a \exp(-bD)\, dD \quad . \tag{A2.2}$$

The resultant loss integrated across the size distribution ($0 \leqslant D \leqslant \infty$) is

$$F_D = -\left(\frac{\pi E' a}{2}\right)\left(\frac{\gamma}{b^3}\right) f_1 \quad , \tag{A2.3}$$

where E' is the integral mean value of E and $f_1 = [1-(\alpha/\gamma)/(1 + \beta/b)^3]$. The spray volume flux can be evaluated from

$$Q/A = \left(\frac{\pi}{6}\right) \int U\, D^3\, N\, dD = \left(\frac{\pi}{6}\right) \int [\gamma - \alpha \exp(-\beta D)]\; D^3\; [a \exp(-bD)]\, dD \quad . \tag{A2.4}$$

Integrating from D = 0 to ∞ gives the volume flux for the polydisperse spray as

$$Q/A = \pi a \left(\frac{\gamma}{b^4}\right) f_2 \quad , \tag{A2.5}$$

where $f_2 = [1-(\alpha/\gamma)/(1 + \beta/b)^4]$. Dividing equation (A2.3) by equation (A2.5) to determine the fog droplet loss rate in terms of the volume flow rate (Q) gives

$$F_D = (1/n)\, dn/dt = -(E'Q/2A) b f_1/f_2 \quad , \tag{A2.6}$$

or

$$n = n_o \exp\left\{-\left[\left(\frac{E'Q}{2A}\right)\left(\frac{bf_1}{f_2}\right)\right] t\right\} \quad . \tag{A2.7}$$

Since A = Lut, then

$$n = n_o \exp\left\{-\left[\left(\frac{b}{2}\right)\left(\frac{f_1}{f_2}\right)\left(\frac{E'Q}{Lu}\right)\right]\right\} \quad , \tag{A2.8}$$

where u is the component of the wind velocity normal to the spray curtain and L is the length of spray curtain.

Standard values for the terminal velocity relation, applicable for drops having a diameter greater than 0.3 mm, are γ = 965 cm s^{-1}, α = 1030 cm s^{-1}, and β = 6 cm^{-1} [12]. An exponential fit can be made on the measured spray drop spectra to determine the value of b and thus permit evaluation of equation (A2.8).

A3.0 COLLISION, COALESCENCE, AND COLLECTION EFFICIENCIES

The concept of "collision efficiency" is used to describe the effect of hydrodynamic deflection of approaching drops on the collection rate. Simply, it is the probability that a larger drop will collide with a smaller one in its direct path. It is defined as the ratio of the actual collision cross section, πY_c^2, to the geometric cross section, $\pi(R+r)^2$, where Y_c is the initial horizontal separation of drop centers on a grazing trajectory; R is the radius of the larger drop and r is the radius of the smaller drop.

It is possible that colliding drops may bounce apart before surface contact is made, due to the presence of an air film trapped between their surfaces, or disrupt following a temporary union. The fraction of colliding drops that actually coalesce is termed the "coalescence efficiency." Disruption occurs if the surface energy for the coalesced drops is exceeded by the excess kinetic energy for an inelastic collision (e.g., see Beard et al. [13]) or the rotational kinetic energy [14, 15]. When disruption takes place satellite drops are produced for the more glancing interactions and disintegration of one or both drops occurs in more direct collisions [16]. The appropriate dimensionless energy parameters are functions of the collision Weber number (see Appendix A8.0) and the size ratio.

The net efficiency of the process, the collection efficiency, is given by the product of the collision and coalescence efficiencies. Being a sensitive function of the relative drop size as well as the surface energy, the collection efficiency fraction under these conditions can range from zero to unity.

Figure A3-1 [17] gives the calculated collision efficiency of freely falling drops as large as R = 500 μm with fog size droplets. The results of two-sphere hydrodynamics were used at R = 40, 50, and 60 μm [18]. Superposition hydrodynamics were used at R = 73 μm [19]. Large sphere hydrodynamics were applied at R = 100, 200, 300, and 500 μm [20] for 20°C and 1 atm. Collision efficiency values for drops as large as R = 3 mm have been calculated using large sphere hydrodynamics and are tabulated elsewhere [21]. Figure A3-1 along with the tabulated values for larger drops were used to produce Figure A3-2. This figure gives the theoretical collision efficiency (fraction) for a wide range of drop/droplet pairs.

Coalescence efficiencies which are a function of the relative drop size, the relative velocity, and the impact angle must be determined indirectly using measured collection efficiencies and theoretical collision efficiencies. Figure A3-3 gives the coalescence efficiency (fraction) determined empirically [17] for collector drops smaller than 500 μm and extrapolated to larger drops. These extrapolated values are less than the unity value of coalescence efficiency generally used for large drops [21].

Numerical values for the collision and coalescence efficiencies from Figures A3-2 and A3-3 were multiplied together to obtain the best estimate collection efficiencies shown in Figure A3-4. These collection efficiencies are used in computing the fog removal rate.

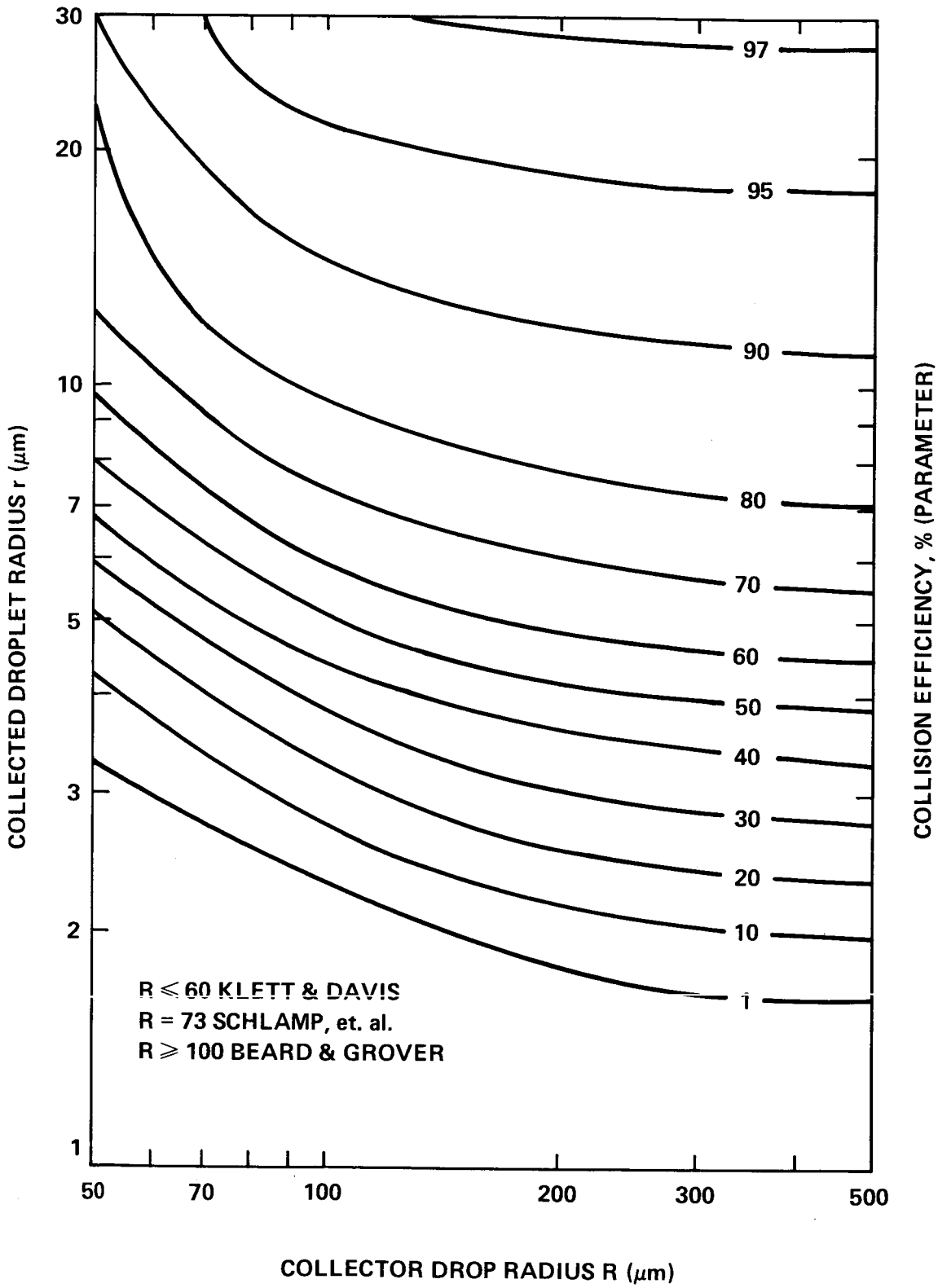

Figure A3-1. Theoretical collision efficiency (%) of freely falling water drops as large as 1 mm diameter for fog size droplets.

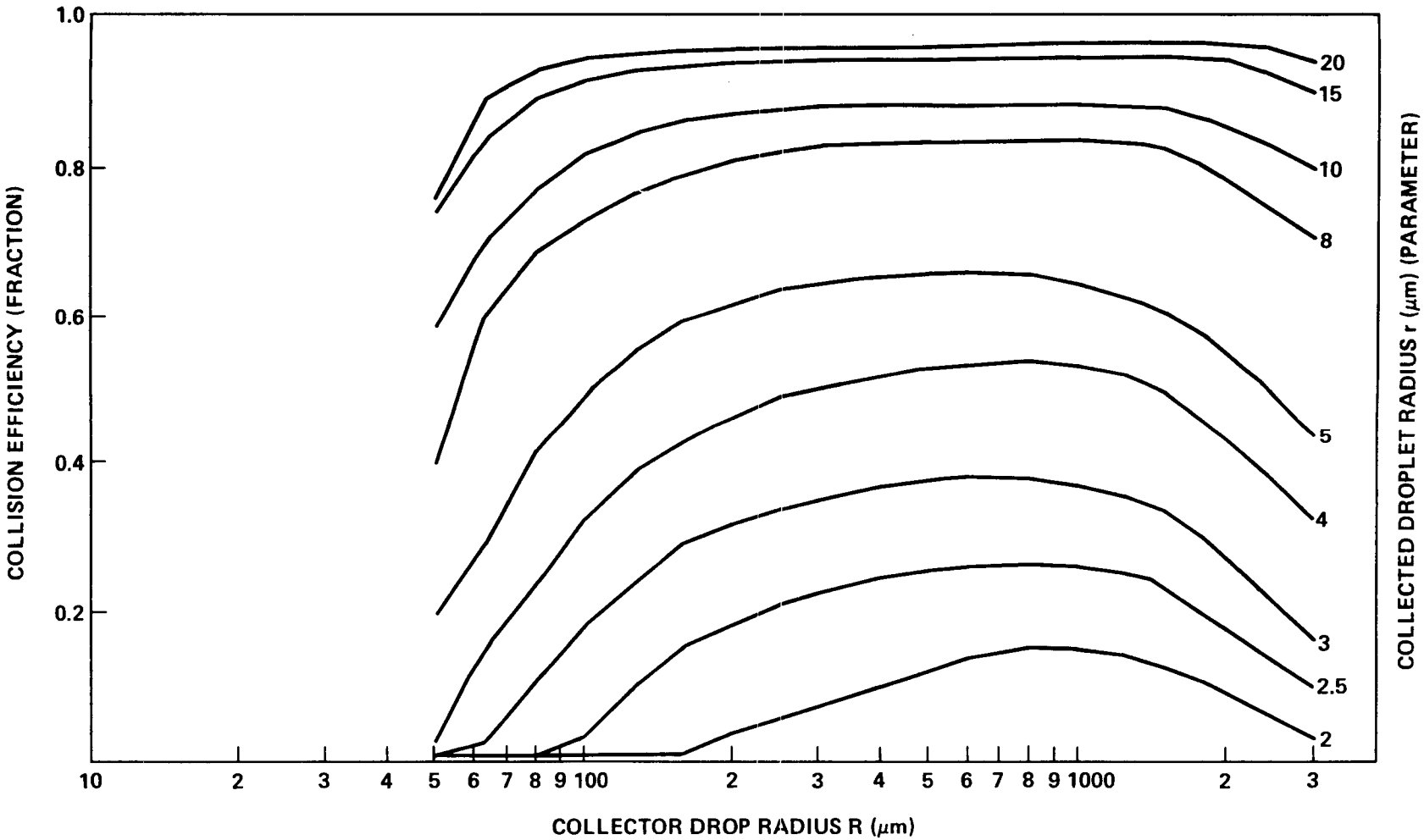

Figure A3-2. Theoretical collision efficiency (fraction) of freely falling water drops as large as 6 mm diameter for fog size droplets.

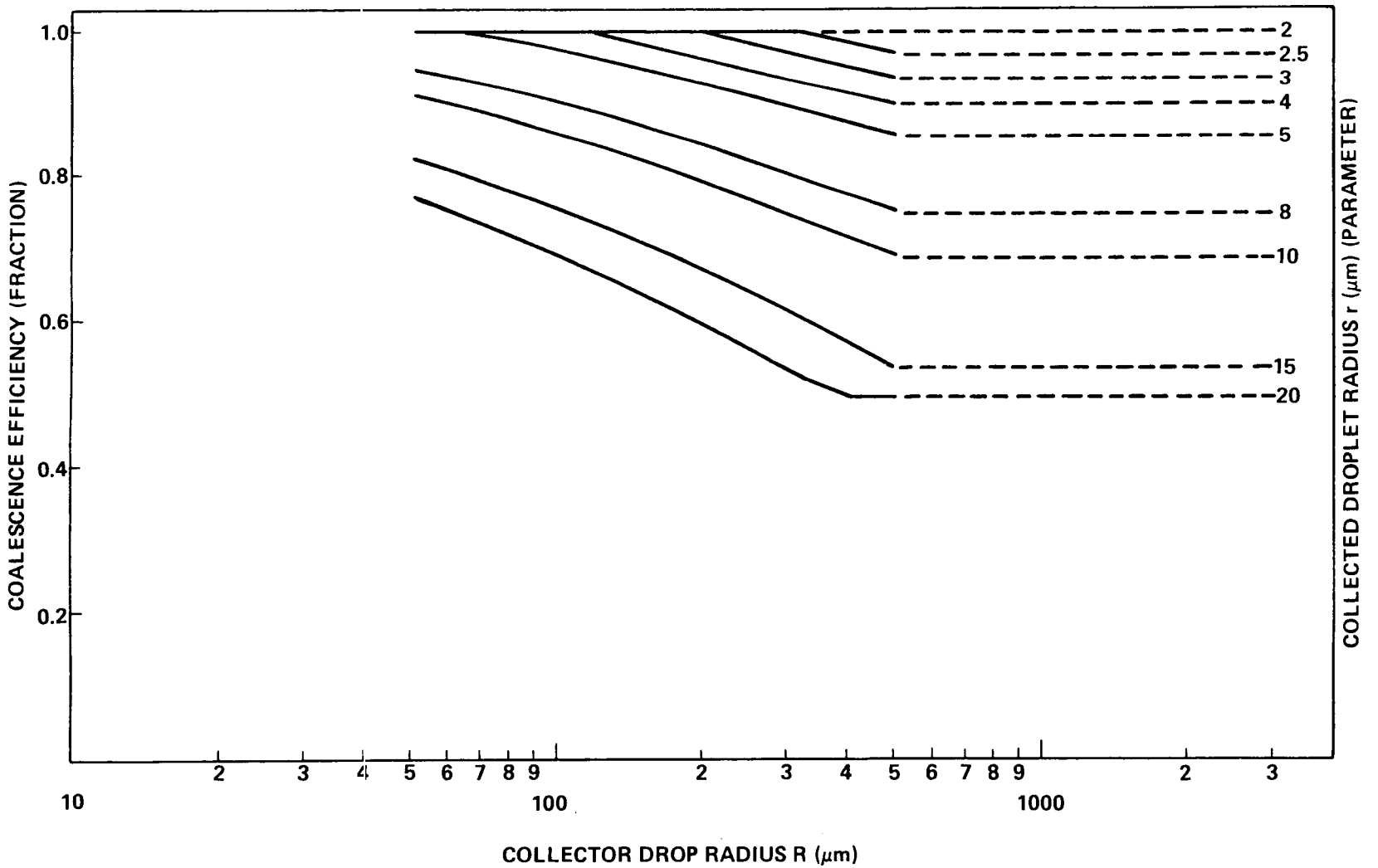

Figure A3-3. Empirically determined coalescence efficiency (fraction) for collector drops smaller than 1 mm diameter and extrapolated to larger drops.

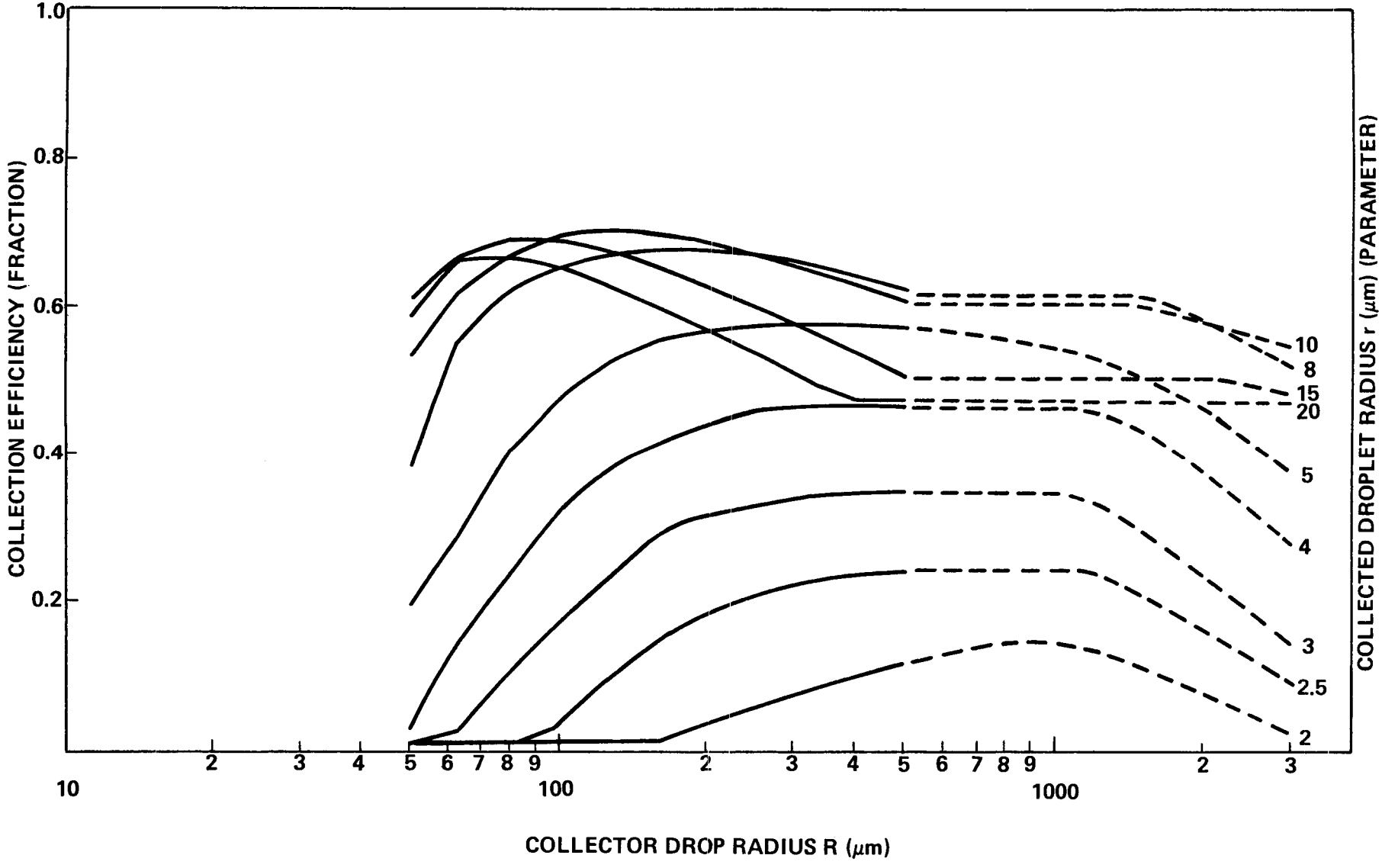

Figure A3-4. Best estimate collection efficiency (fraction) of freely falling water drops for fog size droplets.

A4.0 INSTRUMENTATION DETAILS

The instruments provided by the State University of New York (SUNY) for the October 1984 tests at MSFC are summarized in Table A4-1. In addition a Meteorology Research Inc. (MRI) Model 302 tipping bucket rain gauge was also provided. The magnetic switch was replaced with an infrared triggering system to eliminate spurious tips. Two spectrometer probes, OAP-230X (10 to 300 μm) and GBPP-100 (0.2 to 12.4 mm), were necessary to cover the complete spray size of interest. They, along with the rain gauge, were located near the extended end of the 7.5-m I-beam platform with all cables routed to a central data acquisition system located on the test stand. Two additional droplet spectrometers and two visibility meters were required to characterize fogs occurring during the test period. These droplet spectrometers were located at the 11-m level of the test stand in an area sheltered from the water spray produced during the single nozzle tests. The two forward scatter visibility meters were positioned, respectively, to the east and west of the multiple nozzle array which was located on the access road near the test stand. Figure A4-1, a schematic diagram, illustrates the operating principle of these two instruments. The location of these instruments relative to the test area is shown in Figure 4-1. This arrangement provided the best exposure for the instruments while permitting measurement of the residual spray from the nozzle array. Data and control signals from all these instruments were routed to the central data acquisition system. Data from the spectrometer probes were acquired over 1-min intervals with a Particle Data System which provided real time graphical displays of droplet/aerosol spectra, as well as providing an interface to a cartridge tape recording system. Other data, such as rainfall rates and visual range, were logged at the same location with a PDP-11/23 computer system. This computer was also used for post experiment analysis and verification of good drop spectra data. The visibility meter data were recorded at 30-sec intervals and displayed in real time.

Although initial tests of the single nozzles were conducted with the platform located at the 19-m level, most tests used the 11.5-m level. The precipitation probe (GBPP) was oriented with the long axis parallel to the water stream from the nozzle to minimize the cross axis sizing errors. The cloud droplet probe (OAP) with the attached aspirator and inlet horn was installed vertically to optimize the sampling of large droplets. The early tests were of short duration because the water spray entered the optical system of the probes preventing further measurements. In the case of the GBPP the problem was due to the nearly horizontal trajectory of some of the drops which allowed them to enter the optical system. Modification of the probe optical hoods corrected this problem but made it necessary to correct the measurements for the reduced sample area. This modification was employed during the remainder of the test program (October 19-25, 1984).

Use of the OAP in these tests was particularly difficult because of the conflicting requirement for uniform sampling and prevention of wetting of the probe optics. The initial vertical orientation provided the best sampling configuration but allowed water spray as well as drops resulting from splashing on the inlet horn to enter the probe and foul the optics. Alternate arrangements such as removal of the inlet horn and replacement with a short straight inlet proved equally unsatisfactory. During the last half of the test program, the probe with attached inlet horn was oriented horizontally with its axis perpendicular to the spray direction. While reducing the sampling efficiency at large droplet sizes, this change did permit sustained operation of the instrument.

The anticipated sampling problems due to the orientation of the OAP appear to have been less severe than expected. From the spectra shown in Figures 4-16 to 4-31, it can be seen that the measurements in the region of overlap of the OAP and GBPP are comparable. Some differences in the concentrations measured by the two probes may be due to sampling problems caused by the location of the drop spray. Because of the separation of the instruments and the narrow width of the spray, one or the

other of the instruments may have been momentarily outside of the main curtain of drops. Since the measurements were made outdoors, wind gustiness on some days made targeting and accurate characterization of the drop spectra difficult. In most cases, however, sufficient measurements were made to insure that representative spectra were obtained.

Tables A4-2, A4-3, and A4-4, respectively, give the size range and corrected sampling volume for the FSSP-100, OAP-230x, and GBPP-100 particle probes as a function of channel number. The FSSP and OAP sampling volume assume an aspirated constant velocity of 26 m s^{-1} and 13 m s^{-1}, respectively. The GBPP sampling volume assumes the drops are falling at their terminal fall speed. Figure A4-2 shows plots of one count in each channel for the two larger probes plotted variously as number concentration, surface area, and mass versus drop diameter. These plots can be used to check the adequacy of the total sampling volume for the measured drop spectra. It should be noted that drop flattening corrections applied to the GBPP data sometimes resulted in fractional counts per channel. Figure A4-3 graphically shows the drop flattening relationship which was applied to all the GBPP data in this report. The equivalent spherical diameter for each drop size is plotted versus the horizontal drop dimensions measured by the GBPP. The drop axis ratio (Γ) (vertical/horizontal) measured in heavy rainshowers [22] suggests that raindrops average about half the distortion of the equilibrium shape (Γ_o), that is $\Gamma \sim (1 + \Gamma_o)/2$. This is supposedly a consequence of the asymmetric oscillations [23]. Since energetic drop collisions and breakup are far more frequent in these water sprays than in the heaviest natural rainfall, it would not be surprising if the average axis ratio in the spray was closer to unity than to equilibrium. There is therefore some justification for not correcting the GBPP data for drop flattening. Nonetheless, to be consistent for comparison purposes with other published results, we have corrected the GBPP data for drop flattening.

The most notable consequence of uncertainty in sizing the largest drops is the effect on the mass distribution. We attempted to use the tipping bucket rainfall rate as a check on the GBPP derived value. For natural rainfall rates as high as 100 mm/hr, SUNY in the past has measured the ratio of the GBPP to tipping bucket rainfall rate to be as high as 3, especially under heavy rainfall conditions. Furthermore, due to the time required for the tipping bucket funnel to drain, the tipping bucket is limited to rainfall rates of less than 1400 mm/hr. Since the single nozzle water spray tests produced typical rates of 5,000 to 10,000 mm/hr the comparison could only be made for selected spectra.

TABLE A4-1. SUMMARY OF SUNY INSTRUMENTATION USED IN THE OCTOBER 1984 WATER SPRAY TESTS

Spectrometer Probes:

GBPP-100.....Ground Based Precipitation Probe
Particle Measuring Systems Inc.
Size Range 0.2 to 12.4 mm
Resolution 62 channels 0.2 mm width

OAP-230x.....Optical Array Probe
Particle Measuring Systems Inc.
Size Range 10 to 300 micrometers
Resolution 30 channels 10 um width

FSSP-100.....Forward Scatter Spectrometer Probe
Particle Measuring Systems Inc.
Size Range 0.5 to 47 micrometers
Resolution 60 channels (4 ranges) 0.5 to 3 um

ASASP-X.....Axial Scatter Spectrometer Probe
Particle Measuring Systems Inc.
Size Range 0.12 to 6 micrometers
Resolution 32 logarithmically spaced channels

Visual Range Instruments:

FOG-15.....Forward Scatter Meters (Two)
Wright and Wright Inc.
Range 100 feet to 100,000 feet

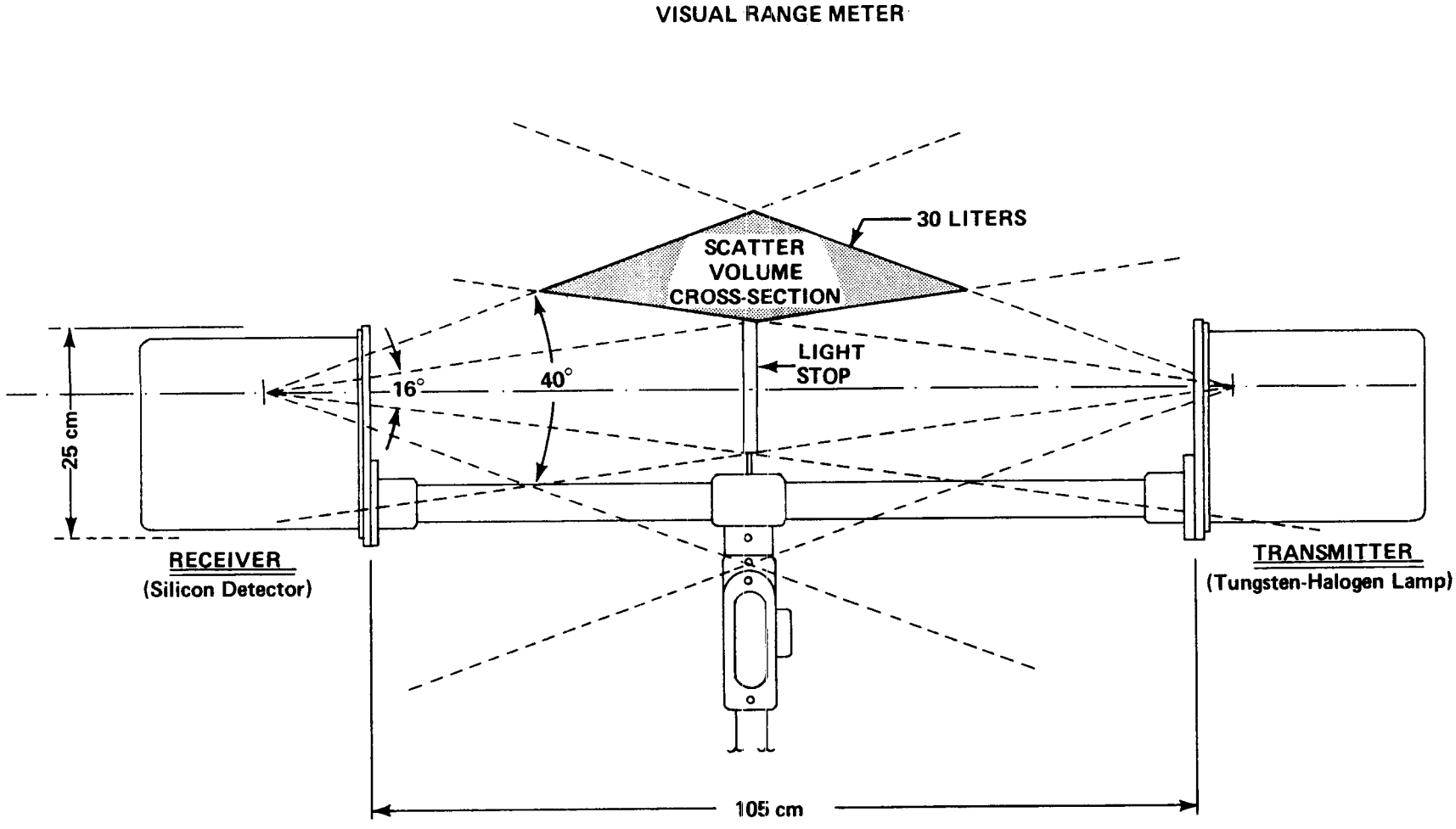

Figure A4-1. Schematic diagram which illustrates the operating principle of the Wright and Wright Fog-15 forward scatter visibility meters.

TABLE A4-2. SIZE RANGE AND CORRECTED SAMPLING VOLUME FOR THE FSSP-100 PARTICLE PROBE

FSSP-100 Channel number, size range and sample volume (for a 60 second sample)

Channel #	Size Range (um)	Sample Volume (cm^3)	Channel #	Size Range (um)	Sample Volume (cm^3)
1	2.0 - 5.0	5.424E+02	9	26.0 - 29.0	5.424E+02
2	5.0 - 8.0	5.424E+02	10	29.0 - 32.0	5.424E+02
3	8.0 - 11.0	5.424E+02	11	32.0 - 35.0	5.424E+02
4	11.0 - 14.0	5.424E+02	12	35.0 - 38.0	5.424E+02
5	14.0 - 17.0	5.424E+02	13	38.0 - 41.0	5.424E+02
6	17.0 - 20.0	5.424E+02	14	41.0 - 44.0	5.424E+02
7	20.0 - 23.0	5.424E+02	15	44.0 - 47.0	5.424E+02
8	23.0 - 26.0	5.424E+02			

TABLE A4-3. SIZE RANGE AND CORRECTED SAMPLING VOLUME FOR THE OAP-230x PARTICLE PROBE

OAP-230X Channel number, size range and sample volume (for a 60 second sample)

Channel #	Size Range (mm)	Sample Volume (m^3)	Channel #	Size Range (mm)	Sample Volume (m^3)
1	0.0071 - 0.0170	2.262E-05	16	0.1550 - 0.1650	7.384E-03
2	0.0170 - 0.0269	1.751E-04	17	0.1650 - 0.1750	6.892E-03
3	0.0269 - 0.0368	5.100E-04	18	0.1750 - 0.1850	6.400E-03
4	0.0368 - 0.0467	9.499E-04	19	0.1850 - 0.1950	5.907E-03
5	0.0467 - 0.0566	1.368E-03	20	0.1950 - 0.2050	5.415E-03
6	0.0566 - 0.0664	1.908E-03	21	0.2050 - 0.2150	4.923E-03
7	0.0664 - 0.0762	2.461E-03	22	0.2150 - 0.2250	4.430E-03
8	0.0762 - 0.0861	3.056E-03	23	0.2250 - 0.2350	3.938E-03
9	0.0861 - 0.0968	3.712E-03	24	0.2350 - 0.2450	3.446E-03
10	0.0968 - 0.1059	4.352E-03	25	0.2450 - 0.2550	2.954E-03
11	0.1059 - 0.1156	4.949E-03	26	0.2550 - 0.2650	2.461E-03
12	0.1156 - 0.1255	5.571E-03	27	0.2650 - 0.2750	1.969E-03
13	0.1255 - 0.1353	6.175E-03	28	0.2750 - 0.2850	1.477E-03
14	0.1353 - 0.1452	6.747E-03	29	0.2850 - 0.2950	9.845E-04
15	0.1452 - 0.1550	7.273E-03	30	0.2950 - 0.3050	4.842E-04

TABLE A4-4. SIZE RANGE AND CORRECTED SAMPLING VOLUME FOR THE GBPP-100 PARTICLE PROBE

GBPP-100 Channel number, size range and sample volume (for a 60 second sample)

Channel #	Size Range (mm)	Sample Volume (m^3)	Channel #	Size Range (mm)	Sample Volume (m^3)
1	0.142 - 0.340	6.526E-02	32	6.300 - 6.500	1.221E+00
2	0.340 - 0.538	4.623E-01	33	6.500 - 6.700	1.182E+00
3	0.538 - 0.736	6.718E-01	34	6.700 - 6.900	1.143E+00
4	0.736 - 0.934	8.640E-01	35	6.900 - 7.100	1.103E+00
5	0.934 - 1.132	1.029E+00	36	7.100 - 7.300	1.063E+00
6	1.132 - 1.328	1.154E+00	37	7.300 - 7.500	1.023E+00
7	1.328 - 1.524	1.253E+00	38	7.500 - 7.700	9.839E-01
8	1.524 - 1.722	1.337E+00	39	7.700 - 7.900	9.445E-01
9	1.722 - 1.936	1.415E+00	40	7.900 - 8.100	9.052E-01
10	1.936 - 2.118	1.475E+00	41	8.100 - 8.300	8.658E-01
11	2.118 - 2.312	1.523E+00	42	8.300 - 8.500	8.265E-01
12	2.312 - 2.510	1.565E+00	43	8.500 - 8.700	7.871E-01
13	2.510 - 2.706	1.597E+00	44	8.700 - 8.900	7.477E-01
14	2.706 - 2.904	1.619E+00	45	8.900 - 9.100	7.084E-01
15	2.904 - 3.100	1.634E+00	46	9.100 - 9.300	6.690E-01
16	3.100 - 3.300	1.641E+00	47	9.300 - 9.500	6.297E-01
17	3.300 - 3.500	1.641E+00	48	9.500 - 9.700	5.903E-01
18	3.500 - 3.700	1.637E+00	49	9.700 - 9.900	5.510E-01
19	3.700 - 3.900	1.625E+00	50	9.900 - 10.100	5.116E-01
20	3.900 - 4.100	1.609E+00	51	10.100 - 10.300	4.723E-01
21	4.100 - 4.300	1.589E+00	52	10.300 - 10.500	4.329E-01
22	4.300 - 4.500	1.566E+00	53	10.500 - 10.700	3.936E-01
23	4.500 - 4.700	1.540E+00	54	10.700 - 10.900	3.542E-01
24	4.700 - 4.900	1.510E+00	55	10.900 - 11.100	3.148E-01
25	4.900 - 5.100	1.477E+00	56	11.100 - 11.300	2.755E-01
26	5.100 - 5.300	1.445E+00	57	11.300 - 11.500	2.361E-01
27	5.300 - 5.500	1.409E+00	58	11.500 - 11.700	1.968E-01
28	5.500 - 5.700	1.373E+00	59	11.700 - 11.900	1.574E-01
29	5.700 - 5.900	1.337E+00	60	11.900 - 12.100	1.181E-01
30	5.900 - 6.100	1.299E+00	61	12.100 - 12.300	7.871E-02
31	6.100 - 6.300	1.259E+00	62	12.300 - 12.500	3.936E-02

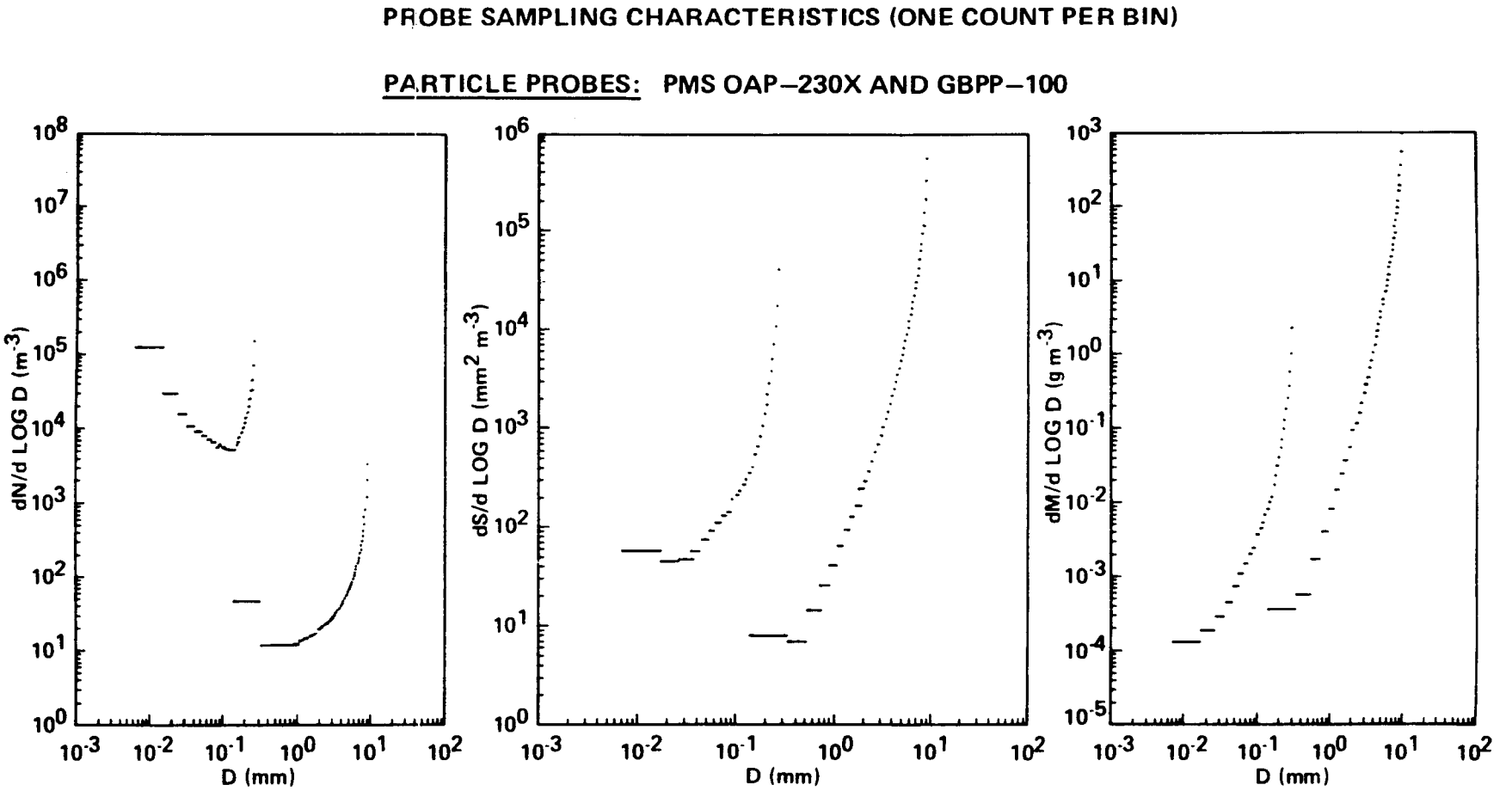

Figure A4-2.: Plots of one count in each channel (threshold values) for the two larger particle probes, OAP-230x and GBPP.

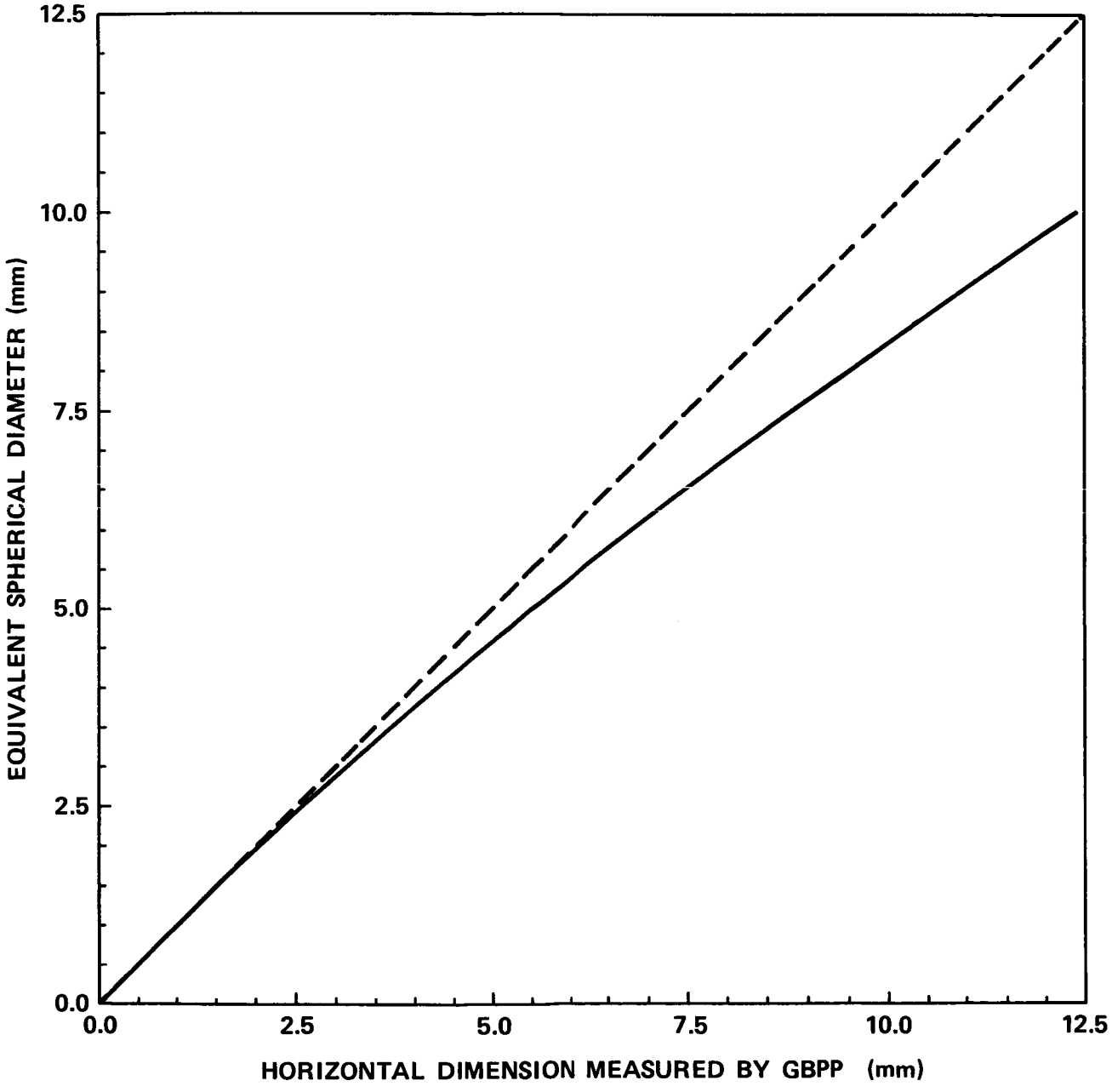

Figure A4-3. Drop flattening correction applied to all drop spectra from the Ground Based Precipitation Probe (GBPP). Dotted line gives one-to-one relationship for reference.

A5.0 COMPUTER CODE FOR FOG DROPLET WASHOUT

A numerical model was developed to evaluate the time dependent washout of fog by a polydisperse water spray. A copy of the FORTRAN program "WSHB" and an example of its output is included in this section. A brief explanation of critical variables, steps and equations used in the main program is also given.

Principal Equations

Visual range (meters): $VR = 0.03912 \{ 2\pi \Sigma [N(r) r^2] \}^{-1}$

Washout factor (sec^{-1}): $DF = (A1\pi/4) E \varepsilon U D^2 \Delta D \exp(-A2 D)$
where E is the collision efficiency, ε is the coalescence efficiency and the spray concentration is given by $A1 \exp(-A2 D) \Delta D$

Depleted concentration (cm^{-3}): $XN = N(I) \exp[-F(I) T]$

Main Program Variables
(in order of appearance)

D(15)	fog droplet diameter: 3.5, 6.5, 9.5, . . . , 39.5 μm
DB(16)	size category boundaries (μm) given in DATA statement
F(15)	washout factor in exponential depletion (sec^{-1})
N(15)	number concentration of fog droplets (cm^{-3})
NPU(15)	measured fog spectrum ($cm^{-3}\ \mu m^{-1}$), 10/24/84; 802:09 OAP data
LWC	liquid water content ($g\ m^{-3}$)
A1, A2	coefficients for exponential spray distribution
C	constant in washout equation
DD	spacing factor in logarithmic interval of spray sizes
RS	fog droplet radius (cm)
XK	exponent for calculating 10 per decade of spray drops
DL	spray drop diameter (cm)
D1, D2	size category boundaries (cm)
U	spray drop terminal velocity (cm/sec, Johnson's coefficients)
RL	spray drop radius (cm)
DF	washout factor for particular drop sizes
T	time (seconds)
SS	sum for extinction coefficient (cm^{-1})
SN	sum of the number concentration of fog drops (cm^{-3})
SL	sum of the liquid water content of fog drops ($g\ m^{-3}$)
XN	number of fog drops in category after washout (cm^{-3})
XNPU	dN/dD for fog drops in category after washout ($cm^{-3}\ \mu m^{-1}$)
VR	visual range (meters)

Main Program Steps

6	DATA NPU	initial fog spectrum ($cm^{-3}\ \mu m^{-1}$)
9	DATA DB	size category boundaries (μm)
17	CALL INITIAL	constants for coalescence efficiency subroutine
18	DO 1 I=1,22	LWC and concentration of initial fog spectrum
24	DO 3 I=1,22	outer loop -- fog drop size for washout factor
27	DO 2 J=1,17	inner loop -- spray drop size for washout factor
35	DF =	washout factor for particular size fog and spray drops
	E(U,RS,RL)	FUNCTION E is the collision efficiency
	EPS(RS,RL)	FUNCTION EPS is the coalescence efficiency
36	F(I) =	total droplet depletion factor from all spray drop sizes
39	DO 5 J=1,5	outer loop -- time from 0 to 4 seconds
43	DO 4 I=1,22	inner loop -- fog drop category for washout calculation
45	XN =	depleted fog drop concentration in category
55	VR =	visual range for depleted fog spectrum

```
      PROGRAM WSHB(INPUT,OUTPUT)
C  COMPUTES DEPLETION OF FOG BASED ON OAP DATA AT 802:09
      DIMENSION D(22),DB(23),F(22)
      REAL N(22),NPM(22),LWC
C  MEASURED FOG SPECTRUM NO. PER CC PER UM-DIAMETER INTERVAL
      DATA NPM/1.26,.359,.209,.115,.0574,.0153,.00381,.000760,.000529.
     *,.000277,.000188,.000109,.000099,.000030,0,0,.000014,0,0,0,0,0/
C  DIAMETER CATEGORY BOUNDARIES IN MICRONS
      DATA DB/7.1,17.,26.9,36.8,46.7,56.6,66.4,76.2,86.1,96.8,105.9,
     *115.6,125.5,135.3,145.2,155.,165.,175.,185.,195.,205.,215.,225./
      PI=2.*ASIN(1.)
C  CONSTANTS (A1,A2) FOR EXP SPRAY DROP DISTR CORRECTED FOR AXIS RATIO
      A1=.2760
      A2=7.4277
      C=.25*PI*A1
      DD=10.**.1
      CALL INITIAL
      DO 1 I=1,22
C  DROPLET CONCENTRATION (NO/CC) & MEAN DIAMETER IN CATEGORY (MICRON)
      N(I)=NPM(I)*(DB(I+1) - DB(I))
      D(I)=.5*(DB(I+1) + DB(I))
    1 CONTINUE
C  WASHOUT LOOP -- EXPONENTIAL FACTOR (1 SEC DEPLETION FACTOR)
      DO 3 I=1,22
      RS=.00005*D(I)
      F(I)=0.0
      DO 2 J=1,17
      XK=1. + 1.*J
      DL=.01*10.**(.1*XK)
C  LOG CATEGORIES OF SPRAY DROP SIZE (10 PER DECADE)
      D1=DL/DD
      D2=DL*DD
      U=961.8 - 1030.*EXP(-6.*DL)
      RL=0.5*DL
      DF=C*E(U,RS,RL)*EPS(RS,RL)*U*DL*DL*(D2-D1)*EXP(-A2*DL)
    2 F(I)=F(I) + DF
    3 CONTINUE
C  TIME LOOP TO GET OUTPUT (LWC, NO/CC, VIS RNG AND NO/(CC-UM))
      DO 5 J=1,5
      T=J-1
      SS=SN=SL=0.0
      PRINT 202
      DO 4 I=1,22
      RS=.00005*D(I)
      XN=N(I)*EXP(-T*F(I))
      SN=SN + XN
      LWC=(1./6E6)*XN*PI*D(I)**3
      SL=SL + LWC
      XNPM=XN/(DB(I+1) - DB(I))
      SS=SS + XN*RS**2
    4 PRINT 100,D(I),LWC,XN,SS,XNPM
      PRINT 102,SL,SN,SS
      PRINT 200
C      VISUAL RANGE (METERS)
      VR=.03912/(2.*PI*SS)
      PRINT 106,T,VR
    5 PRINT 200
      STOP
  100 FORMAT(F6.1,F12.6,F10.5,F11.9,F12.6)
```

```
  102 FORMAT("TOTALS  =",F10.6,F10.5,F11.9)
  106 FORMAT("TIME (SEC)= ",F4.2,"VISUAL RANGE (METERS) = ",F8.1)
  200 FORMAT(" ")
  202 FORMAT(" D(UM)   LWC(G/M3)    N(/CC)   SS(/CM)        DN/DD(/(CC-UM))")
      END
      FUNCTION E(U,RS,RL)
C  COLLISION EFFICIENCIES FROM BEARD AND GROVER (1974)
      REAL K,K0
      P=RS/RL
      RE=2*RL*U/.15
      IF(RE.LT.400)GOTO2
      K0=.21
      GO TO 4
   2  F=ALOG(RE)
      G=-.1007-.358*F+.0261*F**2
      K0=EXP(G)
   4  K=P*P*.998*RE/9./.0012
      Z=ALOG(K/K0)
      H=.1465+1.302*Z-.607*Z*Z+.293*Z**3
      IF(H .GT.0.0)GOTO          3
      YC0=0.0
      GO TO 1
   3  YC0=(2./3.1416)*ATAN(H)
   1  XX=YC0 + P
      E=(XX/(1.+P))**2
      RETURN
      END
      SUBROUTINE INITIAL
C  CONSTANTS FOR FUNCTION EPS
      COMMON  XN,B0,B1,C,E0
      XN=.44
      A0=+5.0740810
      A1=-5.9360579
      A2=+7.2737249
      A3=-5.2863216
      P=A2/A3
      Q=A1/A3
      A=(3.*Q - P*P)/3.
      E0=-P/3.
      C=(A**3)/27.
      B0=(2.*P*P*P - 9.*P*Q)/(2.*27.) + A0/(A3*2.)
      B1=-1./(A3*2.)
      RETURN
      END
      FUNCTION EPS(RS,RL)
C  COALESCENCE EFFICIENCIES FROM BEARD AND OCHS (1984)
      COMMON  XN,B0,B1,C,E0
      AS=RS*10000.
      AL=RL*10000.
      BETA=ALOG(AS*(AL/200.)**XN)
      B=B0 + B1*BETA
      A=SQRT(B*B + C)
      X=(A-B)**(1./3.) - (A+B)**(1./3.)
      EPS=X+E0
      IF(EPS.LT..5)EPS=.5
      IF(EPS.GT.1.)EPS=1.
      RETURN
      END
```

Washout Model Output
OAP fog data (10/24/84, 0802:09, spray off)
GBPP spray data (10/25/84, 1210:53, corrected for axis ratio)

D(μm)	LWC(g m^{-3})	N(cm^{-3})	Σ σ (cm^{-1})	dN/dD ($cm^{-3}\mu m^{-1}$)
12.1	.008182	8.93133	.000003242	.902154
22.0	.014101	2.54649	.000006309	.257221
31.9	.024880	1.47071	.000010039	.148556
41.8	.030606	.80323	.000013539	.081134
51.7	.028799	.39917	.000016202	.040320
61.5	.012793	.10504	.000017195	.010718
71.3	.004955	.02611	.000017527	.002664
81.2	.001470	.00525	.000017613	.000531
91.5	.001581	.00395	.000017696	.000369
101.4	.000958	.00176	.000017741	.000193
110.8	.000904	.00127	.000017780	.000131
120.6	.000689	.00075	.000017807	.000076
130.4	.000786	.00068	.000017836	.000069
140.3	.000297	.00021	.000017846	.000021
150.1	.000000	.00000	.000017846	.000000
160.0	.000000	.00000	.000017846	.000000
170.0	.000259	.00010	.000017853	.000010
TOTALS =	.131261	14.29604	.000017853	

TIME (SEC) = .50 VISUAL RANGE (METERS) = 348.7

D(μm)	LWC(g m^{-3})	N(cm^{-3})	Σ σ (cm^{-1})	dN/dD ($cm^{-3}\mu m^{-1}$)
12.1	.005858	6.39479	.000002321	.645939
22.0	.010103	1.82454	.000004519	.184297
31.9	.017685	1.04537	.000007170	.105593
41.8	.021593	.56669	.000009640	.057241
51.7	.020229	.28040	.000011510	.028323
61.5	.008962	.07359	.000012205	.007509
71.3	.003465	.01826	.000012437	.001863
81.2	.001027	.00367	.000012498	.000371
91.5	.001103	.00275	.000012555	.000257
101.4	.000668	.00122	.000012587	.000135
110.8	.000630	.00089	.000012614	.000091
120.6	.000480	.00052	.000012633	.000053
130.4	.000547	.00047	.000012653	.000048
140.3	.000207	.00014	.000012660	.000014
150.1	.000000	.00000	.000012660	.000000
160.0	.000000	.00000	.000012660	.000000
170.0	.000180	.00007	.000012665	.000007
TOTALS =	.092737	10.21338	.000012665	

TIME (SEC) = 1.00 VISUAL RANGE (METERS) = 491.6

D(μm)	LWC(g m^{-3})	N(cm^{-3})	Σ σ (cm^{-1})	dN/dD ($cm^{-3}\mu m^{-1}$)
12.1	.004195	4.57864	.000001662	.462489
22.0	.007239	1.30727	.000003237	.132048
31.9	.012570	.74305	.000005121	.075055
41.8	.015234	.39980	.000006863	.040384
51.7	.014210	.19696	.000008177	.019895
61.5	.006278	.05155	.000008664	.005260
71.3	.002423	.01277	.000008827	.001303
81.2	.000717	.00256	.000008869	.000259
91.5	.000770	.00192	.000008909	.000180
101.4	.000465	.00085	.000008931	.000094
110.8	.000439	.00062	.000008950	.000064
120.6	.000334	.00036	.000008963	.000037
130.4	.000381	.00033	.000008977	.000033
140.3	.000144	.00010	.000008982	.000010
150.1	.000000	.00000	.000008982	.000000
160.0	.000000	.00000	.000008982	.000000
170.0	.000125	.00005	.000008985	.000005
TOTALS =	.065524	7.29684	.000008985	

TIME (SEC) = 1.50 VISUAL RANGE (METERS) = 692.9

D(μm)	LWC(g m^{-3})	N(cm^{-3})	Σ σ (cm^{-1})	dN/dD ($cm^{-3}\mu m^{-1}$)
12.1	.003003	3.27829	.000001190	.331140
22.0	.005187	.93665	.000002318	.094611
31.9	.008935	.52815	.000003658	.053349
41.8	.010748	.28207	.000004887	.028492
51.7	.009982	.13836	.000005810	.013975
61.5	.004398	.03611	.000006151	.003685
71.3	.001694	.00893	.000006265	.000911
81.2	.000501	.00179	.000006294	.000181
91.5	.000537	.00134	.000006322	.000125
101.4	.000324	.00060	.000006337	.000065
110.8	.000306	.00043	.000006350	.000044
120.6	.000233	.00025	.000006360	.000026
130.4	.000265	.00023	.000006369	.000023
140.3	.000100	.00007	.000006373	.000007
150.1	.000000	.00000	.000006373	.000000
160.0	.000000	.00000	.000006373	.000000
170.0	.000087	.00003	.000006375	.000003
TOTALS =	.046300	5.21330	.000006375	

TIME (SEC) = 2.00 VISUAL RANGE (METERS) = 976.6

Parameters from Droplet Spectra

OAP data for 802:09

D(μm)	LWC(g m^{-3})	N(cm^{-3})	Σ σ (cm^{-1})	dN/dD($cm^{-3}\mu m^{-1}$)
12.1	.011428	12.47400	.000004528	1.260000
22.0	.019680	3.55410	.000008809	.359000
31.9	.035003	2.06910	.000014056	.209000
41.8	.043381	1.13850	.000019018	.115000
51.7	.040997	.56826	.000022808	.057400
61.5	.018262	.14994	.000024225	.015300
71.3	.007086	.03734	.000024700	.003810
81.2	.002105	.00752	.000024824	.000760
91.5	.002267	.00566	.000024942	.000529
101.4	.001374	.00252	.000025007	.000277
110.8	.001297	.00182	.000025063	.000188
120.6	.000990	.00108	.000025102	.000109
130.4	.001129	.00097	.000025143	.000099
140.3	.000428	.00030	.000025158	.000030
150.1	.000000	.00000	.000025158	.000000
160.0	.000000	.00000	.000025158	.000000
170.0	.000373	.00015	.000025168	.000015
TOTALS =	.185800	20.01126	.000025168	

VISUAL RANGE (METERS) = 247.4

OAP data for 809:34

D(μm)	LWC(g m^{-3})	N(cm^{-3})	Σ σ (cm^{-1})	dN/dD($cm^{-3}\mu m^{-1}$)
12.1	.003728	4.06890	.000001477	.411000
22.0	.008333	1.50480	.000003290	.152000
31.9	.018088	1.06920	.000006001	.108000
41.8	.024331	.63855	.000008784	.064500
51.7	.025070	.34749	.000011101	.035100
61.5	.013010	.10682	.000012111	.010900
71.3	.008872	.04675	.000012705	.004770
81.2	.006759	.02416	.000013103	.002440
91.5	.006042	.01509	.000013419	.001410
101.4	.003383	.00621	.000013578	.000682
110.8	.003739	.00526	.000013739	.000542
120.6	.002470	.00269	.000013837	.000272
130.4	.003004	.00259	.000013947	.000264
140.3	.002360	.00163	.000014027	.000165
150.1	.002672	.00151	.000014112	.000154
160.0	.000581	.00027	.000014130	.000027
170.0	.004476	.00174	.000014255	.000174
180.0	.001432	.00047	.000014293	.000047
190.0	.000607	.00017	.000014309	.000017
200.0	.000000	.00000	.000014309	.000000
210.0	.000000	.00000	.000014309	.000000
220.0	.001260	.00023	.000014336	.000023
TOTALS =	.140216	7.84451	.000014336	

VISUAL RANGE (METERS) = 434.3

Parameters from OAP Data on Spray
(10/25/84, 1210:53)

D (μm)	dN/dlnD (cm^{-3})	LWC ($g\ m^{-3}$)	N (cm^{-3})	$\Sigma\ \sigma$ (cm^{-1})	dN/dD ($cm^{-3}\mu m^{-1}$)
12.1	.270	.000216	.23574	.000000086	.023812
22.0	.170	.000432	.07802	.000000180	.007880
31.9	.140	.000742	.04387	.000000291	.004432
41.8	.120	.001089	.02859	.000000415	.002888
51.7	.090	.001248	.01730	.000000531	.001748
61.5	.130	.002528	.02076	.000000727	.002118
71.3	.120	.003135	.01652	.000000937	.001686
81.2	.067	.002290	.00818	.000001072	.000827
91.5	.120	.005629	.01406	.000001366	.001314
101.4	.080	.003918	.00719	.000001550	.000790
110.8	.070	.004363	.00613	.000001738	.000632
120.6	.075	.005653	.00616	.000001962	.000622
130.4	.065	.005674	.00489	.000002170	.000499
140.3	.060	.006120	.00424	.000002378	.000428
150.1	.050	.005782	.00327	.000002562	.000333
160.0	.040	.005363	.00250	.000002722	.000250
170.0	.037	.005600	.00218	.000002880	.000218
180.0	.030	.005091	.00167	.000003015	.000167
190.0	.020	.003781	.00105	.000003110	.000105
200.0	.010	.002095	.00050	.000003160	.000050
	TOTALS =	.070752	.50282	.000003160	

VISUAL RANGE (METERS) = 1970.5

A6.0 THERMAL RELAXATION TIME CONSTANT FOR DROPS

Suppose a water drop having an initial temperature, T_i, is released at some height, z, above the ground so that it falls through an incremental volume of air having a temperature, T_a, and a saturated water vapor density (absolute humidity) $\rho_s(T_a)$. Assume that this same volume of air contains N other water drops or fog droplets at the temperature T_a. As the drop falls through the volume, a distance, Δz, in a time, Δt, water vapor from the air condenses onto the drop if the drop temperature is initially colder than the air ($T_i < T_a$) or the water drop partially evaporates providing additional water vapor to the air if the drop temperature is initially warmer than the air ($T_i > T_a$). In this case a vapor density gradient $[\rho_s(T_i) - \rho_s(T_a)]$ exists, directed from the drop surface which is at higher temperature T_i and higher vapor density $\rho_s(T_i)$ to the air at T_a, $\rho_s(T_a)$. Subsequent evaporation decreases the mass of the drop so that it leaves the volume with a mass $(m_i - \Delta m_d)$; the subscript d denotes mass lost by diffusion.

Since the mass of water evaporated from the drop increases the vapor pressure of the air, a new vapor pressure gradient must be established between the water surfaces of the other drops and the surrounding air. In this case, the other drops grow in response to this vapor gradient until a new equilibrium condition between drops and air is achieved. Therefore, for $T_i > T_a$, the direction of water mass transfer is from the larger, faster falling, warmer water drops to the vapor, and then, from the vapor to the other smaller, slower falling, cooler water drops.

As the previously described large warm drop falls through an incremental volume it evaporates and cools due to the escape of the most energetic water molecules. This evaporative cooling is supplemented by direct heat conduction and convection losses to the air, as well as by collection of cooler drops through the coalescence process. Hence, there is a net transfer of both heat and water vapor from the evaporating drop to the air. This excess water vapor then recondenses onto the other cooler drops within the incremental volume. The water vapor condensing on these remaining drops releases latent heat of condensation in proportion to the quantity of vapor deposited resulting in a slight temperature increase for each of these drops. With continued fall into successive volume elements the drop temperature approaches the temperature of the air with a relaxation time constant characteristic for its size. Figure A6-1 illustrates the net transfer of water vapor as a function of drop fall distance for both the case where the spray drops are initially warmer than the ambient air and the case where they are colder than the air. Up (down) arrows indicate net transfer of water vapor from (to) that particular size spray drop or fog droplet. It should be noted that the distance required for water drops falling in air to approach their terminal fall speed is primarily a function of drop size. When released from rest under atmospheric conditions of P = 700 mb and T = 10°C drop diameters of 200, 400, 600, 800 μm, 1.0 mm, 2.0 mm, and 4.0 mm assume 99 percent of their terminal fall speed within a distance 0.18, 0.90, 2.1, 3.6, 5.4, 12.6, and 19.8 m, respectively [24].

The thermal relaxation time constant for water drops falling freely through air [25] is given by

$$\tau = \frac{R^2 \rho_L c_p}{3[K + L D (d\rho/dT)_s] [f]} , \qquad \text{(A6.1)}$$

where

R = drop radius (cm)

ρ_L = density of liquid water = 1 g cm^{-3} for water

c_p = specific heat of the drop = 1 cal g^{-1} $°C^{-1}$ for water

K = thermal conductivity of air = 6.05 x 10^{-5} cal cm^{-1} s^{-1} $°C^{-1}$ at +15°C

L = latent heat of condensation = 588.9 cal g^{-1} at +15°C

D = diffusivity of water vapor in air = 0.249 cm^2 s^{-1} at +15°C and 1000 mb

$(d\rho/dT)_s$ = the mean slope of the saturated vapor density = $\dfrac{\rho_s(T_{drop}) - \rho_s(T_{air})}{(T_{drop} - T_{air})}$.

f = the "ventilation factor" for mass transfer .

In the formulation of Kinzer and Gunn

$$f = [1 + F(N_{Sc}N_{Re}/4\pi)^{0.5}]$$

where

F = non-dimensional number given by Kinzer and Gunn

N_{Re} = Reynolds number = $\dfrac{2\,R\,U}{\nu}$.

where R is the drop radius, U is the drop velocity, and ν = 0.148 cm^2 s^{-1} is the kinematic viscosity of air at +15°C and 1000 mb, N_{Sc} = Schmidt number = ν/D, where ν and D are the kinematic viscosity and water vapor diffusivity, respectively.

The values of the non-dimensional "ventilation coefficient," F, given by Kinzer and Gunn were only approximate. More applicable values for the "ventilation factor," f, are obtained from the formulas [26,27]

$$f = 1 + 0.091\ N_{Re} \qquad \text{(for small drops } D \leqslant 120\ \mu m)$$

and

$$f = 0.78 + 0.275\ (N_{Re})^{0.5} \qquad \text{(for large drops } D > 120\ \mu m) \quad .$$

The calculations which follow use these latter values.

C.2

As an example, assume a large warm water drop having a temperature of +25°C is suddenly injected into an environment where the air temperature is +15°C. The time required for the drop temperature to change from 25°C to 18.7°C, i.e., a change of 63 percent of 25°C minus 15°C is given by equation (A6.1). If the equivalent drop diameter is 4.0 mm then the terminal fall speed is 8.8 m s^{-1}, f~ 14 and

$$(d\rho/dT)_s = \frac{\rho_s(T = 25°C) - \rho_s(T = 18.7°C)}{(25.0°C - 18.7°C)} = 1.116 \times 10^{-6} \text{ g cm}^{-3} \text{ °C}^{-1} \quad .$$

The time constant for a 4.0 mm drop is then $\tau \sim 4.2$ sec. Similarly, 3.0, 2.0, and 1.0 mm diameter drops have time constants of 2.8, 1.7, and 0.7 sec, respectively. Of course four time constants are required for a drop to assume 98 percent of the temperature of the environment. These relaxation times apply regardless of the magnitude of the initial temperature difference between the drop and the air. If sweepout of smaller drops through the coalescence process is considered, these relaxation times are somewhat shorter.

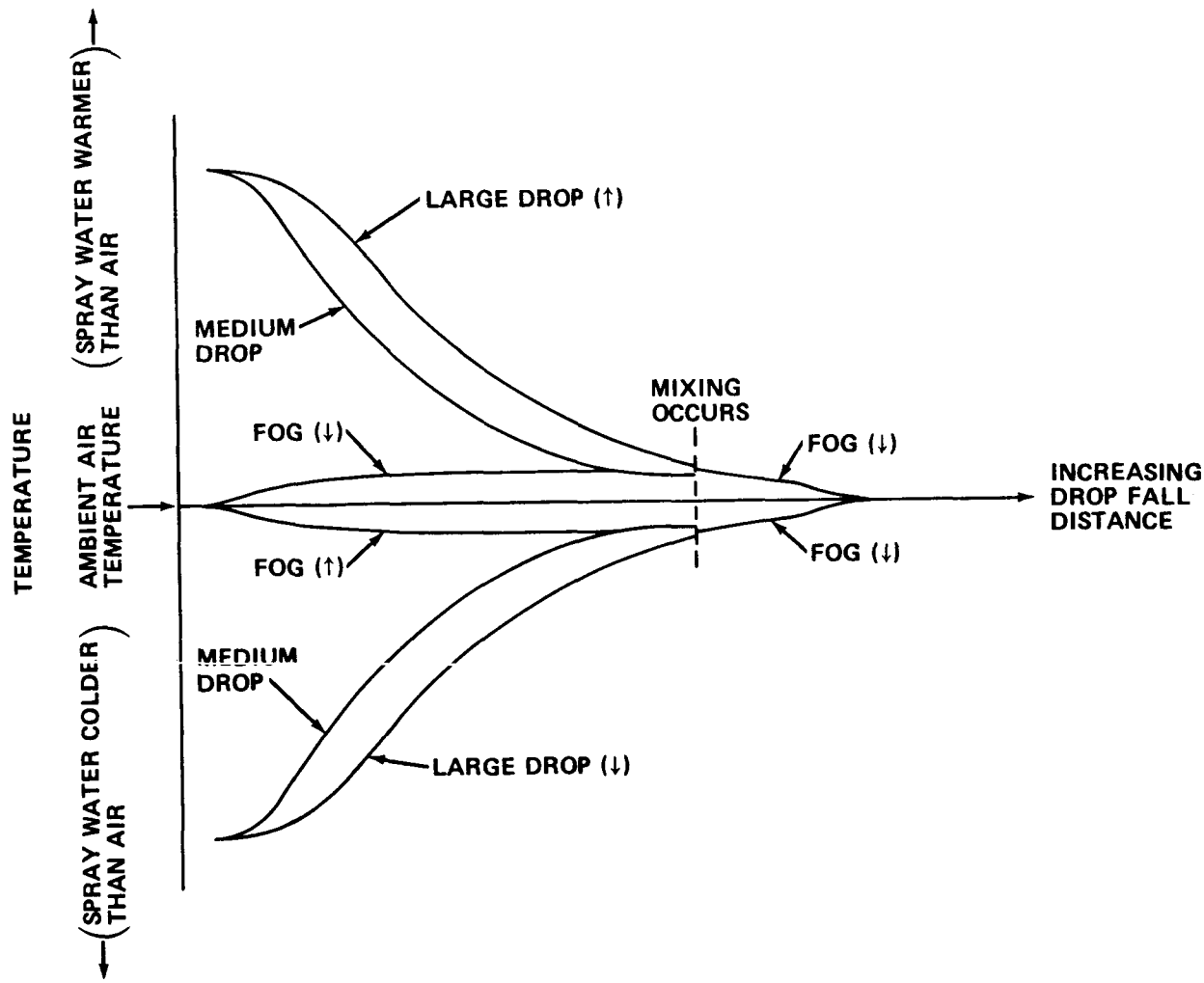

Figure A6-1. While falling spray drops are relaxing to the ambient air temperature net transfer of water vapor takes place. Up (down) arrows indicate net transfer from (to) a particular size drop.

A7.0 WATER PARTITIONING: VAPOR, SPRAY, FOG

The mass of water evaporated from the falling water spray drops before they achieve thermal equilibrium can be approximated using the equation

$$dm/dt = -(4\pi Rf)\ D\ [\rho_s(T_{drop}) - \rho_s(T_{air})] \qquad (A7.1)$$

where

R = equivalent spray drop radius (cm)

f = the "ventilation factor" for mass transfer (see Appendix A6.0)

D = diffusivity of water vapor in air

$\rho_s(T_{drop})$ = the saturated vapor density at the drop temperature

$\rho_s(T_{air})$ = the saturated vapor density at the air temperature

and the negative sign indicates evaporation.

Assume that initially the drop temperature is 20°C and the air temperature is 16°C as in the observed natural fog case. For R = 2 mm (the approximate "effective" mean radius of the curtain spray drops used in the MSFC field tests), $N_{Re}^{0.5} \sim 49$, $\rho_s(T_{drop}) = 17.30$ g m^{-3}, $\rho_s(T_{air}) = 13.63$ g m^{-3}, D = 0.25 cm^2 s^{-1}, and $dm/dt = -3.2 \times 10^{-5}$ g s^{-1}. As was seen in Appendix A6.0 the thermal response time constant for this large a drop is about 4.2 sec. Therefore, as a first approximation, a single drop loses a mass $dm = (3.2 \times 10^{-5}\ g\ s^{-1})(4.2\ s) = 1.3 \times 10^{-4}$ g. Since the original drop mass was $m = 4/3\ \pi\ R^3\ \rho_L = 3.3 \times 10^{-2}$ g, the percentage of change in drop mass due to evaporation is

$$dm/m \times 100\% = 1.3 \times 10^{-4}/3.3 \times 10^{-2} = 0.4\% \ .$$

Applying this same percentage change to all the spray water implies a loss rate of 25 l s^{-1} (400 gpm) per 6300 l s^{-1} (100,000 gpm) of spray. Of course, the actual amount of water spray converted to vapor can not exceed that amount corresponding to saturated air at the final mean temperature of the air. However, water can be transferred from large warm drops to smaller cooler drops within the spray curtain by this mechanism as discussed in Appendix A6.0. For this temperature (16°C) the saturated air contains 13.6 g m^{-3} of water vapor. For a clearing volume of 10^7 m^3 this implies a total of 1.36×10^5 liter (36,000 gallons) of water in the form of vapor initially. For typical wind speeds, i.e., 1 to 2 m s^{-1}, a clearing volume of this size would be replaced with advected air roughly once per minute. Since a typical fog has a liquid water content of about 0.1 g m^{-3} this same clearing volume would have contained 10^3 liter (260 gallons) of water in the form of fog droplets.

A8.0 SURFACTANT/SURFACE TENSION EFFECTS

This section addresses the potential for improving the fog washout process by reducing the surface tension of the spray water through the addition of a surfactant. It deals with the reduced surface tension effects on the spray drop size spectrum, on the collection efficiency, and, finally, on the fog washout rate and resultant visibility improvement.

The surface tension of falling spray drops determines the shape and thereby the terminal velocity of the drops; that is, the ratio of surface tension forces to hydrodynamic forces determines the sphericity of the drop. Water drops falling at terminal velocity are nearly perfect spheres if d_o, the diameter of the equivalent volume sphere, is less than about 280 μm ($N_{Re} < 20$). Above this size the hydrodynamic forces begin to deform the drops slightly so that they resemble oblate spheroids. The ratio of minor to major axis, d_v/d_h, is about 0.98 for millimeter sized drops, $N_{Re} \sim 260$, and it decreases to 0.85 as the diameter increases to 2.8 mm. At this point the Reynolds number is of order 1.4×10^3 and the drop begins to flatten on the bottom. As the size is increased the flattening becomes more pronounced and a concave depression develops in the base of the drop. If the size is increased further, the concavity deepens until at some critical point the drop becomes hydrodynamically unstable and breakup occurs. At breakup the concavity expands explosively into a thin bubblelike surface which ruptures into many small drops. The portion of the drop surrounding the concavity forms a ring-like structure which breaks up into a few large drops. For water in still air the critical (equivalent sphere) diameter is about $d_o = 9$ mm [24].

For falling, non-interacting drops the ratio of the aerodynamic pressure of distortion to the intrinsic pressure is given by the dimensionless Weber number, N_{We}. The Weber number is a measure of the relative strength of the aerodynamic pressure difference across a drop in separated flow ($\sim 0.5\ \rho_a\ U^2$) to an internal opposing pressure from Laplace's equation for mechanical equilibrium for a curved surface ($\sim 2\ \sigma/R_o$). Instability results from exposure to an external pressure increase from air blast, or for interacting drops, an external pressure increase from collisions ($\sim 0.5\ \rho_L\ \Delta U^2$). In these equations, ρ_a is the density of the air, U the terminal fall speed of the drop, σ its surface tension, R_o the radius of the equivalent volume sphere, ρ_L the density of water, and ΔU the change in drop speed due to a collision.

Since for the plain deluge nozzles the primary drop forming mechanism is aerodynamic breakup, it would appear that a reduction in the liquid surface tension should result in production of smaller drops. As was discussed earlier, smaller drops have higher collection efficiencies for fog droplets as well as represent a much larger total collecting surface area for the same mass of spray water. Therefore, reducing the surface tension should result in increased fog washout.

This effect can be quantified by developing the mathematical expressions for conservation of mass and energy flux of the untreated and treated water sprays. The spray mass flux per size interval is U M N dD. Hence, the assumption that the mass flux is unchanged by the effect of a surfactant (consistent with constant input mass flux Q/A), leads to a relation between untreated and treated spray given by

$$a \int U\ D^3 \exp(-bD)\ dD = a' \int U\ D^3 \exp(-b'D)\ dD \quad .$$

Note that all symbols have the same definitions as given in Appendix A2.0. The prime indicates the corresponding parameter for the treated spray.

At a given height the gravitational potential energy is fixed and the kinetic energy flux is determined by the assumptions of constant mass flux and constant terminal fall speed. Thus, a constant energy flux for untreated and treated spray is found from the surface energy fluxes as

$$\sigma\, a \int U\, D^2 \exp(-bD)\, dD = \sigma'\, a' \int U\, D^2 \exp(-b'D)\, dD \quad .$$

Values of a' and b' for the spectrum of treated spray can be determined from the two conservation equations resulting in $a' \sim 16a$ and $b' \sim 2b$ for $\sigma' = \sigma/2$.

Integration of the flux conservation equations (for D = 0 to ∞), results in $f_2 a/b^4 = f'_2 a'/b'^4$ for mass flux, and $f_1 a/b^3 = f'_1 a'/b'^3$ for energy flux so that

$$b' = (\sigma/\sigma')b(f_1/f_2)(f'_2/f'_1) \quad .$$

Since the fractional loss of fog droplets [$F_D = (1/n)dn/dt$] at a constant volume flow rate is $F_D = -(EQ/2A)bf_1/f_2$, the effect of surface tension can be estimated from

$$F_D'/F_D = (E'b'/bE)(f_2/f_1)(f'_1/f'_2) = (E'/E)(\sigma/\sigma') \quad .$$

Thus, the enhancement of fog washout for $\sigma' = \sigma/2$ assuming the collection efficiency (E) is unaffected by the change in surface tension is simply $F_D' = 2F_D$, i.e., halving the surface tension doubles the fog washout.

It is important to know the accuracy of the assumption that the collection efficiency is unaffected by the change in surface tension. A simple estimate of the altered size distribution on collection efficiency can be made using the effective drop size as determined in Section 5.0. The effective drop size was found to be R = 2.2 mm (based on the measured water spray spectrum). The result for a surface tension altered to $\sigma' = \sigma/2$ is R' = 1.1 mm. Thus, the effective collection efficiency changes from E(R) to E'(R'). Both the collision (E) and coalescence (ϵ) efficiencies may be appreciably altered in such a size change, so the collection efficiency ($E = E\epsilon$) must be considered in two separate aspects. Also, the coalescence efficiency may be directly affected by a change in surface tension.

For simplicity consider R = 2 and R' = 1 mm and fog droplets of r = 5, 10, and 20 μm. The collision efficiencies for 2 mm are E = 83, 96, and 98 percent, and for 1 mm are E' = 80, 95, and 98 percent [20]. Thus, it is a good assumption to treat the collision efficiencies as constant for this problem.

The coalescence efficiency (ϵ) has not been measured for these sizes – nor has the collection efficiency (E). However, measurements have been made for R $\sim$ 0.05 to 0.5 mm and r $\sim$ 10 to 20 μm for freely falling drops [28, 29], and for R $\sim$ 0.5 to 1.8 mm and r = 35 μm with the large drop suspended on the end of a capillary tube [30].

The results of the two studies are quite contradictory (although the size ranges do not overlap). The free fall studies indicate a strong decrease in the coalescence efficiency as the sizes R and r increase,

whereas the capillary study shows a decrease in the coalescence efficiency only with r. The semiempirical formula from the capillary experiment is $\epsilon = (1+r/R)^{-2}$, so that $\epsilon = 1$ for the sizes considered here.

Extrapolation of the free fall findings using the formula given in Beard and Ochs [17], results in ϵ = 71, 48, and 25 percent for R = 2 mm, and ϵ' = 80, 60, and 32 percent for R′ = 1 mm (both for r = 5, 10, and 20 μm). Thus, the effect of a reduced mean size from a surfactant (where $\sigma' = \sigma/2$) is to increase the coalescence efficiency by about 25 percent for larger fog droplets. This increases the collection efficiency by a comparable amount since $E \sim \epsilon$ and results in a surfactant enhancement of washout for large fog droplets given by

$$F'_D = (E'/E)(\sigma'/\sigma)F_D = (1.25)(2)F_D = 2.5F_D \quad .$$

However, this result does not include any direct effects of surface tension on the coalescence efficiency.

An assumption that has proven useful in scaling the coalescence efficiency is to make use of the fact that $\epsilon = \epsilon$ (R, N_{We}), i.e., the coalescence efficiency is the same as long as the collector drop radius and the Weber number are the same [31]. Thus, the direct effect of surface tension can be estimated using $N_{We}'/N_{We} = \sigma/\sigma'$ (i.e., R and therefore U are fixed).

The efficiencies given earlier in this section for R′ = 1 mm are adjusted from the original Weber number to a higher one given by $N_{We}' = 2\,N_{We}$. The altered efficiencies are obtained at R = 1 mm and a droplet size of 2r (to yield twice the Weber number at fixed surface tension). Estimates of these efficiencies are ϵ = 60, 32, and 15 percent for r = 5, 10, and 20 μm. This is a reduction in efficiency of about 32 percent for large fog droplets when compared to the spray unaffected by surfactant (i.e., where ϵ = 71, 48, and 25 percent).

The increase in coalescence efficiency which results from the surfactant induced decrease in mean size of the spray spectrum tends to be compensated by the decrease in coalescence efficiency from the direct influence of surface tension. This conclusion is based on extrapolation of semiempirical results from data on freely falling drops with R < 0.4 mm. The alternative experiment (with a capillary supported large drop and r = 35 μm) also leads to a similar conclusion for a weak effect of surfactant on coalescence efficiency since $\epsilon \sim 1$. However, this conclusion is also based on extrapolation. Thus, the findings in this section are somewhat uncertain with regards to the coalescence aspect of the collection efficiency and the resultant dependence of E on surface tension. At this stage it is reasonable to treat the collection efficiency as constant when assessing fog washout by spray drop distributions affected by a surfactant.

Recall from Section 5.0 that model calculations based on the "measured" water spray drop distribution showed that the visual range in the fog increased to a range of 430 m in 0.82 sec of washout. Model calculations were made using a hypothetical spray drop distribution treated with surfactant to reduce the surface tension to one half its original value. Figure A8-1 shows the increase in visual range with time for fog removal by untreated and treated spray. The lower curve is that for the untreated spray. The upper curve is that for the treated spray. The visual range for the treated spray is 430 m after 0.45 sec of washout. It takes only one half the time to achieve the same increase in visual range using the treated spray as it does using the untreated spray. The visual range increases considerably for washout by the treated spray in a comparison at the same processing time. At 1 sec the range is increased by a factor of 1.8 (from 490 to 860 m). At 2 sec the range is increased by a factor of 2 (from 970 m to 1900 m). This finding indicates that a surfactant treated spray may improve fog removal significantly

since it could greatly enhance visibility for the available processing time. The most important model findings are a 50-percent reduction in the local clearing time from the effect of surfactant and a significantly improved visibility for a fixed washout time over the untreated spray (a factor of about 2).

The effect of surfactant concentration on surface tension has been briefly considered for 1-decanol [32]. This substance is a simple chain alcohol (CH_3 based) with a boiling point of 229°C and a density of 0.83 g cm^{-3}. The quantity of 1-decanol needed to achieve a 50 percent reduction in surface tension is about 24 mg L^{-1}, i.e., about 25 gallons per 1,000,000 gallons of water. (In contrast, the more complicated compound, lauryl sulfonic acid, requires 20 times the concentration to achieve the same effect.] Alcohol chains longer than 1 decanol achieve the same reduction in surface tension at a lower concentration (one added group decreases the required concentration by about one-half). A detailed search for a suitable surfactant must include such parameters as potential environmental impact, foaming, availability and cost.

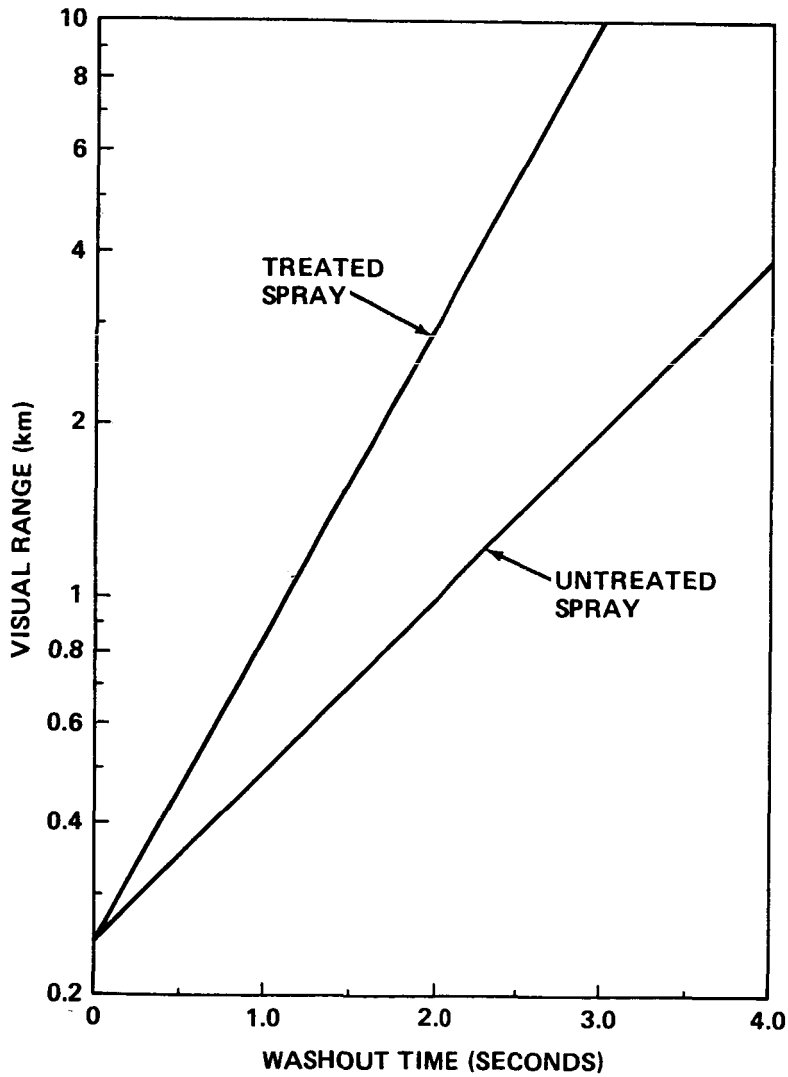

Figure A8-1. The computed effect on fog removal for treating the water spray with a surfactant. The washout calculation for the visual range of the untreated spray is the same as discussed for Figure 5-1. The treated spray drop distribution was obtained by altering the untreated spray drop distribution to maintain constant fluxes of mass and energy with a reduction in surface tension of one-half.

A9.0 PRELIMINARY FOG DISPERSAL PROJECT OUTLINE

PROJECT OVERVIEW

I. Phase A: Feasibility Assessment

   A. MSFC Warm Fog Dispersal Study (Completed)

   B. Cost/Benefit Ratio: KSC and VAFB

II. Phase B: Operational System Design

   A. Fog Measurements at KSC Shuttle Strip and VAFB

   B. Concept Engineering of Operational System

   C. Field Test of Method

   D. Final Concept Definition

III. Phase C: Final Design For Full Scale Implementation

PROJECT OUTLINE

I. Phase A: Feasibility Assessment

A. MSFC Warm Fog Dispersal Study (Completed)

B. Cost/Benefit Ratio: KSC and VAFB

1. Fog frequency and characteristics
-Evaluate existing data

i) Fog frequency/type
ii) Fog droplet spectra
iii) Visibility/visual range
iv) Wind speed/direction
v) Atmospheric stability

2. Launch/landing delay costs

II. Phase B: Operational System Design

A. Fog Measurements At KSC Shuttle Strip and VAFB

1. Fog frequency/type

2. Fog droplet spectra

a. Particle sizing probes (examples)

i) PMS-FSSP (3 to 47 um) with aspirator
ii) PMS-OAP260-X (10 to 600 um) with aspirator and coincidence rejection
iii) PMS-CSAS (0.5 to 3 um) with aspirator

b. Data system (example)
-PDS-400 (4 probe version)

c. Recording instrumentation (example)

i) Tape transport/formatter with software
ii) Printer/plotter with software

3. Visibility

a. Transmissometers

b. Forward scatter visual range meters

c. Slant visual range

4. Wind

   a. Speed

   b. Direction
      -Prevailing wind during fog events

5. Temperature

   a. Air

   b. Water

6. Height of inversion

B. Concept Engineering of Operational System

1. Analytical studies to optimize clearing efficiency

   a. Reduce mean drop size of spray

      i) Surface tension
      ii) Nozzle design improvements

   b. Fog nozzles and deluge nozzles intermixed in the array

   c. Increase collection efficiencies via electrical charging

   d. Optimize the array of nozzles

      i) Spacing
      ii) Air circulation

   e. Evaluate impact of temperature differences between spray and air

2. Pumps and drivers

   a. Total flow rate required is determined by:

      i) Fog removal efficiency
      ii) Visual range requirement
      iii) Cleared volume required
         -Length of runway to be cleared
         -Height of clearing

   b. Head pressure influences

      i) Spray projection height
      ii) Spray drop size and fog removal efficiency
      iii) Energy requirements
      iv) Cost

c. Large units/small units trade-off

i) Minimize capital costs
-Cost per unit
-Number of units required
ii) Minimize operation costs
-Number of operators required
-Energy requirements
-Maintenance
-Shelters required
iii) Maximize reliability
-Impact of unit failure
vi) Portability/versatility considerations

3. Nozzles and monitors

a. Best type(s)

i) Optimum drop sizes
ii) Maximum projection height

b. Flow capacity/quantity trade-offs

i) Uniform spray curtain
ii) Spray induced air circulation
iii) Cost

4. Water system

a. Reservoir

i) Capacity
ii) Location
-Nearby
-Optimally underground
iii) Cost

b. Distribution

i) Lines from pumps to nozzles
ii) Valving

c. Drainage

i) Runoff collection
ii) Return to reservoir

d. Injection of surfactant

5. Development testing

   a. Alternate nozzles

   b. Effect of surfactant on spray height/drop spectra

   c. Required particle sizing probes (example)

      i) PMS-GBPP (0.2 to 12 mm)
      ii) PMS-OAP260-X (10 to 600 um) with aspirator and coincidence rejection
      iii) PMS-FSSP (3 to 47 um) with aspirator

C. Field Test of Method

1. Planning

   a. Site Selection

      i) High incidence of fog
         -High probability of fog in short test period
         -Repeat tests varying one parameter at a time
      ii) Readily accessible recyclable water supply
         -Good drainage
         -Permits surfactant testing
      iii) Logistics support

   b. Test period selection
   -Period of highest incidence of fog varies from site to site
   -Test period as short as possible but at least five weeks

   c. Required instrumentation/measurements

      i) Fog spectra measurements
         -Particle sizing probes, data system and recording instrumentation
      ii) Visibility
         -Transmissometers
         -Forward scatter meters
         -Slant visual range
      iii) Wind
         -Speed
         -Direction
      iv) Temperature
         -Air
         -Water
      v) Height of inversion
      vi) Atmospheric stability
      vvi) Spray induced air circulati[illegible]ptimize nozzle array
         -Smoke tracer
         -Handheld anemometer
         -Doppler lidar

d. Required support equipment

i) Large volume pumping system (~60,000 gpm)
ii) Water distribution system
-Water lines
-Valving
iii) Nozzles and monitors
iv) Water pressure and flow instrumentation

e. Personnel

f. Transferability of results
-Fog spectra differences

2. Conduct field test

a. Long lead procurements

b. Site preparation

c. Test

3. Analysis of results

D. Final concept definition

1. KSC specia!

a. Cost/benefit ratio

b. Design/implementation concept definition

i) Water recirculation
-Difficult to change temperature of very large volumes
ii) Clearing height/volume required for STS

c. Environmental quality issues

2. Generic

a. Cost/benefit ratio

b. Design/implementation concept definition

c. Environmental quality

III. Phase C: Final Design For Full Scale Implementation

REFERENCES

1. FAA Fog Dispersal System Task Team: Ground-Based Warm Fog Dispersal Systems—Technique Selection and Feasibility Determination with Cost Estimates. FAA Report No. FAA-RD-75-126, 1975.

2. Junge, C. E.: Methods of Artificial Fog Dispersal and Their Evaluation. Air Force Surveys in Geophysics, No. 105, GRD 1958, 1958.

3. Jiusto, J. E.: Investigation of Warm Fog Properties and Fog Modification Concepts. NASA CR-72, 1964.

4. Silverman, B. A. and Weinstein, A. I.: Fog, Chapter 9. In Weather and Climate Modification (W. N. Hess, ed.), John Wiley and Sons, New York, New York, 1974.

5. Keller, V. W.: Warm Fog Dissipation Using Large Volume Water Sprays. NASA Patent Case No. MFS-25962, 1983.

6. Plank, V. G.: Fog Modification By Cold-Water Seeding. Air Force Geophysical Research Papers, No. 31, AFCRC-TR-54-201, 1954.

7. Burns, R. A.: Firefighting Module Development. NASA TM-82444, 1981.

8. Hatton, A. P. and Osborne, M. J.: The Trajectories of Large Fire Fighting Jets. Int. J. Heat and Fluid Flow, Vol. 1, No. 1, 1979, pp. 37-41.

9. NASA TM-82473: Terrestrial Environment (Climatic) Criteria Guidelines For Use in Aerospace Vehicle Development, 1982 Revision, p. 4.30.

10. Meyer-Arendt, J. R.: Introduction To Classical and Modern Optics. Prentice-Hall, Inc., Englewood Cliffs, N.J., 1972, p. 353.

11. Beard, K. V.: Rain Scavenging of Particles by Electrostatic-Inertial Impaction and Brownian Diffusion. Precipitation Scavenging-1974, U.S. Atomic Energy Commission, 1977, pp. 183-194.

12. Johnson, D. B.: Raindrop Multiplication by Drop Breakup. J. of Applied Meteorology (JAM), Vol. 21, 1982, pp. 1048-1050.

13. Beard, K. V., Johnson, D. B., and Jameson, A. R.: Collisional Forcing of Raindrop Oscillations. J. Atmos. Sci., Vol. 40, No. 2, 1983, pp. 455-462.

14. Brazier-Smith, P. R., Jennings, S. G., and Latham, J.: The Interaction of Falling Water Drops: Coalescence. Proc. Roy. Soc., London, Vol. A326, 1972, pp. 393-408.

15. Brazier-Smith, P. R., Jennings, S. G., and Latham, J.: Raindrop Interactions and Rainfall Rates Within Clouds. Quart. J. Roy. Meteor. Soc., Vol. 99, 1973, pp. 260-272.

16. McTaggart-Cowan, J. D. and List, R.: Collision and Breakup of Water Drops at Terminal Velocity. J. Atmos. Sci., Vol. 32, 1975, pp. 1401-1411.

17. Beard, K. V. and Ochs, H. T.: Collection and Coalescence Efficiencies for Accretion. J. Geophys. Res., Vol. 89, 1984, pp. 7165-7169.

18. Klett, J. D. and Davis, M. H.: Theoretical Collision Efficiencies of Cloud Droplets at Small Reynolds Numbers. J. Atmos. Sci., Vol. 30, 1973, pp. 107-117.

19. Schlamp, R. J., Grover, S. N., Pruppacher, H. R., and Hamielec, A. E.: A Numerical Investigation of the Effect of Electric Charges and Vertical External Electric Fields on the Collision Efficiency of Cloud Drops. J. Atmos. Sci., Vol. 33, 1976, pp. 1747-1755.

20. Beard, K. V. and Grover, S. N.: Numerical Collision Efficiencies for Small Raindrops Colliding With Micron Size Particles. J. Atmos. Sci., Vol. 31, 1974, pp. 543-550.

21. Mason, B. J.: The Physics of Clouds. Clarendon Press, Oxford, England, 1971, p. 580.

22. Mueller, E. A. and Sims, A. L.: Investigation of the Quantitative Determination of Point and Areal Precipitation by Radar Echo Measurements. Tech. Rep. ECOM-00032-F, (NTIS AD645218), 1966, 88 pp.

23. Beard, K. V.: Raindrop Oscillations: Evaluation of a Potential Flow Model with Gravity. J. Atmos. Sci., Vol. 41, No. 10, 1984, pp. 1765-1774.

24. Pruppacher, H. R. and Klett, J. D.: Microphysics of Clouds and Precipitation. D. Reidel Publishing Co., Dordrecht, Holland, 1980.

25. Kinzer, G. D. and Gunn, R.: The Evaporation, Temperature and Thermal Relaxation-Time of Freely Falling Waterdrops. Jour. of Meteorology, Vol. 8, No. 2, 1951, pp. 71-83.

26. Beard, K. V. and Pruppacher, H. R.: A Wind Tunnel Investigation of the Rate of Evaporation of Small Water Drops Falling at Terminal Velocity in Air. J. Atmos. Sci., Vol. 28, No. 8, 1971, pp. 1455-1464.

27. Pruppacher, H. R. and Rasmussen, R.: A Wind Tunnel Investigation of the Rate of Evaporation of Large Water Drops Falling at Terminal Velocity in Air. J. Atmos. Sci., Vol. 36, No. 7, 1979, pp. 1255-1260.

28. Beard, K. V. and Ochs, H. T.: Measured Collection Efficiencies for Cloud Drops. J. Atmos. Sci., Vol. 40, 1983, pp. 146-153.

29. Ochs, H. T. and Beard, K. V.: Laboratory Measurements of Collection Efficiencies for Accretion. J. Atmos. Sci., Vol. 41, 1984, pp. 863-867.

30. Whelpdale, D. M. and List, R.: The Coalescence Process in Raindrop Growth. J. Geophys. Res., Vol. 76, 1971, pp. 2836-2856.

31. Czys, R. R., Ochs, H. T., and Beard, K. V.: Laboratory Measurements of Collection Efficiencies for Small Precipitation Drops. J. Atmos. Sci., (submitted in February), 1985.

32. Defay, R., Prigogine, I., Bellemans, A., and Everett, D. H.: Surface Tension and Adsorption. John Wiley and Sons, New York, New York, 1966, pp. 95 and 112.

1. REPORT NO.	2. GOVERNMENT ACCESSION NO.	3. RECIPIENT'S CATALOG NO.
NASA TP-2607		

4. TITLE AND SUBTITLE	5. REPORT DATE
Development Testing of Large Volume Water Sprays for Warm Fog Dispersal	June 1986
	6. PERFORMING ORGANIZATION CODE
7. AUTHOR(S) V. W. Keller, B. J. Anderson, R. A. Burns, G. G. Lala,* M. B. Meyer,* and K. V. Beard**	8. PERFORMING ORGANIZATION REPORT #
9. PERFORMING ORGANIZATION NAME AND ADDRESS George C. Marshall Space Flight Center Marshall Space Flight Center, Alabama 35812	10. WORK UNIT NO. M-528
	11. CONTRACT OR GRANT NO.
	13. TYPE OF REPORT & PERIOD COVERED Technical Paper
12. SPONSORING AGENCY NAME AND ADDRESS National Aeronautics and Space Administration Washington, D.C. 20546	14. SPONSORING AGENCY CODE

15. SUPPLEMENTARY NOTES

Prepared by Systems Dynamics Laboratory, Science and Engineering Directorate.
*State University of New York at Albany, Albany, N.Y. 12222.
**University of Illinois at Urbana-Champaign, Urbana, IL 61801

16. ABSTRACT

A new brute-force method of warm fog dispersal is described. The method uses large volume recycled water sprays to create curtains of falling drops through which the fog is processed by the ambient wind and spray induced air flow. Fog droplets are removed by coalescence/rainout. The efficiency of the technique depends upon the drop size spectra in the spray, the height to which the spray can be projected, the efficiency with which fog laden air is processed through the curtain of spray, and the rate at which new fog may be formed due to temperature differences between the air and spray water. Results of a field test program, implemented to develop the data base necessary to assess the proposed method, are presented. Analytical calculations based upon the field test results indicate that this proposed method of warm fog dispersal is feasible. Even more convincingly, the technique was successfully demonstrated in the one natural fog event which occurred during the test program. Energy requirements for this technique are an order of magnitude less than those to operate a thermokinetic system. An important side benefit is the considerable emergency fire extinguishing capability it provides along the runway.

17. KEY WORDS	18. DISTRIBUTION STATEMENT
Nozzles Water Spray Fog Dispersal	Unclassified-Unlimited Subject Category 16

19. SECURITY CLASSIF. (of this report)	20. SECURITY CLASSIF. (of this page)	21. NO. OF PAGES	22. PRICE
Unclassified	Unclassified	111	A06

For sale by National Technical Information Service, Springfield, Virginia 22161

NASA-Langley, 1986